



Dominik Dödlinger, BSc

**ActiveTX Reference Model  
for an Automotive  
Immobilizer System**

**MASTER'S THESIS**

to achieve the university degree of

Diplom-Ingenieur

Master's degree programme: Electrical Engineering

submitted to

**Graz University of Technology**

Supervisor

Ass.Prof. Dipl.-Ing. Dr.techn. Peter Söser

Institute of Electronics

Graz, January 2015



## **AFFIDAVIT**

I declare that I have authored this thesis independently, that I have not used other than the declared sources/resources, and that I have explicitly indicated all material which has been quoted either literally or by content from the sources used. The text document uploaded to TUGRAZonline is identical to the present master's thesis dissertation.

---

Date

---

Signature





Master's Thesis:  
**ActiveTX Reference Model  
for an Automotive  
Immobilizer System**

Dominik Dödlinger

Graz, January 2015

Supervisors: Ass.Prof. Dipl.-Ing. Dr.techn. Peter Söser  
Dipl.-Ing. (FH) Sven Simons



# Acknowledgment

I would have never been able to finish my Master's Thesis without the guidance and support of many people. Although it is not possible to mention all, I would like to express my special thanks to a few of them.

I would like to express my sincere gratitude to my supervisor from NXP, Dipl.-Ing. Sven Simons, whose expertise, support and patience was of great importance for a successful project implementation. Furthermore, I would like to thank Dipl.-Ing. Robert Kofler for providing me the very interesting topic of this Master's Thesis.

I am thankful to my colleague Dipl.-Ing. Christian Liebinger for providing me support with the CAD drawings for the mechanical design. I would like to thank Nikolaos Korkakakis, MSc for helping me with the embedded microcontroller software.

Also special thanks to the Institute of Electronics, and especially to Ass.Prof. Dipl.-Ing. Dr.techn. Peter Söser for the excellent academic supervision.

Finally, I would like to thank my girlfriend Anita Grillnberger for reviewing the documentation with respect to style of the text.



# Abstract

An immobilizer system fulfills the purpose of protecting a car from getting stolen. Such a system consists of a basestation, which is located in the car, and a transponder. The transponder is typically mounted on a PCB inside the key fob. Only when both components share the same secret key, the engine lock is released. The transponder has no battery connected and supplies itself only from the emitted basestation magnetic field.

Current at NXP available immobilizer solutions are using a technique called *Load Modulation* for the transponder to basestation communication. The method has the disadvantage of a limited communication distance due to the necessity of supplying the transponder also during the load modulation communication with the emitted basestation field. To overcome this problem, an alternative so-called *activeTX* concept will be developed at NXP. In this solution, the harvested transponder energy is stored in a support capacitor. Then, the basestation driver is turned off, while the transponder actively responds with its own generated field, using the stored energy in the capacitor.

With respect to the current available load modulation system, the new approach requires changes on both basestation and transponder side. To get a detailed insight into the system, a solid activeTX reference model is required. In this Master's Thesis, a precise Matlab- and lab model of the whole system, with a special focus on transponder energy consumption and active transponder response, is implemented. The Matlab model fulfills the purpose of a free configurable solid prediction tool for the system performance, while the lab setup is intended as a first in-place demonstration hardware. One important requirement that is proven in detail in this document is the matching between lab setup and Matlab model. Also a use case is presented, in which the Matlab model is used for an extraction of important performance and specification parameters of an activeTX example system.



# Kurzfassung

Wegfahrsperrern werden verwendet, um Autos vor Diebstahl zu schützen. Das Gesamtsystem besteht aus zwei Komponenten, der Basisstation und dem Transponder. Typischerweise befindet sich die Basisstation im Auto und der Transponder im Schlüsselgehäuse. Die Wegfahrsperrre, welche den Motor elektronisch blockiert, kann nur gelöst werden, wenn beide Komponenten denselben geheimen Schlüssel teilen. Eine Versorgung des Transponders über eine Batterie ist nicht vorgesehen, wodurch nur eine Feldversorgung über das abgestrahlte Magnetfeld der Basisstation möglich ist.

Die zurzeit bei NXP verfügbaren Wegfahrsperrern-Systeme verwenden ein Konzept, genannt *Lastmodulation*, für die Kommunikation vom Transponder zur Basisstation. Da bei dieser Methode der Transponder auch während der Lastmodulationskommunikation über das Magnetfeld versorgt werden muss, besteht der Nachteil einer geringen Kommunikationsreichweite. Um dieses Problem zu lösen, wird bei NXP ein sogenanntes *activeTX* Konzept entwickelt. Bei diesem System wird die vom Transponder gesammelte Energie in einem Stützkondensator zwischengespeichert, dann wird die Basisstation abgeschaltet und der Transponder verwendet die gespeicherte Energie, um die Antwort über sein eigenes erzeugtes Magnetfeld zu senden.

Im Vergleich zum Lastmodulationssystem sind auf Basisstations- und Transponderseite Veränderungen erforderlich. Um einen genauen Einblick ins activeTX-System zu erhalten, wird ein zuverlässiges Referenzmodell benötigt. Es ist nun Aufgabe dieser Masterarbeit ein exaktes Matlab- und Labormodell des gesamten Systems zu entwickeln, wobei der Schwerpunkt auf dem Energieverbrauch des Transponders sowie auf der aktiv gesendeten Transponderantwort liegt. Das Matlab Modell wird als frei konfigurierbares Simulationstool zur Vorhersage des Systemverhaltens verwendet. Der Laboraufbau ist als erste bei NXP verfügbare Demonstrationshardware für das activeTX-System vorgesehen. Eines der Kernziele dieser Arbeit, die Konsistenz zwischen Matlab- und Labormodell zu gewährleisten, konnte genauestens nachgewiesen werden. Die Arbeit stellt auch ein Anwendungsbeispiel eines activeTX-Systems vor, bei welchem das Matlabmodell zur Spezifizierung von wichtigen Systemparametern verwendet wird.



# Contents

<b>1</b>	<b>Introduction</b>	<b>1</b>
1.1	Project Goals . . . . .	2
1.2	Structure of the document . . . . .	2
<b>2</b>	<b>Immobilizer Systems</b>	<b>5</b>
2.1	Inductive RFID Systems . . . . .	5
2.1.1	Energy Supply and Data Communication . . . . .	6
2.1.2	Frequency Range . . . . .	8
2.1.3	Security . . . . .	9
2.1.4	Transponder . . . . .	10
2.1.5	Basestation . . . . .	11
2.2	Immobilizer System Application . . . . .	11
2.3	ActiveTX Immobilizer System . . . . .	12
<b>3</b>	<b>Matlab Model</b>	<b>17</b>
3.1	Modeling Approaches . . . . .	17
3.2	Coil Coupling Model . . . . .	19
3.2.1	Reference Coils and Arrangements . . . . .	19
3.2.2	Inductive Coupling Theory . . . . .	20
3.2.3	Implemented Coupling Factor Model . . . . .	23
3.2.4	Coupling Factor Measurement . . . . .	29
3.3	ActiveTX Model . . . . .	31
3.3.1	3D-Coil Simulink Model . . . . .	34
3.3.2	Basestation Simulink Model . . . . .	34
3.3.3	Transponder Simulink Model . . . . .	35
3.3.4	ActiveTX Top Level Model . . . . .	44
3.3.5	Solver . . . . .	46
3.4	Graphical User Interface . . . . .	47
<b>4</b>	<b>Lab Setup</b>	<b>51</b>
4.1	Mechanical Distance Setup . . . . .	51
4.1.1	Requirements . . . . .	51
4.1.2	Approaches for the Mechanical Setup . . . . .	52
4.1.3	Implemented Mechanical Setup . . . . .	52
4.2	Requirements and Overview of the Electronic Setup . . . . .	54
4.3	Transponder Hardware . . . . .	56
4.3.1	Transponder Approaches . . . . .	56
4.3.2	Implemented Hardware . . . . .	57

4.4	Transponder Software . . . . .	60
4.5	Basestation Hardware . . . . .	63
4.6	Basestation Software . . . . .	65
4.6.1	Driver Software . . . . .	66
4.6.2	Receiver Amplifier Software . . . . .	67
4.7	Complete Lab Setup . . . . .	68
4.7.1	Configuration Principle of the Lab Setup . . . . .	69
4.7.2	Transponder Current Consumption Measurement Principle . . . . .	70
4.7.3	Measurement GUI . . . . .	71
<b>5</b>	<b>Results</b>	<b>73</b>
5.1	Comparison between Lab Setup and Matlab Model . . . . .	73
5.1.1	Explanation of the Differences . . . . .	73
5.1.2	Comparison Plots . . . . .	80
5.1.3	Discussion . . . . .	84
5.2	Use Case of the ActiveTX Model . . . . .	84
5.2.1	Coil Inductance Calculation . . . . .	84
5.2.2	Calculation of the Transponder Support Capacitance . . . . .	86
5.2.3	System Optimization . . . . .	87
5.2.4	System Specification . . . . .	89
<b>6</b>	<b>Conclusion</b>	<b>91</b>
6.1	Outlook . . . . .	91
	<b>List of Figures</b>	<b>92</b>
	<b>List of Tables</b>	<b>95</b>
	<b>Bibliography</b>	<b>97</b>
<b>A</b>	<b>Coupling Factor Values</b>	<b>99</b>
<b>B</b>	<b>Mechanical Distance Setup Drawings</b>	<b>101</b>
<b>C</b>	<b>Schematic and Layout of the Transponder Adapter Board</b>	<b>117</b>
<b>D</b>	<b>Schematic and Layout of the Transponder Coil PCB</b>	<b>121</b>
<b>E</b>	<b>Layout of the Basestation Coil PCB</b>	<b>125</b>

# Chapter 1

## Introduction

An immobilizer system is used as anti-theft protection in the automotive sector. Basically it is a sub-category of an inductively coupled Radio Frequency Identification (RFID) system. The two main components are a basestation and a transponder IC. In a typical application, the battery supplied basestation is located in the car, with its coil wound around the ignition lock. The transponder and its associated coil are mounted on a PCB inside the key fob. Since the transponder has no battery connected, it is only supplied by the harvested energy from the emitted basestation magnetic field.

When the key is inserted into the ignition lock, the basestation begins to communicate with the transponder. Only when both components share the same secret key, the engine lock is released and the driver is allowed to start the car. From a manufacturers point of view, it is desired to have a large transponder operating distance because this gives freedom in choosing the location of the basestation coil inside the car. For example, a 5 cm operating distance makes it much harder for choosing a suitable place compared to a 10 cm operating distance.

As this project is made in co-operation with *NXP Semiconductors Austria* located in Gratkorn, the limitations in operating distance of the in-place available transponder are well known. The current system uses a method called *Load Modulation* for the communication from the transponder to the basestation. This technique requires the basestation carrier to be always turned on since the transponder changes its load impedance to influence the emitted field so that the basestation receiver is able to detect a telegram. The signal modulated on top of the basestation carrier is by orders of magnitude smaller than the carrier itself. Through the inherent noise of the generated carrier, even the best receiver won't be able to detect a transponder telegram for larger distances between basestation and transponder coil.

An alternative approach for the immobilizer system is the so-called *activeTX* concept. The major difference compared to the load modulation system is the transponder to basestation communication. In the activeTX solution, the basestation is turned off while the transponder transmits the response with its own generated magnetic field. Since the basestation carrier is not activated, the important advantage of a larger signal-to-noise ratio leads to a larger communication distance. The fact that no basestation magnetic field is available during the transponder response requires an appropriate transponder support capacitor, in which the previously extracted energy is stored. According to this, the basestation protocol also needs to include charge times (i.e. a constant emitted magnetic field) to reload the capacitor. In other words, the protocol has to be optimized in a way that the transponder supply is always

larger than the ICs power on reset voltage level to guarantee a properly working transponder.

In the next period, an activeTX system will be developed at NXP. Compared to the current available load modulation system, changes on both transponder and basestation side are necessary. For the development process, a solid reference model is required. It is now scope of this Master's Thesis to develop a Matlab and physical lab model of the activeTX system. The Matlab model should allow simulating relevant system parameters such as the transponder energy consumption or the efficiency of different protocol timings. It should be possible to use the model for a prediction of important performance parameters like the transponder operating distance. The lab model fulfills the purpose of having a first in-place demonstration hardware. It is very useful to have a physical setup for getting a feeling of the new system's behavior. Another important aim of the lab model is the advantage of having a cross check tool, which allows the evaluation of the Matlab model's correctness. Because the first step of the activities at NXP will be the development of the new basestation, it should also be possible to use the lab setup as test system for this IC.

## 1.1 Project Goals

The project goals are:

1. The development of a Matlab model of the activeTX immobilizer system with the following properties:
  - A detailed model of the air interface, including all relevant coil antenna parameters
  - A simple model of the basestation
  - A detailed model of the transponder with a special focus on the transponder current consumption and transponder to basestation response
2. The development of a lab model of the activeTX immobilizer system with the following major requirements:
  - The development of a mechanical setup, which should allow an accurate distance adjustment
  - A detailed transponder implementation with electronically adjustable current consumption
  - A basestation implementation, which should allow an accurate measurement of the received transponder response
3. To proof if the Matlab model and the lab setup are consistent

## 1.2 Structure of the document

Chapter 2 discusses the basics of immobilizer systems. This includes a short introduction into important RFID system properties. After an explanation of an immobilizer application, the new activeTX system is introduced.

Chapter 3 contains the description of the implemented activeTX Matlab model. It starts with a discussion of the possible modeling approaches and continues with the description of

the used coil coupling model. The core of this chapter is the explanation of the implemented activeTX Matlab model. At the end, the implemented Graphical User Interface (GUI), which is necessary for a clear visualization of the simulation results, is presented.

Chapter 4 deals with the lab setup. It contains a short description of the designed mechanical parts and goes into more detail for the electronic components. The description of the electronic setup starts with the requirements for the activeTX system, followed by a detailed hardware and software explanation.

Chapter 5 contains the results of this Master's Thesis. It begins with an accurate check of the consistence between Matlab model and lab setup. The second part presents a use case, which demonstrates how the Matlab model can be used for a determination of important performance parameters.



## Chapter 2

# Immobilizer Systems

Chapter 2 gives an overview of inductively coupled automotive immobilizer systems, as well as an introduction to the activeTX system. To be able to understand such a system, the basics and most important parts of inductively coupled Radio Frequency Identification (RFID) systems are explained in section 2.1. As RFID is a very broad topic, there are also other coupling mechanism such as acoustic, electrical, or electromagnetic coupling. Because only inductive coupling is of importance for the activeTX system, the other mechanism are not explained in more detail. For more insights please refer to [7].

Section 2.2 describes an example of an immobilizer system application. The above mentioned knowledge allows the activeTX system to be introduced in section 2.3. This section contains the motivation and an explanation of the advantages and disadvantages of the system.

### 2.1 Inductive RFID Systems

The most important requirement for an inductive RFID system is that transponder and basestation are located in the near field of each other. This is valid as long as the distance between them is smaller than the wavelength of the signal divided by  $2\pi$ . A block diagram of an inductively coupled RFID system is illustrated in figure 2.1. The system consists of a basestation and a transponder, with each part connected to a coil. Communication is done via magnetic coupling. The quality of the coupling depends on the coil geometries, orientation and distance between the coils. A detailed mathematical representation of the coupling mechanism is discussed in section 3.2.2. [7, p. 40-43]

The basestation consists of a matching network, driver (TX), receiver (RX) and microcontroller and is typically supplied externally (i.e. a car battery in an immobilizer system). An effective and simple form of the basestation coil connection is a tuned series resonance circuit, resulting in a matching network, which consists of a series connection of a resistor and a capacitor. The resonance frequency matches the frequency of the voltage generated by the basestation driver. Due to the resonance effect, a large current flows, only limited by the ohmic resistance of the matching circuit. Because of the proportionality to the magnetic field, in most cases such a large current is desired. [7, p. 40-42]

The transponder side includes a matching network, receiver and microcontroller, but there exist differences in the supply. If the basestation driver is turned on, the emitted time varying magnetic field induces a voltage in the transponder coil. The induced voltage can be maxi-

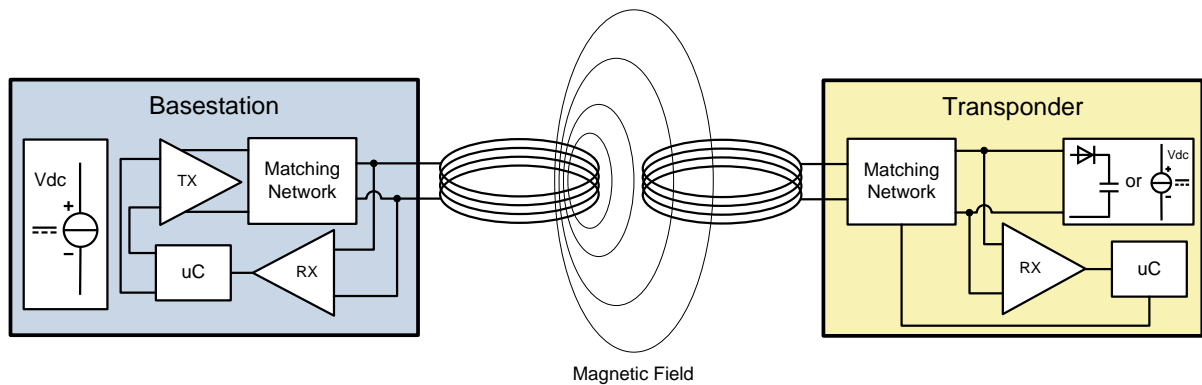


**Figure 2.1:** Block diagram of an inductively coupled RFID system.

mized with a parallel resonance circuit, tuned to the same frequency as the basestation field (i.e. a parallel connection of resistor and capacitor used as matching circuit). Depending on the supply, the transponder can be distinguished to be either active or passive. An active transponder has an external supply (i.e. a battery), whereat a passive transponder generates its supply only from harvesting the magnetic energy of the emitted basestation field. A simple example for a passive supply is a rectifier and a support capacitor directly connected to the transponder coil. [7, p. 22-24, 40-42]

The next subsections outline the most important properties of inductive RFID systems, which are also necessary for the activeTX system.

### 2.1.1 Energy Supply and Data Communication

As already mentioned, in most cases the basestation is externally supplied and the transponder supply is either active or passive. But there is also an important difference in the elementary communication procedure. The procedures are: [7, p. 39-40]

- **FDX:** full-duplex procedure
- **HDX:** half-duplex procedure
- **SEQ:** sequential procedure

The differences between the procedures are illustrated in figure 2.2. Because energy transfer is of little importance for active supplied transponders, it has to be admitted that the following considerations are obtained for passive transponders. FDX and HDX have a continuous energy transfer, which means that the basestation field is always available. In contrast, in the SEQ procedure, the basestation field is turned on during the downlink (basestation to transponder communication) and turned off during the uplink (transponder to basestation communication). This means that energy must be stored during the downlink (i.e. in a capacitor), which can then be used for the uplink. The only difference between FDX and HDX is that in the FDX procedure, the uplink and downlink are used simultaneously, which means that transponder and basestation are also able to transmit during the reception. To

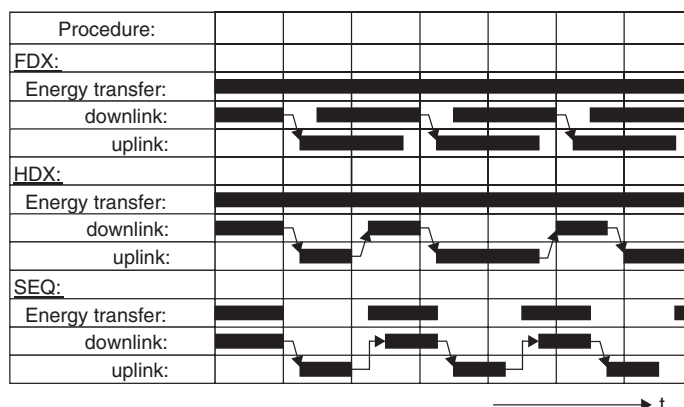


**Figure 2.2:** Diagram of FDX, HDX and SEQ over time. [7, p. 40]

accomplish this, methods are used in which the transponder uses a different frequency for the transmission (i.e. subharmonics of the basestation frequency). [7, p. 39-40]

A commonly used uplink communication method for HDX systems is the *Load Modulation*. This principle relies on the effect that due to the magnetic coupling between transponder and basestation coil, a change in the transponder load impedance is seen on the basestation side. Since the transponder usually has a high load impedance during normal operation, the whole transponder system, consisting of coil and IC, has a large quality factor (Q factor) and thus a large coil voltage. Because of the resonance circuit, a large voltage leads to a large coil current. The current's direction is set up in such a way that its magnetic field opposes the emitted basestation field (Lenz Law). This reduction in the magnetic field produces a reduction of the basestation coil voltage. When the transponder reduces its load impedance, with i.e. switching on a transistor as illustrated in figure 2.3, the Q factor decreases. This results in a smaller coil voltage and current, which leads to a negligible influence on the basestation field. Summarized, by switching on a parallel transistor at the right time, a modulation scheme like Amplitude Shift Keying (ASK) can be generated very easily for the uplink communication. [7, p. 43-45, 98]

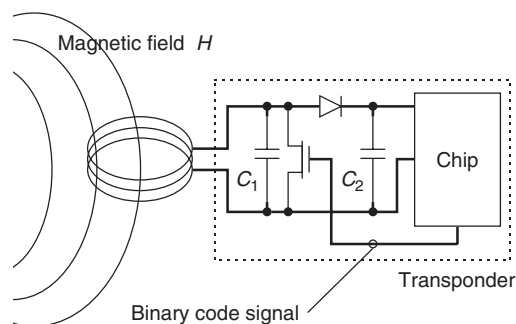


**Figure 2.3:** Block diagram of a circuit for a load modulation signal generation. [7, p. 44]

An example for a widely used HDX downlink communication method is the Pulse Pause Coding (PPC). Figure 2.4 shows an example of a PPC coded baseband signal. The basestation

transmission signal can be easily generated by multiplying this baseband signal with the carrier. Information is stored in the pulse length of the baseband signal. A short pulse length represents a logic one and a long pulse length represents a logic zero. The transponder simply demodulates the signal by counting the time between two rising or falling edges. As can be seen, the low pulses, in which the basestation is not emitting a field, are very short. This has the advantage that the transponder can extract energy almost during the whole downlink process. [7, p. 180-181]

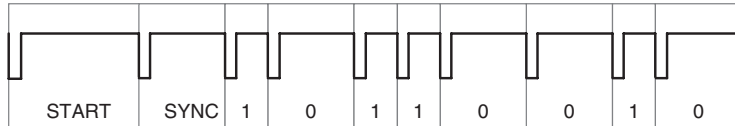


**Figure 2.4:** Baseband signal of a pulse pause coding sequence. [7, p. 181]

Because in an SEQ procedure, no basestation carrier is present during the uplink, modulation methods like ASK, BPSK (Binary Phase Shift Keying) or 2-FSK (Binary Frequency Shift Keying) can be used. The missing basestation carrier leads to the advantage of a much higher communication distance compared to the load modulation concept. This topic is discussed in more detail in section 2.3. [7, p. 180-181]

For an SEQ downlink communication, the same conditions apply as in the HDX case, which means that for energy reasons, PPC is a good choice.

### 2.1.2 Frequency Range

The frequency range for inductive RFID can be defined from 27.125 MHz downwards. Of course niche products can use higher frequencies, but the transition to the near field limits the most available products to frequencies in the mentioned range. For example, for a 30 MHz system, the near field begins at 1.6 m. [7, p. 162-164]

Frequencies smaller than 135 kHz are denoted as LF (Low Frequency). Because the induced transponder coil voltage is proportional to the frequency, for energy reasons, the lowest used frequencies are bounded to approximately 9 kHz. The advantages of LF are listed below: [7, p. 156, 162-164]

- High distances possible because regulations allow high power for basestation field
- Low transponder energy consumption due to low clock rate
- Low magnetic damping in metal environment and high penetration depth in non magnetic materials and water
- Frequencies free accessible for all applications

Frequencies between 135 kHz and 27.125 MHz are known as HF (High Frequency). The most common used frequencies are 6.78 MHz and 13.56 MHz because they fall into the ISM-band. ISM stands for a free of charge usage for industrial, scientific and medical applications. Many applications, such as Near Field Communication (NFC) systems, prefer a 13.56 MHz carrier.

Some advantages of the HF frequency range are listed below: [7, p. 156, 162-164]

- Fast communication rate due to high carrier frequency
- Only small inductances necessary (i.e. inductance realizable directly on PCB)
- Tuning capacitors for resonance circuit realizable on chip

### 2.1.3 Security

Security is a very important issue for RFID systems. Many methods, such as relay or denial of service attacks, exist for getting unauthorized access to secure basestation or transponder data. A hacked system can lead to large economical damage for the manufacturer. Thus, efficient methods for securing the communication channel are available. As an example, the method of authenticated encryption, which is also used in immobilizer systems, is now explained in more detail. [7, p. 226]

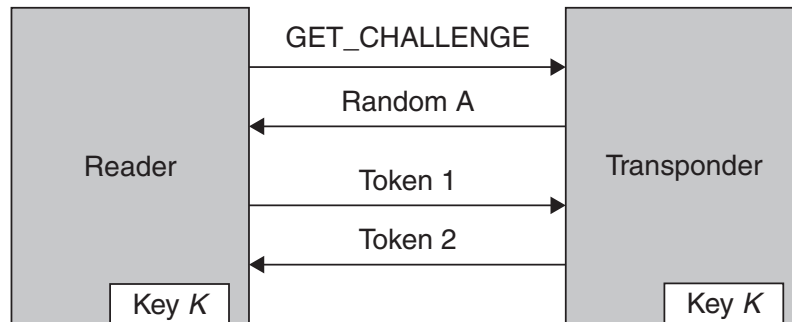


**Figure 2.5:** Implementation of a mutual symmetrical authentication. [7, p. 227]

A mutual symmetrical authentication between basestation and transponder is also known as *Three Pass Mutual Authentication*. The requirement for this method is an encryption unit. An example is an Advanced Encryption Standard (AES) unit, which uses a secret key to encrypt the plaintext. Symmetric in the context of this authentication method means that transponder and basestation are in possession of the same secret key. A possible implementation of the whole authentication process is illustrated in figure 2.5. At the beginning, when the transponder enters the basestation operating distance, both do not know if they belong to each other. The start of the authentication is a GET\_CHALLENGE command, transmitted by the basestation. Afterwards, the transponder sends a pseudo random number (Random A). The basestation takes Random A and adds additional data and a self generated pseudo random number (Random B) to build a data package (Token 1). This data package is encrypted and transmitted to the transponder. When the transponder decrypts the encrypted telegram with its secret key and is able to recognize Random A, the proof that the basestation belongs to the transponder is given. In the next step, the transponder uses Random B and adds a new generated pseudo random number (Random C) and additional data to produce a data package (Token 2). The data package is encrypted and transmitted to the basestation, which then decrypts the telegram. When the basestation is able to recognize Random B, it knows that the transponder uses the same secret key and the mutual authentication is finished. [7, p. 226-228]

Two important advantages can be stated for the explained method. The first one is that always two random numbers are transmitted in one encrypted telegram. Thus, a secret key retrieval from using Token 1 and Random A is not possible. The second advantage is the usage of pseudo random numbers, which eliminates a recording and replay attack. [7, p. 227-228]

### 2.1.4 Transponder

As an example for an inductively coupled transponder, an automotive IC developed by *NXP Semiconductors* is presented. The block diagram can be seen in figure 2.6. The IC is a combination between an active and passive transponder. It has both Passive Keyless Entry (PKE) and immobilizer function. The PKE part is battery supplied, whereas the immobilizer part is used with field supply. Usually, the IC is connected to a coil and both are integrated into a car key fob. [18]

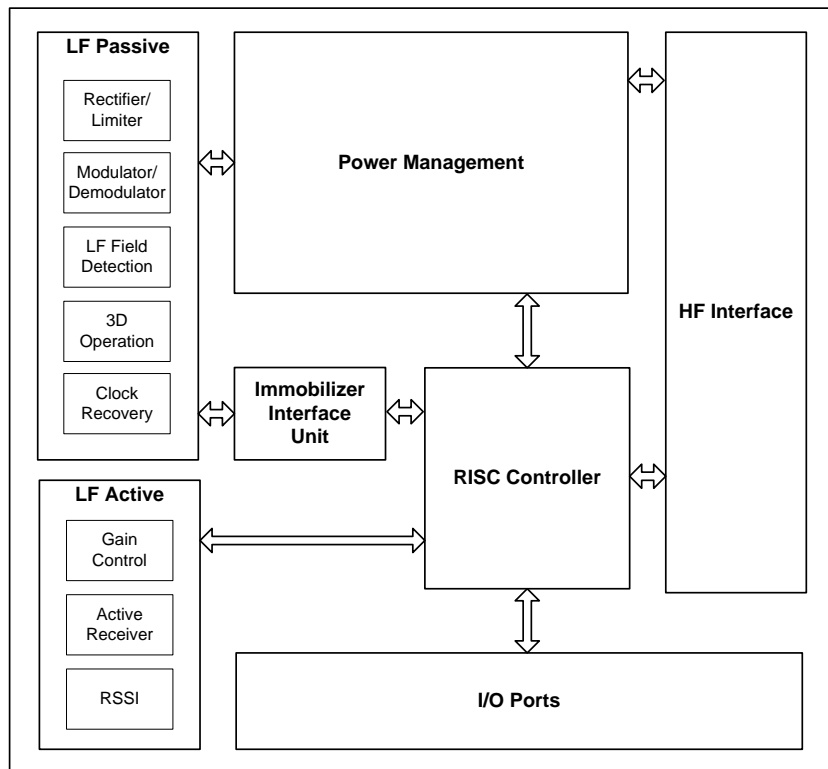


**Figure 2.6:** Block diagram of an automotive transponder IC developed by *NXP Semiconductors*. [18]

The battery supplied LF Active block is the analog part of the PKE system. When the IC enters the basestation operating distance, the Gain Control block preprocesses the received signal for the Active Receiver. After analog-to-digital conversion, the RISC controller checks if the received telegram is valid. Via the RSSI block, the PKE system is able to measure the amplitude of the magnetic field and thus, the distance between transponder and basestation can be calculated. [18]

The more interesting part for this Master's Thesis is the immobilizer. When the battery of the key fob is empty, the immobilizer is the only possibility to start the car. Hence, it can be seen as a backup system. The LF Passive block is the analog frontend of the immobilizer.

With the LF Field Detection, the IC is able to detect if a strong enough basestation field for supplying the IC is available. The Rectifier with connected external support capacitor generates a DC supply from the AC coil voltage. When the basestation field is too strong, the coil voltage is regulated to a sufficiently low value by the Limiter. The Power Management is responsible for generating different regulated supply domains for the whole transponder. Transmission and reception of commands is done via load modulation modulator and PPC demodulator. The immobilizer state machine is implemented on the RISC Controller. [18]

### 2.1.5 Basestation

The now presented IC is the counterpart of the above explained transponder. This IC, which was also developed by *NXP Semiconductors*, is used as basestation for immobilizer applications. According to the IC's block diagram in figure 2.7, a state machine (Control Unit) is responsible for controlling all circuit parts. Due to the voltage regulator with included temperature sensor, the basestation can be directly supplied by the car battery. An external series resonance circuit, containing of coil and tuning capacitor, is required to be connected to the driver pins. The driver's output is a rectangular voltage with adjustable duty cycle. Due to the resonance circuit, which acts like a bandpass filter, a sinusoidal coil current is generated. The implemented coding for the driver is PPC. A synchronous demodulator with switched capacitor filters and adjustable amplifiers is used for the demodulation of the received load modulation signal. [17]

To be able to communicate with the car's body control unit, a LIN-transceiver is available. An SPI interface is also included so that a controlling by a an external microcontroller is possible. [17]

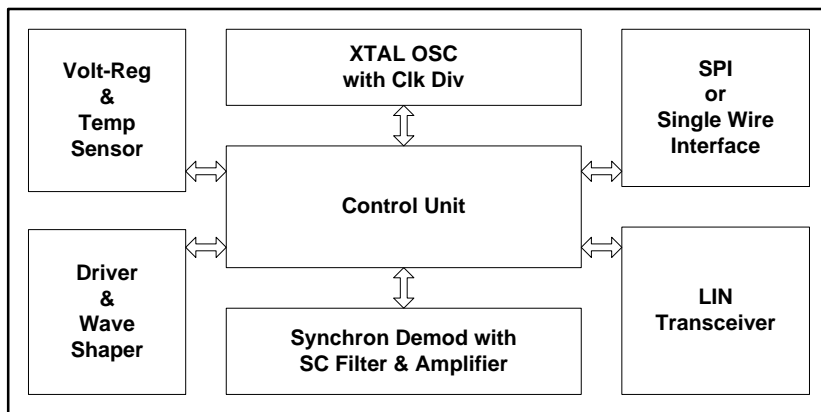


**Figure 2.7:** Block diagram of an automotive basestation IC developed by *NXP Semiconductors*. [17]

## 2.2 Immobilizer System Application

Basically, the purpose of an immobilizer system is to prevent the car from getting stolen. This can be achieved by blocking the engine start activity as long as no valid transponder is recognized. A diagram of an immobilizer system is shown in figure 2.8. [4] [5]

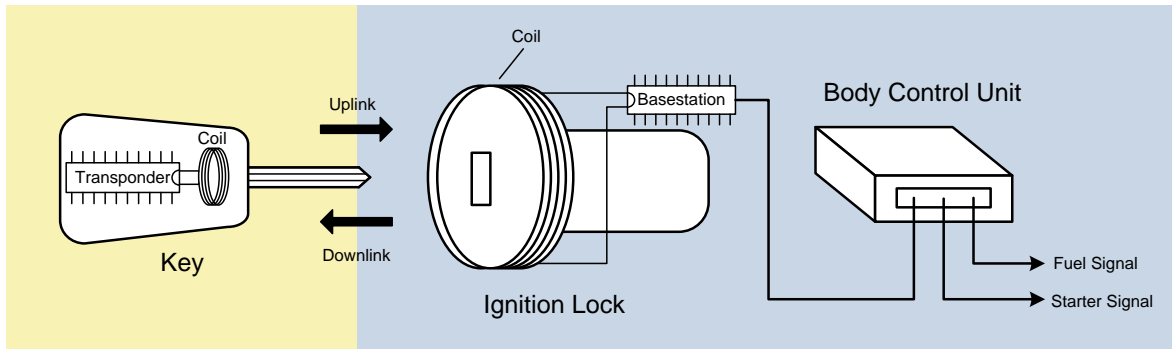


**Figure 2.8:** Basic diagram of an immobilizer system. [4]

The key fob contains a PCB with mounted transponder and coil. There exist also one-part-solutions, where the coil is wound around the transponder and both parts are cast with plastic. The transponder can then be placed anywhere in the key fob. For both mounting types, no battery is required. An included battery is only necessary if the car has also Remote Keyless Entry (RKE) or Passive Keyless Entry (PKE) function. This feature allows the car to be opened by pressing a button on the key fob. It must be noted that RKE and PKE are independent systems, which have nothing to do with the immobilizer function. [4]

The basestation is located in the car and also connected to a coil. In most cases, this coil is wound around the ignition lock. Controlling of the basestation is done by the Body Control Unit (BCU), which is also the centerpiece for many other functions such as power windows, power mirrors, air conditioning or central locking. [4] [5]

When the key is inserted into the ignition lock and turned around, the body control unit informs the basestation to begin the communication. To identify if the transponder belongs to the car, a mutual symmetrical authentication, as described in section 2.1.3, can be used. This requires the transponder and the BCU to have an encryption unit. The basestation does not need to have one because after reception, the encrypted telegram is directly transmitted to the body control unit. A decryption and subsequent transmission of the plaintext by the basestation would result in a major security risk due to the possibility of scanning the plaintext on the connection wire between basestation and BCU. When the authentication finishes successfully, the BCU releases the lock by informing the Engine Control Unit (ECU) to begin with the start activity. [5]

The already presented transponder and basestation in section 2.1.4 and 2.1.5 can be used to implement a fully functional immobilizer system.

## 2.3 ActiveTX Immobilizer System

The currently at NXP available transponders are using load modulation for the uplink communication and thus are part of an HDX system. An activeTX immobilizer is of SEQ type. The differences between FDX/HDX and SEQ have already been explained in section 2.1.1.

To get more insight into the activeTX system, a simplified representation is shown in figure 2.9. The basestation has an external resistor ( $R_b$ ) for a Q factor adjustment and two external series capacitor ( $C_b$ ) connected to the coil. Compared to a one capacitor solution, two

capacitors have the advantage that the receiver can be implemented differentially. Both driver and receiver are controlled via microcontroller.

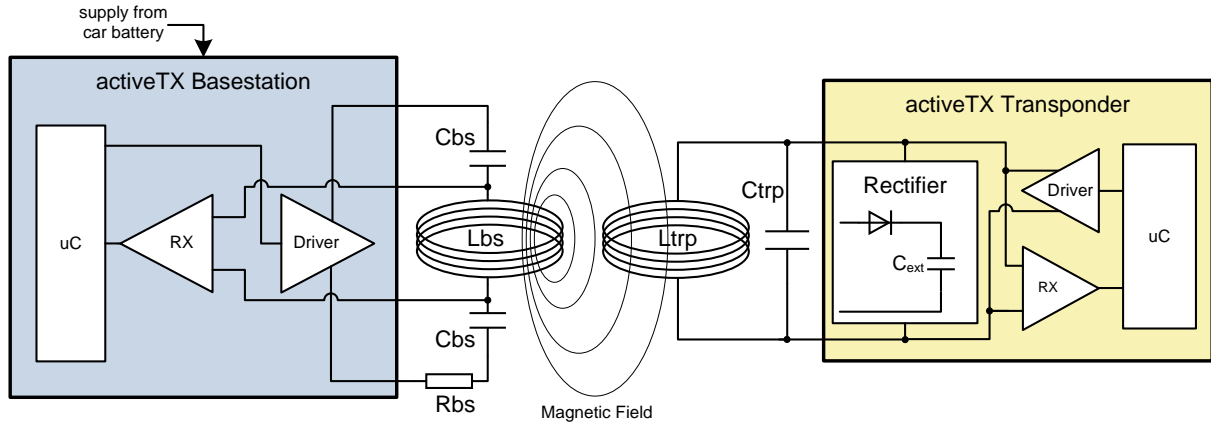


**Figure 2.9:** Simplified diagram of the activeTX immobilizer system.

The transponder has only a parallel capacitor connected. In most cases, a parallel resistor for a Q factor adjustment is not necessary because the ohmic resistance of the coil sets the Q factor to sufficient low values. As for all passive transponders, the energy for supplying the IC is extracted from the magnetic field. A rectifier with a connected external support capacitor ( $C_{ext}$ ) generates the required DC supply. Because pulse pause coding is used for the downlink, the receiver can simply be designed as envelope detector. The most important part of the new system, which also gives it the name activeTX, is the active transponder transmitter (Driver). To exploit the advantage of the resonance rise of the parallel circuit consisting of coil ( $L_{trp}$ ) and tuning capacitor ( $C_{trp}$ ), the only possibility for the transmitter is a current driver. As a parallel resonant circuit acts like a bandpass for the coil current, also rectangular driving currents can be used to generate sinusoidal coil currents. The microcontroller fulfills the task of controlling all transponder circuit parts.

An important part of activeTX is the behavior of the transponder supply voltage during different communication phases. Figure 2.10 shows a simplified example sequence. During the first charging time ( $t_{charge_1}$ ), the voltage at the support capacitor  $C_{ext}$  rises approximately like an RC-loading curve. This is a very simple assumption because in the normal case, this curve depends strongly on the transponder current consumption. When the basestation transmits its first PPC command ( $t_{dl_1}$ ), the voltage drops a little bit due to the inherent small low pauses of the magnetic field. During the first transponder command ( $t_{ul_1}$ ), the basestation is turned off and the supply voltage drops strongly. In this phase, the stored energy in  $C_{ext}$  is used for transmission and for supplying the transponder. It is important that the voltage does not drop below the Power On Reset (POR) voltage threshold before the next charging phase begins. Otherwise the transponder would stop operating.

The motivation for the new system is an improved communication distance compared to a load modulation system. Because the basestation is driving large currents in normal operation, also large voltages appear on the coil. As an example, a 125 kHz system, which uses a basestation drive current with an amplitude of 1 A, generates a voltage in the range of  $400 V_{pk}$  on a  $500 \mu H$  coil. For distances larger than 5 cm between basestation and transponder, typically a signal

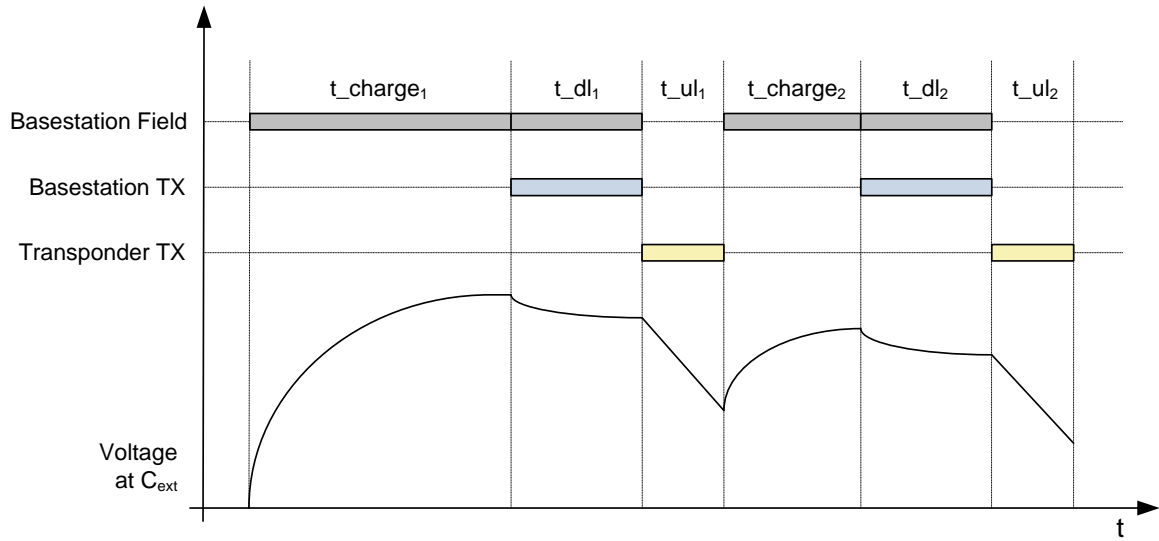


**Figure 2.10:** Voltage behavior at the external support capacitor of the activeTX transponder during different communication phases.

of only tens of a millivolt is modulated on top of this large carrier via a transponder load modulation communication. It can be imagined easily that a small variation of the carrier, i.e. in the amplitude or phase, can destroy an uplink command. An activeTX system has no carrier activated and thus, also actively sent transponder commands, which generate a basestation RX voltage smaller than 1 mV, can be recognized by a well designed receiver. This leads to a big improvement in the communication distance.

A big disadvantage of the activeTX system is a smaller energy distance compared to a load modulation system. The explanation therefor is that the load modulation transponder is always supplied by the basestation, while the activeTX transponder is not during the uplink. From this fact, it follows that the transponder current consumption is one of the most important parameters for the system. A comparison between the activeTX and load modulation system is given in table 2.1 (with respect to the particular property, a check mark is provided for the preferable system).

The big challenge for the activeTX system is to find a balance between the energy and communication distance, with the goal of reaching an overall better performance as with a load modulation system. With the presented Matlab model in chapter 3 and the lab setup in chapter 4, the behavior of the system can be studied in detail. It will be shown that the model provides the ability to adjust all necessary parameters, such as transponder current consumption, coil detuning or protocol timings, for optimizing the system and defining a specification for the future ICs.

<b>Property</b>	<b>ActiveTX System</b>	<b>Load Modulation System</b>
Larger communication distance	✓	✗
Larger energy distance	✗	✓
Shorter protocol duration	✗	✓
Advantage of a smaller external support capacitor	✗	✓
Advantage of a smaller required dynamic range for the basestation ADC	✓	✗
Advantage of an inaccurate system clock requirement on basestation side	✓	✗
More freedom for the car manufacturer in placing the basestation coil due to larger operating distance	✓	✗

**Table 2.1:** Comparison between activeTX and load modulation concept



# Chapter 3

## Matlab Model

This chapter contains the description of the complete activeTX Matlab model implementation. Section 3.1 starts with a comparison of the modeling approaches. Since the coupling factor between basestation and transponder coil is a very important parameter, the coupling model and the necessary theory are presented in section 3.2. The activeTX Simulink and Matlab top level model are explained in section 3.3. To be able to visualize the simulation results in a comfortable way, a Graphical User Interface (GUI) is implemented. This GUI is described in section 3.4.

### 3.1 Modeling Approaches

Basically, there exist three different possibilities to implement the activeTX model in Matlab:

1. Implement the whole model with only Matlab scripts. The model's algebraic differential equations appear then in source code documents, which are executed sequentially.
2. Use the Simulink environment's standard blocks to define the model's behavior. Only the model parametrization is done with Matlab scripts, while the simulation is executed in the Simulink environment. [16]
3. Use the Simulink environment's included Simscape toolbox to define the model's behavior. The difference between case 2 is that this toolbox supports a physical network approach. Again, only the parametrization is done with Matlab scripts. [13]

The first option with only Matlab scripts has the disadvantage of many complex scripts and thus, a verification will get time consuming. In contrast, a Simulink implementation has a graphical representation of the model, resulting in a more convenient design and validation process. Because the model of the activeTX system should be time-based and Simulink is specially tailored for such types of simulations, it will be used as main environment.

The difference between case 2 and 3 is that the Simscape toolbox offers the advantage of a physical model development. Specifically, the model can be implemented using physical blocks instead of integrator or gain blocks. To make this more clear, the differences for an RLC series resonance circuit are illustrated in figure 3.1. Both systems produce the same capacitor voltage ( $v_c$ ), when they are simulated with the same solver settings. For the basic

Simulink block variant, first of all the following RLC circuit system equations must be derived by hand:

$$\begin{bmatrix} \frac{di}{dt} \\ \frac{dv_c}{dt} \end{bmatrix} = \begin{bmatrix} -\frac{R}{L} & -\frac{1}{L} \\ \frac{1}{C} & 0 \end{bmatrix} \cdot \begin{bmatrix} i \\ v_c \end{bmatrix} + \begin{bmatrix} \frac{v_{in}}{L} \\ 0 \end{bmatrix} \quad (3.1)$$

$$y = v_c$$

With this knowledge, the system can be implemented with integrator, gain and sum blocks. In contrast, the system, which uses the Simscape toolbox, can be described with the physical structure (i.e. the needed circuit parts), without having any knowledge about the underlying differential equations. [13]

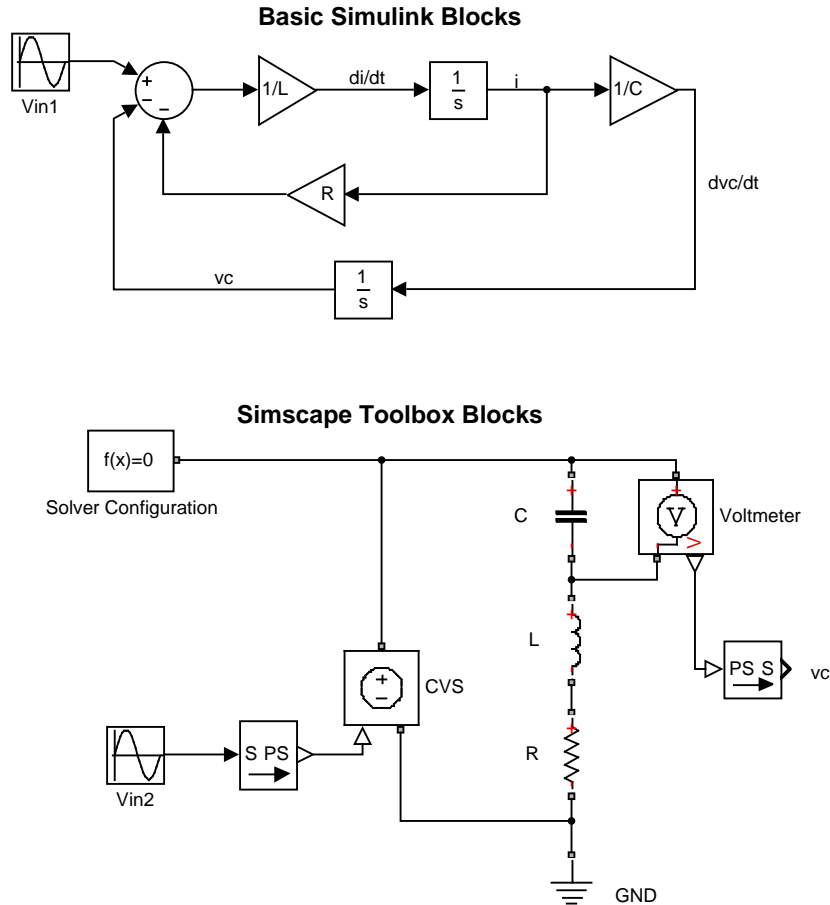


**Figure 3.1:** Simulink basic block model versus Simscape toolbox model.

The big advantage of Simscape arises for example, when another capacitor needs to be switched in parallel to the resistor. For the system with basic blocks, a new differential system has to be derived by hand. With Simscape, the capacitor simply needs to be placed

in parallel. When a circuit contains more than ten parts, a significant amount of time can be saved with this development method. This advantage is the key point for choosing the variant with Simscape as framework for the activeTX Matlab model implementation.

Because Simscape uses a physical network approach, some differences arise compared to the standard Simulink modeling procedure. Simscape blocks, such as capacitors, diodes or mechanical parts, cannot be connected directly with Simulink blocks. As can be seen in figure 3.1, converters (i.e. the SPS block) exist, which make it possible for the voltage source (CVS) to be controlled via the basic sine wave source ( $V_{in2}$ ). This is necessary because Simscape blocks exchange energy when interacting with each other. For example, a port of a capacitor block consists of voltage and current variables. Energy can flow into the port or out of the port. In contrast, a Simulink connection is only a signal which has one direction.

A simulation with Simscape blocks can be started in the same way as with basic Simulink blocks, but differences exist in the underlying simulation principle. In a basic Simulink system, all connected blocks are simulated one after another. If for example an integrator is identified, the simulator only solves this single block using numerical integration to get the value of the next time step. Afterwards, the next block is executed. In contrast, the Simscape toolbox derives the algebraic differential equations automatically and then solves the whole model simultaneously. With this approach, algebraic loops, which slow down the simulation, are avoided. A big disadvantage of the direct solving method is the simulation time rise since large matrices have to be solved. Also of major importance is the usage of the appropriate solver settings. This topic will be explained in section 3.3.5 in more detail. [13]

Simscape also offers an object oriented modeling language to define custom components such as a MOS transistor model. This feature is very important for the activeTX model because the behavior of most of its parts cannot be modeled with the included simple toolbox components.

## 3.2 Coil Coupling Model

The coupling model between basestation and transponder coil is very important. When comparing model and lab setup, a deviation of the coupling factor must be eliminated to be able to focus only on the basestation and transponder behavior. Before presenting the coupling model, the reference coils are explained in the following section.

### 3.2.1 Reference Coils and Arrangements

The used reference coil on basestation side is shown in figure 3.2a. It is an air-coil with a non magnetic plastic body and copper windings. For reasons of clarity, the copper windings are drawn thicker and also only one winding layer is shown. Since the coil has more than ten layers, the given coil diameter of 33 millimeters is an average value which is measured from the middle of these layers.

On transponder side, a 3D ferrite coil, which is manufactured by an external company [21], is used. The coil is shown in figure 3.2b. Three independent orthogonally arranged coils are wound around a ferrite core. The axes are defined as the normal vectors of the spanned coil surface. For simplicity, again only a few windings are drawn, whereas the real coil has more than hundred. Also, the real coil is mounted on an SMD body to make it easy to integrate it on a PCB.

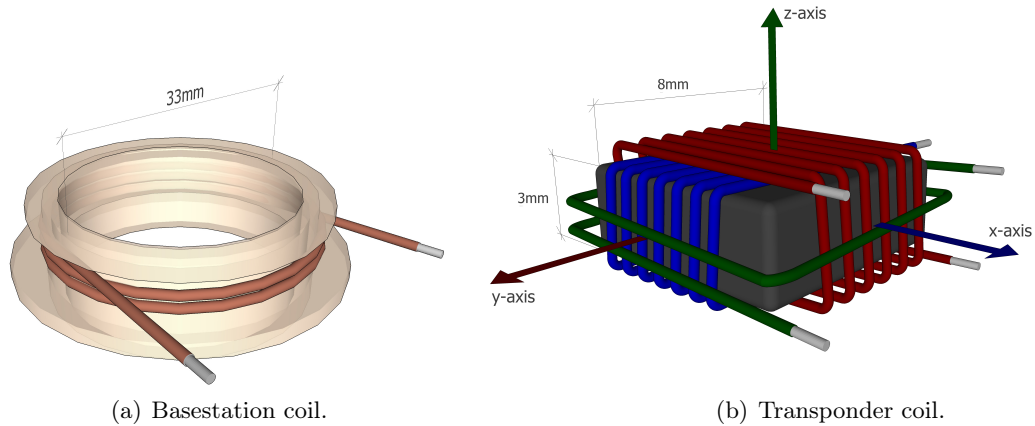


**Figure 3.2:** Reference coils.

Now that the coils are explained, two example arrangements, which explain the used notations in this Master’s Thesis, are defined. Since the transponder coil is a lot smaller than the basestation coil, the drawings are not true to scale. The shown arrangement in figure 3.3 is defined as *coaxial 1D z-axis arrangement*. Coaxial z-axis is used because the centers of the basestation and the green transponder z-coil are exactly aligned on the same rotational axis. The magnetic field lines are perpendicular to the x- and y-coil surfaces and thus, a voltage is only induced in the z-coil, what explains the 1D property.

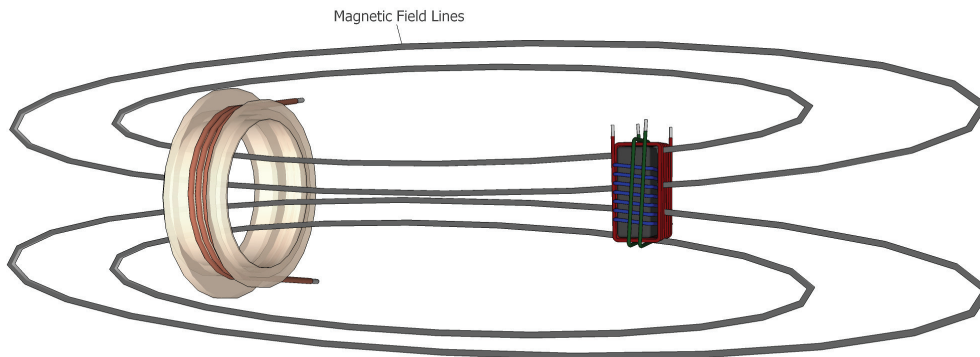


**Figure 3.3:** Coaxial 1D z-axis arrangement.

The *coplanar 3D arrangement* is drawn in figure 3.4. Again, the centers of the coils are aligned, but this time they are located on the same plane (coplanar). The 3D property is used because the transponder coil is arranged in an angle so that a voltage is induced in all three coils.

### 3.2.2 Inductive Coupling Theory

The coupling factor model requires some insights in the inductive coupling theory presented in this section. To be able to calculate the inductance values and coupling factors, in a first step, the generated magnetic field needs to be derived. Because the activeTX system uses 125 kHz as operating frequency, the near field condition is valid and thus, the quasi-stationary Maxwell equations can be applied. When the coil is located in a non conducting enclosed media, no

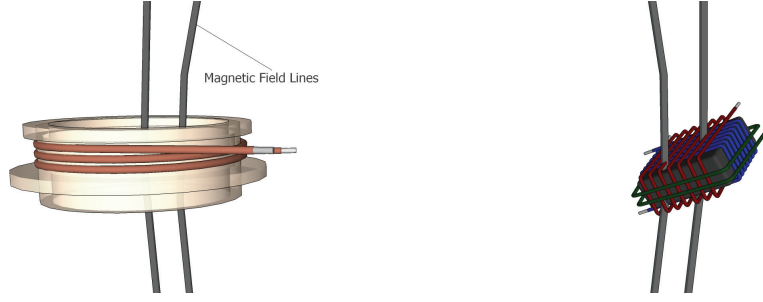


**Figure 3.4:** Coplanar 3D arrangement.

other components are present and the current is known, the emitted magnetic field can be calculated with the following stationary magnetic field formulas [2, p. 91]:

$$\begin{aligned}
 \text{curl } \vec{H} &= \vec{J} \\
 \text{div } \vec{B} &= 0 \\
 \vec{B} &= \mu \vec{H}
 \end{aligned}
 \tag{3.2}$$

The first equation is the Ampere's Law, the second specifies that the magnetic field is source free and equation three describes the material relationship between the magnetic flux density and the magnetic field. Because of equation two, the magnetic vector potential can be introduced as  $\vec{B} = \text{curl} \vec{A}$ . With this vector potential, the three equations can be solved. The result is the Biot Savart's Law specified in formula 3.3. [2, p. 87-90], [23, p. 342-343]

$$\vec{B}(\vec{r}) = \frac{\mu_0 I}{4\pi} \iiint_{\Omega} \vec{J}(\vec{r}') \times \frac{\vec{r} - \vec{r}'}{|\vec{r} - \vec{r}'|^3} d\Omega'
 \tag{3.3}$$

For simple geometries, the Biot Savart's Law can be used to derive closed analytical formulas for the magnetic field, but for most of the problems, it is easier to solve the integrals numerically. A useful analytical result can be obtained when calculating the magnetic field along the coaxial direction of a single loop coil with infinitesimal small wire cross section. The result is given in equation 3.4. [23, p. 353]

$$B_z(z) = \frac{\mu_0 I}{2} \frac{r^2}{(r^2 + z^2)^{\frac{3}{2}}}
 \tag{3.4}$$

$z$  – coaxial direction

$B_z$  – coaxial component of the magnetic field

$r$  – radius of the coil

Another important parameter is the magnetic flux. It is defined as the sum of all magnetic field lines which pass through a certain surface (formula 3.5). [7, p. 66]

$$\Phi = \iint_A \vec{B} \cdot \vec{n} \cdot dA \quad (3.5)$$

When a coil has more than one winding, the flux must be multiplied by the number of windings, what defines the linked flux ( $\Psi = N \cdot \Phi$ ). The self and mutual inductance are now derived using figure 3.5. Because a current is only injected into the left coil, while the right coil is opened, the self inductance ( $L$ ) can be defined as the quotient between the magnetic flux  $\Psi_1$  at the surface  $A_1$  and the current  $I_1$  [7, p. 67]:

$$L = \frac{\Psi_1}{I_1} \quad (3.6)$$

The mutual inductance ( $M_{21}$ ) is the quotient between the magnetic flux in the right coil ( $\Psi_2$ ) and the current in the left coil  $I_1$  [7, p. 67]:

$$M_{21} = \frac{\Psi_2}{I_1} \quad (3.7)$$

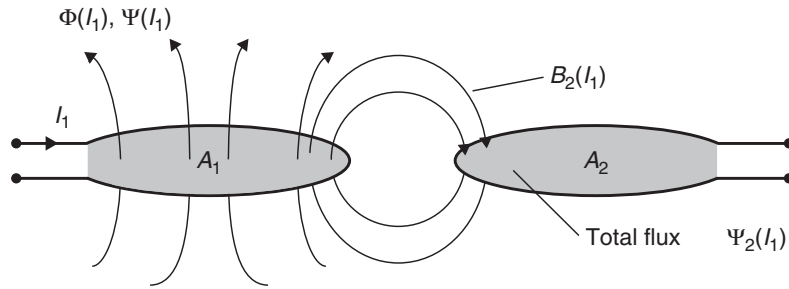


**Figure 3.5:** Basic diagram of coupled coils. [7, p. 67]

Because the system is linear, the mutual inductance remains the same when the current would be applied to coil 2 ( $M = M_{12} = M_{21}$ ). By using Biot Savart's Law, the inductances can then be calculated. Most of the models are represented with infinitesimal small wire cross sections. These models all have the problem that exactly at the conductor, the magnetic field is infinitely high and thus, only approximation formulas exist for the self inductance. This problem does not exist for calculating the mutual inductance if the current conducting wire is not enclosed by the surface of the second coil. [20, p. 357] [7, p. 67]

Since the mutual inductance is only a quantitative coupling description, it is useful to introduce the qualitative coupling factor defined in equation 3.8. This factor specifies the fraction of the emitted magnetic field lines which also pass through the second coil. The value varies

between zero and one, where zero means no coupling (i.e. the second coil is infinitely far away) and one means 100 % coupling (i.e. an ideal transformer).

$$k = \frac{M}{\sqrt{L_1 \cdot L_2}} \quad (3.8)$$

With all needed parameters defined, the circuit model shown in figure 3.6 is now introduced. Using the induction law, the following differential equations can be derived to describe the relationship between the two coils:

$$\begin{aligned} v_1 &= \frac{d\Psi_1}{dt} = L_1 \cdot \frac{di_1}{dt} + M \cdot \frac{di_2}{dt} = L_1 \cdot \frac{di_1}{dt} + k \cdot \sqrt{L_1 \cdot L_2} \cdot \frac{di_2}{dt} \\ v_2 &= \frac{d\Psi_2}{dt} = L_2 \cdot \frac{di_2}{dt} + M \cdot \frac{di_1}{dt} = L_2 \cdot \frac{di_2}{dt} + k \cdot \sqrt{L_1 \cdot L_2} \cdot \frac{di_1}{dt} \end{aligned} \quad (3.9)$$

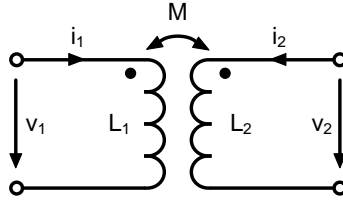


**Figure 3.6:** Circuit diagram of coupled coils.

### 3.2.3 Implemented Coupling Factor Model

#### Winding Calculation

To be able to calculate the coupling factor for different arrangements and distances between transponder and basestation, the geometries and windings of the coils need to be identified. While the geometries can be measured exactly with a sliding caliper, the windings cannot be determined directly. The chosen solution is kind of a back calculation, where the self inductance is measured with an impedance analyzer and then, an approximation formula is used to calculate the windings (N). As already stated in section 3.2.2, it is very difficult to derive exact analytical formulas for the inductance. Thus, a very accurate approximation formula for multilayer coils from [19] is used. The formula is given in equation 3.10 and the geometry parameter illustration is shown in figure 3.7.

$$\begin{aligned} S_1 &= \left(\frac{c}{2 \cdot a}\right)^2 \\ N &= \left[4 \cdot 10^{-7} \cdot \pi \cdot a \cdot L \cdot \left(\left(0.5 + \frac{S_1}{12}\right) \cdot \ln\left(\frac{8}{S_1}\right) - 0.84834 + 0.2041 \cdot S_1\right)\right]^{-\frac{1}{2}} \end{aligned} \quad (3.10)$$

Since the formula is only valid for low frequencies, it has to be proven that this requirement is given for the measured inductance. The equivalent circuit diagram of a coil is shown in

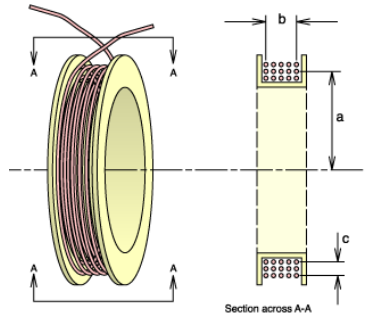


**Figure 3.7:** Parameter illustration for the inductance approximation formula. [19]

figure 3.8, where  $L$  is the inductance,  $R_s$  is the ohmic resistance of the windings and  $C_p$  is the capacity between the windings. It can be concluded that the coil behaves like a parallel resonance circuit. If the measured resonance frequency is much higher than the operating frequency and the inductance values at smaller frequencies are equal to those at the operating frequency, it is proven that the low frequency formula can be used. Measurements of all coils showed that this is the case. For example, the resonance frequency of the basestation coil is 1.3 MHz, which is more than a factor of ten higher than the operating frequency of 125 kHz.

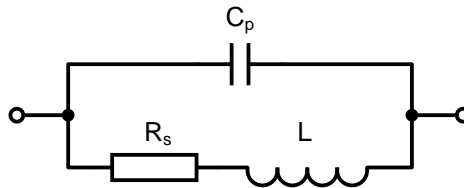


**Figure 3.8:** Coil equivalent circuit.

While the winding calculation formula can be directly applied to the basestation coil, some simplifications must be made for the transponder coil. All three axes of the transponder coil have a common ferrite core, which needs to be included into the formula. If the whole media would be made of ferrite material, the inductance could simply be multiplied with the relative permeability of the ferrite ( $\mu_r$ ). Since the ferrite is only in the middle of the coil and the remaining media is air, the inductance increase is much lower. The used approach is to directly apply formula 3.10, which results in a higher number of windings for the model compared to the real coil. This is valid because the winding value is only used for calculating the coupling factor and not needed anywhere else in the model. An additional requirement is a linear behavior of the ferrite material. Since the core has a very small hysteresis curve, this is true for the needed operating conditions. Another approximation has to be made because the formula requires a circular shaping and the transponder coils have a rectangular geometry. The simple solution is to calculate a circle area, which is equal to the rectangle area, and insert its radius into the formula. Table 3.1 contains the measured inductances and the corresponding calculated winding values.

### Magnetic Field Calculation

Now that all needed parameters are available, the emitted basestation magnetic field can be calculated. Formulas 3.11 from [8, p. 31] describe the magnetic field in free space using Biot

	Measured Inductance	Calculated Windings
Basestation Coil	366 $\mu$ H	80
Transponder Coil x-Axis	7.33 mH	5350
Transponder Coil y-Axis	7.02 mH	3900
Transponder Coil z-Axis	7.37 mH	847

**Table 3.1:** Inductance and winding values of the reference coils

Savart's Law in Cartesian coordinates. The equations are implemented in Matlab, where all integrals are solved numerically. The only simplification which has been made is that the windings of the basestation coil are located on the same position. This approximation is valid because the coil is very short. In exact coaxial and coplanar directions shown in figure 3.9, the magnetic field has only a z-component, while the x- and y-components are zero. These directions are very important for the activeTX model because the mechanical setup presented in section 4.1 is implemented for this configurations.

$$\begin{aligned}
B_{bs\_x}(x, y, z) &= \int_0^{2\pi} \frac{\mu_0 \cdot I_{bs} \cdot N_{bs} \cdot r_{bs} \cdot (-z) \cdot \cos(\phi)}{4\pi \cdot \left[ (r_{bs} \cdot \cos(\phi) - x)^2 + (r_{bs} \cdot \cos(\phi) - y)^2 + (-z)^2 \right]^{\frac{3}{2}}} d\phi \\
B_{bs\_y}(x, y, z) &= \int_0^{2\pi} \frac{\mu_0 \cdot I_{bs} \cdot N_{bs} \cdot r_{bs} \cdot (-z) \cdot \sin(\phi)}{4\pi \cdot \left[ (r_{bs} \cdot \cos(\phi) - x)^2 + (r_{bs} \cdot \cos(\phi) - y)^2 + (-z)^2 \right]^{\frac{3}{2}}} d\phi \quad (3.11) \\
B_{bs\_z}(x, y, z) &= \int_0^{2\pi} \frac{\mu_0 \cdot I_{bs} \cdot N_{bs} \cdot r_{bs} \cdot [r_{bs} - x \cdot \cos(\phi) - y \cdot \sin(\phi)]}{4\pi \cdot \left[ (r_{bs} \cdot \cos(\phi) - x)^2 + (r_{bs} \cdot \cos(\phi) - y)^2 + (-z)^2 \right]^{\frac{3}{2}}} d\phi
\end{aligned}$$

- $\mu_0$  – vacuum permeability
- $I_{bs}$  – basestation current
- $N_{bs}$  – windings of basestation coil
- $r_{bs}$  – radius of basestation coil

The RMS z-component value of the emitted basestation magnetic field, along the coaxial direction, is shown in figure 3.10. A current with 1 A amplitude is used. As can be seen, the field is approximately constant if the distance is smaller than one centimeter. For distances much greater than the coil radius, the field drops with 60dB per decade.

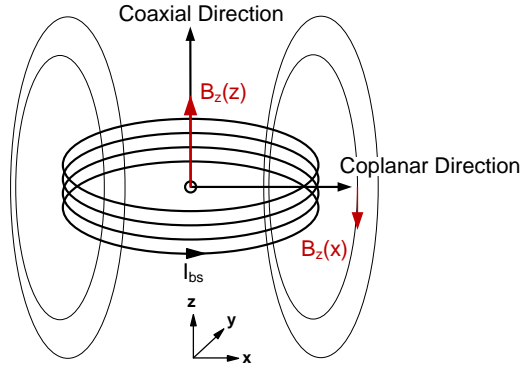


**Figure 3.9:** Basestation magnetic field z-component in coaxial and coplanar direction.

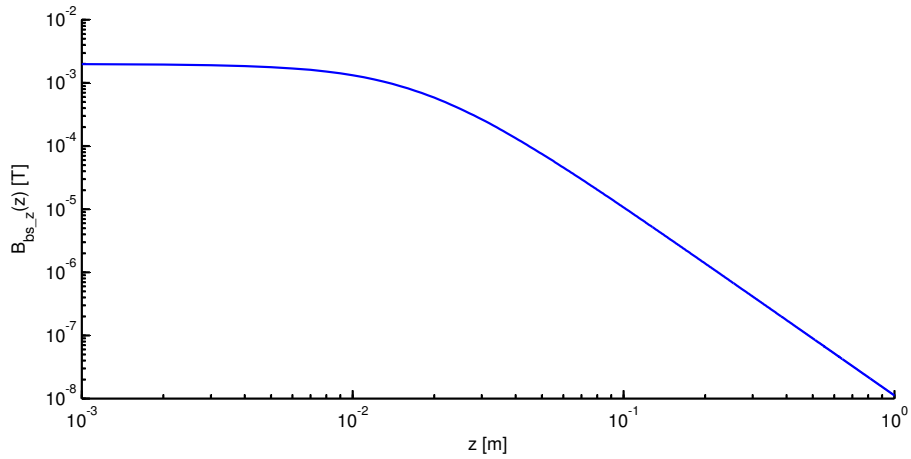


**Figure 3.10:** RMS z-component of the emitted basestation magnetic field in coaxial direction with  $I_{bs} = 1$  A<sub>pk</sub>.

### Coupling Factor Calculation

Before the full coupling factor model can be presented, the coil misalignment angle needs to be defined. It is the angle ( $\alpha$ ) between the two coil's surface normal vectors as illustrated in figure 3.11.

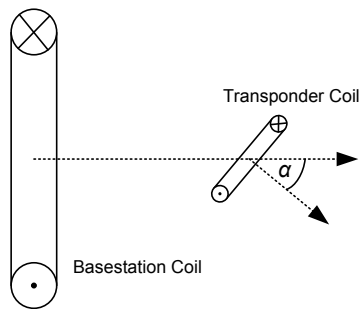


**Figure 3.11:** Misalignment angle between transponder and basestation coil.

The following simplifications are used for the coupling factor calculation:

1. The allowed transponder directions are only exactly coaxial and coplanar, resulting in an emitted basestation field with just a z-component (referred to the the basestation system of coordinates shown in figure 3.9). This constraint is valid because the mechanical setup is implemented only for these directions.
2. The magnetic field, which passes through the transponder coil, is homogenous. This approximation is valid because the transponder coil dimensions are small enough so that the variation of the basestation field in the transponder coil surface can be neglected.
3. The windings of the transponder coil are assumed to be exactly at the same position and the wire cross section is infinitesimal small. This was also already assumed for the basestation coil.

With the knowledge of the coupling theory in section 3.2.2, equations 3.12 can now be derived. The advantage of the above specified simplifications is that the integrals can be replaced by simple multiplications. If the transponder coil is misaligned with the angle  $\alpha$ , only the basestation field component, which is perpendicular to the transponder coil surface, contributes to the magnetic flux. This can be modeled with the misalignment factor  $\cos(\alpha)$ .

$$M(d) = \frac{\Psi_{trp}}{I_{bs}} = \frac{N_{trp} \cdot B_{bs\_z}(d) \cdot A_{trp}}{I_{bs}} \cdot \cos(\alpha) \tag{3.12}$$

$$k(d) = \frac{M(z)}{\sqrt{L_{trp} \cdot L_{bs}}} = \frac{N_{trp} \cdot B_{bs\_z}(d) \cdot A_{trp}}{I_{bs} \cdot \sqrt{L_{trp} \cdot L_{bs}}} \cdot \cos(\alpha)$$

- $d$  – distance between basestation and transponder coil
- $M$  – mutual inductance
- $k$  – coupling factor
- $\alpha$  – coil misalignment angle
- $I_{bs}$  – basestation current
- $B_{bs\_z}$  – z-component of emitted basestation field
- $L_{bs}$  – measured basestation coil self inductance
- $\Psi_{trp}$  – magnetic flux at transponder coil
- $L_{trp}$  – measured transponder coil self inductance
- $N_{trp}$  – number of transponder coil windings
- $A_{trp}$  – transponder coil surface

Since the transponder coil has three axes, equations 3.12 must be applied for each of them. Due to the orthogonally arranged axes, the additional condition for the misalignment factors in equation 3.13 must be satisfied.

$$\cos^2(\alpha) + \cos^2(\beta) + \cos^2(\gamma) = 1 \tag{3.13}$$

- $\alpha$  – misalignment angle of transponder coil x-axis
- $\beta$  – misalignment angle of transponder coil y-axis
- $\gamma$  – misalignment angle of transponder coil z-axis

The equation can be derived using a 2-D vector interpretation of the transponder coil. Figure 3.12a shows the basestation magnetic field vector and two coil axes, while figure 3.12b illustrates the real coil for this configuration. At the beginning, the third axis is not included because the result of the derivation can be generalized for the 3-D case. If the basestation vector is assumed to have a length of 1, the components, which contribute to the magnetic flux on the x- and y-axis, are  $\cos(\alpha)$  and  $\cos(\beta)$ . From the Pythagoras Law, it can be stated that the length of the magnetic field vector is:  $1^2 = \cos^2(\alpha) + \cos^2(\beta)$ . This statement can now be generalized for the third axis, resulting in equation 3.13.

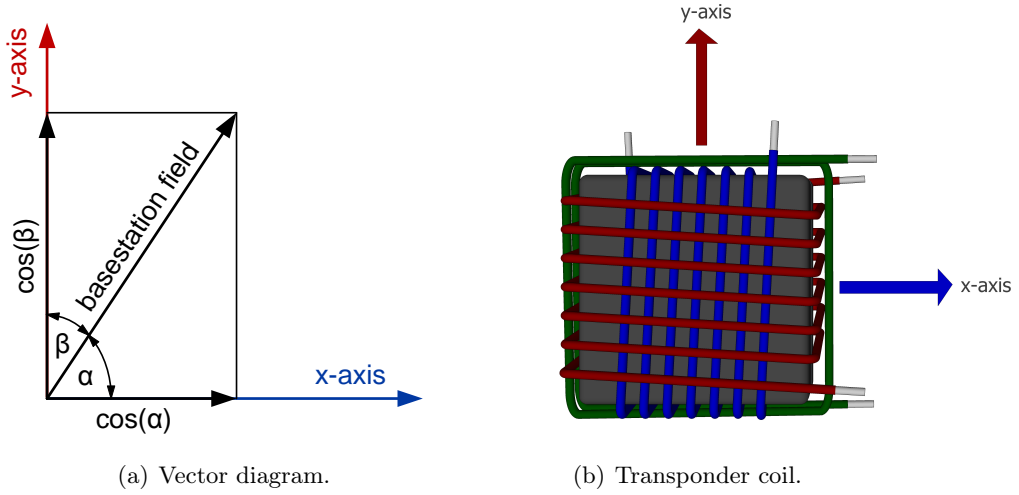


**Figure 3.12:** Vector interpretation for the derivation of equation 3.13.

An interesting misalignment orientation is when  $\alpha = \beta = \gamma$ , which represents the worst case for the induced transponder coil voltages. Thus, it is also very important for the harvested transponder energy. By rearranging formula 3.13, the resulting angles are:

$$\alpha = \beta = \gamma = \arccos\left(\frac{1}{\sqrt{3}}\right) \approx 54.74^\circ \quad (3.14)$$

This angle will later play an important role for the construction of the mechanical setup.

As an example, the calculated coupling factor for the coaxial 1D z-axis arrangement is shown in figure 3.13.  $d$  is defined as the distance between the centers of the coils in meter. The k-factor has a maximum of 13% at zero distance and behaves like the magnetic field shown in figure 3.10.

Because the above presented model is derived using magnetic field theory, it is now possible to calculate the coupling factors for coils with different geometries (i.e. a larger basestation coil radius). This would not be possible if the factors were only measured and then stored in a lookup table.

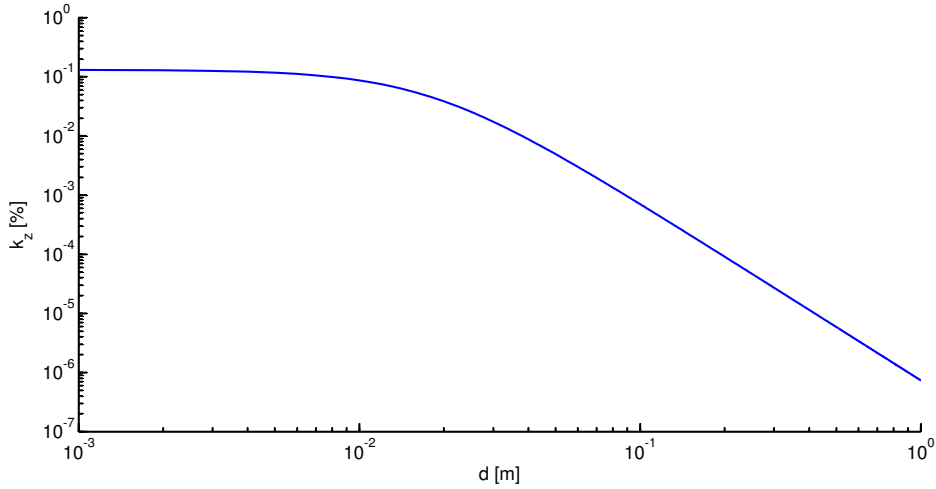


**Figure 3.13:** k-factor plot of the coaxial 1D z-axis arrangement.

### 3.2.4 Coupling Factor Measurement

The validation of the coupling factor model is done with the measurement setup shown in figure 3.14. A basestation is programmed to output a 125 kHz constant carrier. It is connected to a tuned resonance circuit consisting of basestation coil and capacitor. Because the used basestation current ( $I_{bs}$ ) has an amplitude of more than 0.5 A, it can be measured accurately with a current probe. The transponder coil is measured open loop to guarantee that the flowing current is as small as possible and thus cannot reduce the emitted basestation field. A differential measurement is required because a parasitic voltage is induced in the probes. This would introduce an error in a single ended measurement. Since the parasitic voltages appear as common mode signals, they are canceled out in the differential case. The drawn probe impedances on transponder side are already converted from single-ended to differential, resulting in a doubled resistor and half capacitor value.

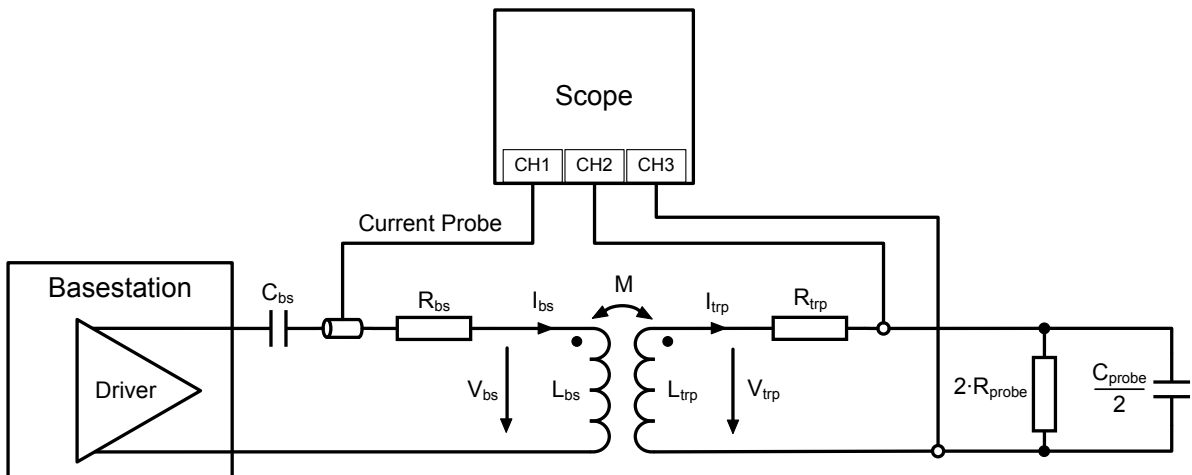


**Figure 3.14:** Block diagram of the k-factor measurement setup.

To derive a simple coupling factor formula from the measured values, the following simplifications are made:

1. For the used operating frequency of 125 kHz, the transponder winding resistance ( $R_{trp}$ ) is much smaller than the inductive reactance ( $\omega L_{trp}$ ) of the coil. Thus,  $R_{trp}$  is neglected.
2. The differential probe resistance ( $2 \cdot R_{probe}$ ) is much larger than the differential capacitive reactance ( $\frac{2}{\omega C_{probe}}$ ). It follows that  $2 \cdot R_{probe}$  can be neglected.

Since all voltages and currents are harmonic, the final coupling factor formula given in equation 3.15 can be determined using AC calculations.

$$k(d) = \frac{V_{trp}(d)}{I_{bs}(d)} \cdot \left( \frac{2 - \omega^2 \cdot L_{trp} \cdot C_{probe}}{2 \cdot \omega \cdot \sqrt{L_{trp} \cdot L_{bs}}} \right) \quad (3.15)$$

- $d$  – distance between basestation and transponder coil
- $k$  – coupling factor
- $V_{trp}$  – measured transponder coil voltage
- $I_{bs}$  – measured basestation current
- $L_{bs}$  – measured basestation coil self inductance
- $L_{trp}$  – measured transponder coil self inductance
- $C_{probe}$  – capacitance of scope probes

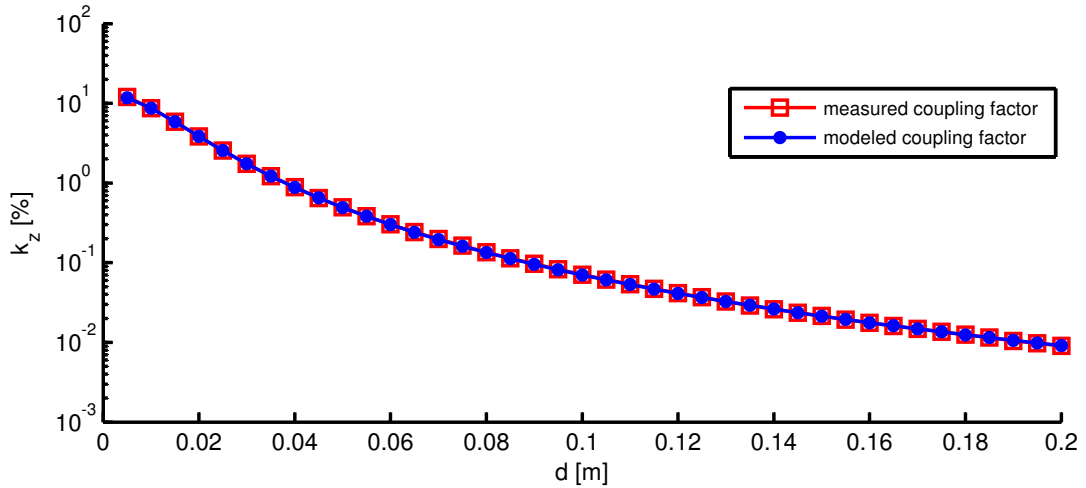


**Figure 3.15:** Coupling factor comparison between measurement and model.

The comparison between measurement and model for the 1D z-axis arrangement is shown in figure 3.15 (please refer to appendix A for the corresponding values). As can be seen, the required accuracy for the coupling factor model is given. A calculation of the relative error shows that it is 3% at a distance of 5 mm. For distances larger than 100 mm it is smaller than 1%. The greater difference at 5 mm can be explained by the simplification of a homogeneous basestation field, which is not exactly valid for small distances.

### 3.3 ActiveTX Model

Although a lab setup is implemented in this Master's Thesis, it is very important to have a solid model which allows a simulation of parameters that cannot easily be tested in the lab. An example would be a different operating frequency or larger basestation currents, for which no real IC with sufficient current capability is available.

The focus of the activeTX model is on transponder energy consumption and active transponder response. Questions, which should be explained are:

- How large is the transponder operating distance for a certain basestation current?
- Is the actively sent transponder response signal large enough to be recognized by the basestation receiver?
- How long are the optimum charging times to ensure a good trade off between protocol duration and operating distance?

It can be imagined from these questions that many different parameters have to be modeled. To cope with this large parameter set, an approach is chosen, in which a clear parameter list is defined in a Matlab script. After some preprocessing, these parameters are handed over to the Simulink Simscape model.

Because some blocks from the old load modulation transponder and basestation can be reused for the new activeTX ICs, the first task is to identify those parts. This is done by reading through all necessary design reports and analog schematics from newer versions of the transponder and basestation presented in sections 2.1.4 and 2.1.5. The behavior of these parts is then described in a simpler way with Simscape models.

An overview of the Simulink model is shown in figure 3.16. The system consists of a tuned 3D-coil, which models the coupling between basestation and transponder. Since the main focus is on transponder side, the basestation IC is modeled only as simple voltage driver.

The transponder IC consists of three input channels, which all have independent *Rectifier & Limiter*, *Active Transmitter* and *Demodulator* parts. The outputs of the rectifier and limiter blocks are interconnected to a small decoupling capacitance  $C_{fd}$ . A *Preswitch* is used to connect the large external support capacitor  $C_{Vddc}$  with  $C_{fd}$ . After the *Counter* detects a 2ms constant carrier, this switch is closed, which also signalizes the IC that it is now in immobilizer mode. Since the support capacitor  $C_{Vddc}$  stores the energy for supplying the IC, it is one of the most important transponder parts.

The analog part of the real transponder IC can be divided into Frontend and Powermanagement. Each of these blocks has a corresponding current consumption model (*Analog Frontend Current Consumption* and *Analog Powermanagement Current Consumption*). The *Power On Reset Detection* senses the supply voltage at  $C_{Vddc}$  and checks if the voltage is large enough for supplying the microcontroller. After the voltage rises above this power on reset threshold, the *Digital Current Consumption* block is informed that it now has to model the current consumption of all digital blocks, including also the microcontroller states (i.e. booting or idle mode).

It can be seen from this explanation that the whole model is kind of a simplified analog representation of the real activeTX system. All signals, voltages and currents of the model can be simulated. The most important signals, which are necessary to decide if the simulated system would work for a certain parameter set, are explained in section 3.3.4.

Sections 3.3.1 - 3.3.3 follow with a description of important parts of the Simulink model. In section 3.3.4, the top level model, which is responsible for starting and parametrizing the simulation, is explained.

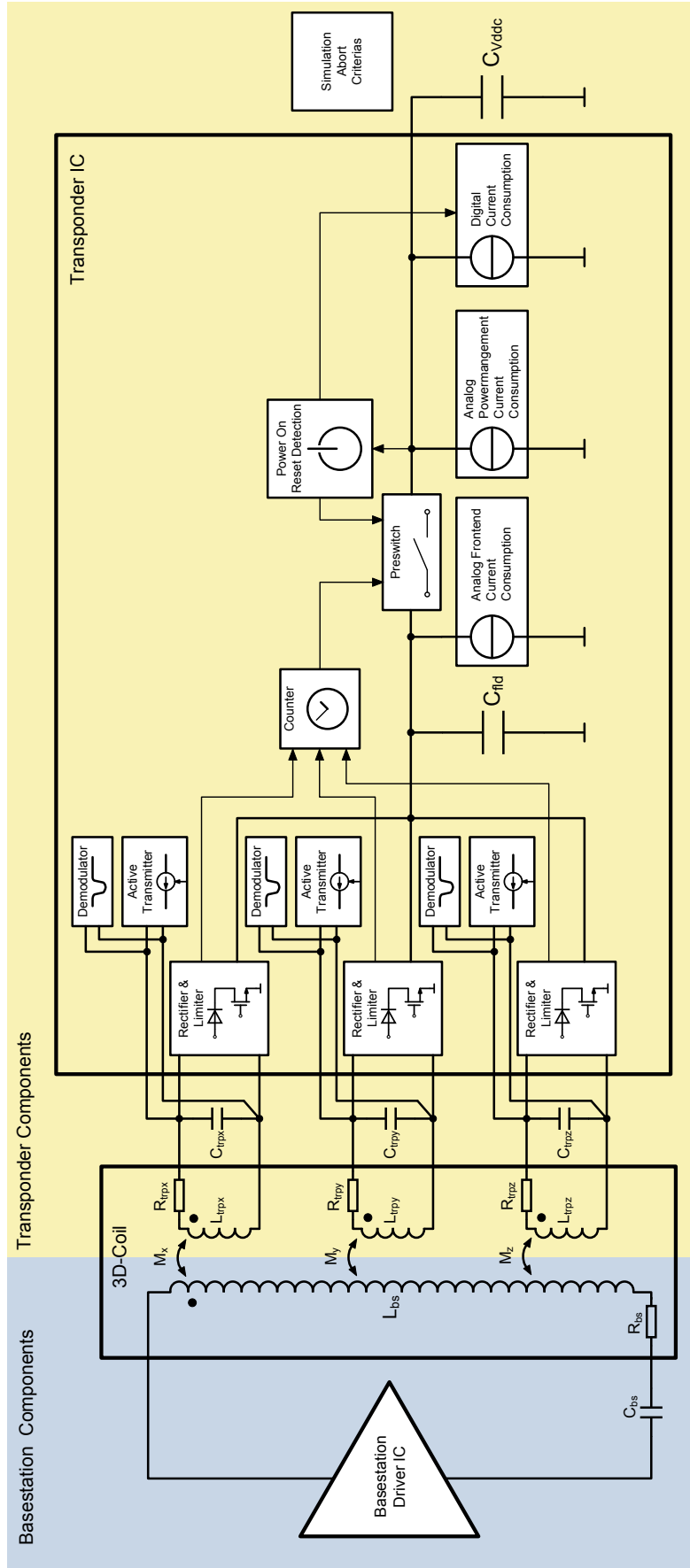


Figure 3.16: Overview of the activeTX Simulink model

### 3.3.1 3D-Coil Simulink Model

The 3D-coil Simulink Simscape model consists of a 3D mutual inductance with the corresponding winding resistances as shown in figure 3.17.

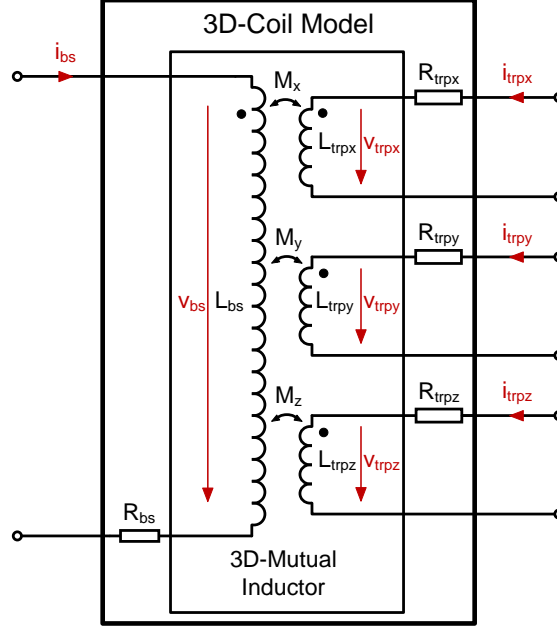


Figure 3.17: 3D-coil Simulink model.

Formula 3.16 describes the implemented differential equation system for the *3D-Mutual Inductor* model.  $k_x$ ,  $k_y$  and  $k_z$  are the coupling factors determined by the coupling model from section 3.2.3. Because the transponder windings are not exactly oriented orthogonally, there exists also a small parasitic coupling between the three coils. This is modeled with the factors  $k_{xy}$ ,  $k_{xz}$ , and  $k_{yz}$ .

$$\begin{bmatrix} v_{bs} \\ v_{trpx} \\ v_{trpy} \\ v_{trpz} \end{bmatrix} = \begin{bmatrix} L_{bs} & k_x \sqrt{L_{bs} \cdot L_{trpx}} & k_y \sqrt{L_{bs} \cdot L_{trpy}} & k_z \sqrt{L_{bs} \cdot L_{trpz}} \\ k_x \sqrt{L_{bs} \cdot L_{trpx}} & L_{trpx} & k_{xy} \sqrt{L_x \cdot L_y} & k_{xz} \sqrt{L_x \cdot L_z} \\ k_y \sqrt{L_{bs} \cdot L_{trpy}} & k_{xy} \sqrt{L_x \cdot L_y} & L_{trpy} & k_{yz} \sqrt{L_y \cdot L_z} \\ k_z \sqrt{L_{bs} \cdot L_{trpz}} & k_{xz} \sqrt{L_x \cdot L_z} & k_{yz} \sqrt{L_y \cdot L_z} & L_{trpz} \end{bmatrix} \cdot \begin{bmatrix} \frac{di_{bs}}{dt} \\ \frac{di_{trpx}}{dt} \\ \frac{di_{trpy}}{dt} \\ \frac{di_{trpz}}{dt} \end{bmatrix} \quad (3.16)$$

### 3.3.2 Basestation Simulink Model

The basestation model (see figure 3.18) is very simple, consisting only of a controlled voltage source (CVS), a basestation coil, a series resistance and a tuning capacitor. CVS represents the driver. It is controlled by a signal (*bs\_driver\_voltage*), which has to be defined in the already mentioned Matlab top level script.

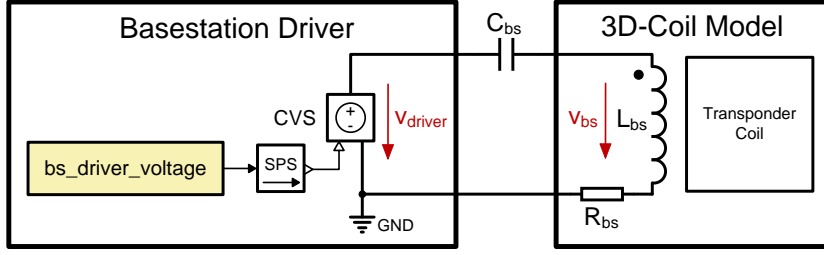


**Figure 3.18:** Basestation Simulink model.

Figure 3.19 shows a simulation output of the driver and basestation coil voltages when no transponder is present (i.e. all coupling factors are zero). What can be seen, is an example signal, consisting of a constant carrier followed by a special variant of a PPC communication sequence. The PPC principle is called Binary Pulselength Modulation (BPLM). [18, p. 43] A long pulse represents a logic one and a short pulse represents a logic zero. The used simulation settings are defined in table 3.2. Because the resonance circuit is exactly tuned to the driver carrier, these values result in a resonance increase of a factor of 10 (circuit Q factor = 10).

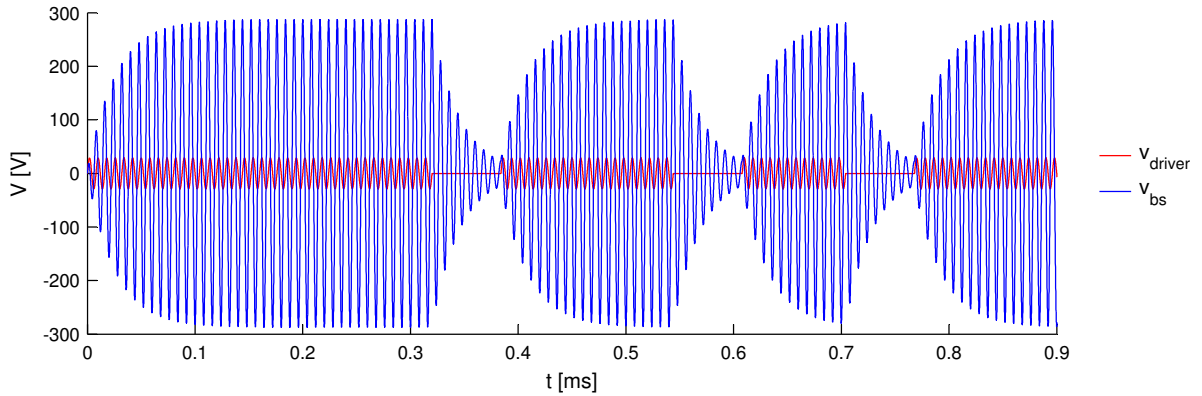


**Figure 3.19:** Simulated basestation driver and coil voltages for the component values defined in table 3.2.

Setting	Value	Setting	Value
$f_{\text{carrier}}$	125 kHz	$C_{\text{bs}}$	4.43 nF
$V_{\text{driver\_pk}}$	28.75 V	$R_{\text{bs}}$	28.75 $\Omega$
$L_{\text{bs}}$	366 $\mu\text{H}$		

**Table 3.2:** Settings for the simulation output in figure 3.19

### 3.3.3 Transponder Simulink Model

This section contains a description of important transponder model blocks. For reasons of clearness, it is necessary to describe each part isolated from the rest of the model. The behavior of the complete model is illustrated in an example simulation output in section 3.4.

## Rectifier and Limiter

The rectifier is necessary to generate a DC voltage for supplying the transponder. If the transponder is located very close to the basestation (i.e. 1 cm), the large coupling factor will lead to a theoretical coil voltage of more than hundreds of volts. This high voltage of course destroys either the coil, the tuning capacitor or the IC. To overcome this problem, a limiter, which regulates the coil and internal supply voltage to a sufficiently low value, is required. Each of the three transponder channels has a separate rectifier and limiter block. Figure 3.20 shows the Simulink model.

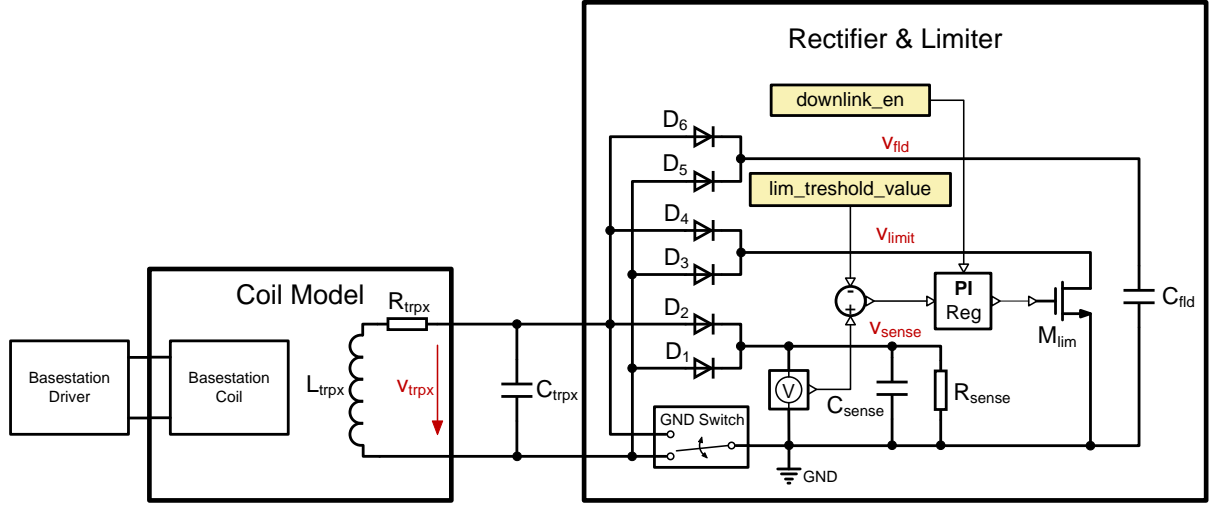


**Figure 3.20:** Rectifier & Limiter Simulink model.

The description of the internal model parts is listed below:

- **Diodes  $D_1 - D_6$ :** The diodes are implemented as piecewise linear model. Pseudocode:

$$\text{if } V_d < V_f \text{ then } I_d = 0$$

$$\text{else } I_d = \frac{V_d - V_f}{R_d}$$

- **NMOS Transistor  $M_{lim}$ :** The square law MOS transistor model from [22, p. 17] is implemented.
- **GND Switch:** The switch simply shorts the input with the lower potential to ground. Pseudocode:

$$\text{if } V_{in1} < V_{in2} \text{ then } V_{in1} = GND$$

$$\text{else } V_{in2} = GND$$

- **PI Regulator:** This block is implemented as anti-windup PI regulator with an additional hold function. The hold function is necessary to prevent the limiter from degrading the modulation depth of a BPLM downlink communication. This block is very

complex and thus, no simple pseudocode example can be given. The behavior will be explained later with the aid of simulation outputs.

The whole rectifier block consists of three independent full wave rectifiers, built up with diodes and a GND switch. The GND switch replaces the two back path diodes and has no voltage drop. This makes the rectifier more efficient. The  $v_{\text{fld}}$  net is connected to a decoupling capacitor ( $C_{\text{fld}}$ ) and is used as DC supply for the transponder. The two nets  $v_{\text{sense}}$  and  $v_{\text{limit}}$  are necessary for the limiter function.  $v_{\text{sense}}$  is a DC replica of the coil voltage.  $v_{\text{limit}}$  is used for drawing current out of the coil to degrade the Q factor of the resonance circuit. As a result,  $v_{\text{trpx}}$  and  $v_{\text{fld}}$  can be decreased dramatically. The limiter feedback loop senses the voltage at  $v_{\text{sense}}$  and compares it with the desired control input  $\text{lim\_thresh\_value}$  (i.e. 5 V). If  $v_{\text{sense}}$  is larger than the control input, the gate voltage of the NMOS transistor  $M_1$  rises. This leads to an increasing drain current. With the PI regulator, the closed feedback loop now regulates  $v_{\text{sense}}$  exactly to the given  $\text{lim\_thresh\_value}$ .

The necessity of the limiter can be demonstrated very clearly with the simulation output in figure 3.21. Again, the values listed in table 3.2 are used for the simulation. The transponder coil settings are shown in table 3.3. A distance of 2 cm between transponder and basestation coil for a coaxial 1D x-axis arrangement is simulated. In the top figure, it can be seen how large the transponder voltages would get without using a limiter. In a real system such a voltage destroys the coil and transponder immediately. The bottom figure shows the voltages with a properly operating limiter.

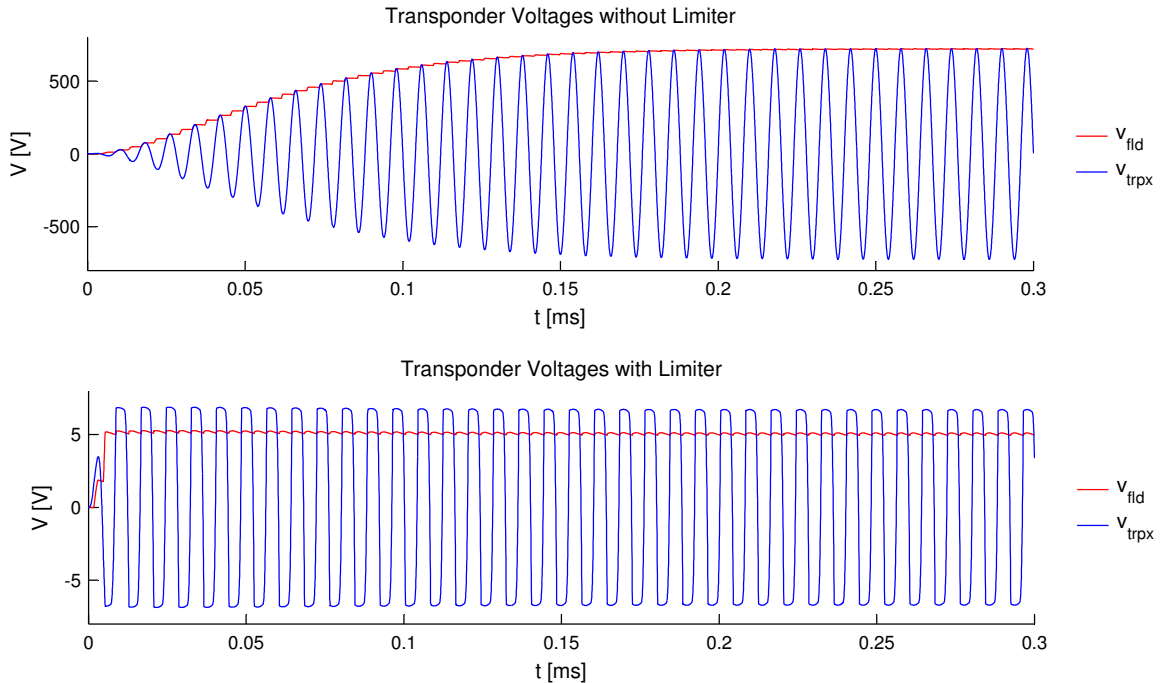


**Figure 3.21:** Simulation output comparison for a transponder with and without limiter.

The limiter also has an included hold function, which freezes the output of the PI regulator if the  $\text{downlink\_en}$  signal is one. This function is necessary because the limiter would decrease the gate voltage during the modulation pauses of a basestation sent BPLM telegram. As a

Setting	Value	Setting	Value
$k_x$	4.4 %	$C_{\text{trpx}}$	221 pF
$L_{\text{trpx}}$	7.3 mH	$R_{\text{trpx}}$	327 $\Omega$

**Table 3.3:** Settings for the simulation output in figure 3.21

result, the transponder would only see a constant carrier. The *downlink\_en* signal ensures that  $M_{\text{lim}}$  reduces the Q factor also during modulation pauses. A comparison of the transponder coil voltages, with and without the freezing function enabled, is shown in figure 3.22. The same basestation signal as in figure 3.19 is transmitted to the transponder. In the top plot, the transponder demodulator sees only a constant carrier, while the BPLM modulation pauses in the bottom plot are strong enough to ensure a valid demodulation.

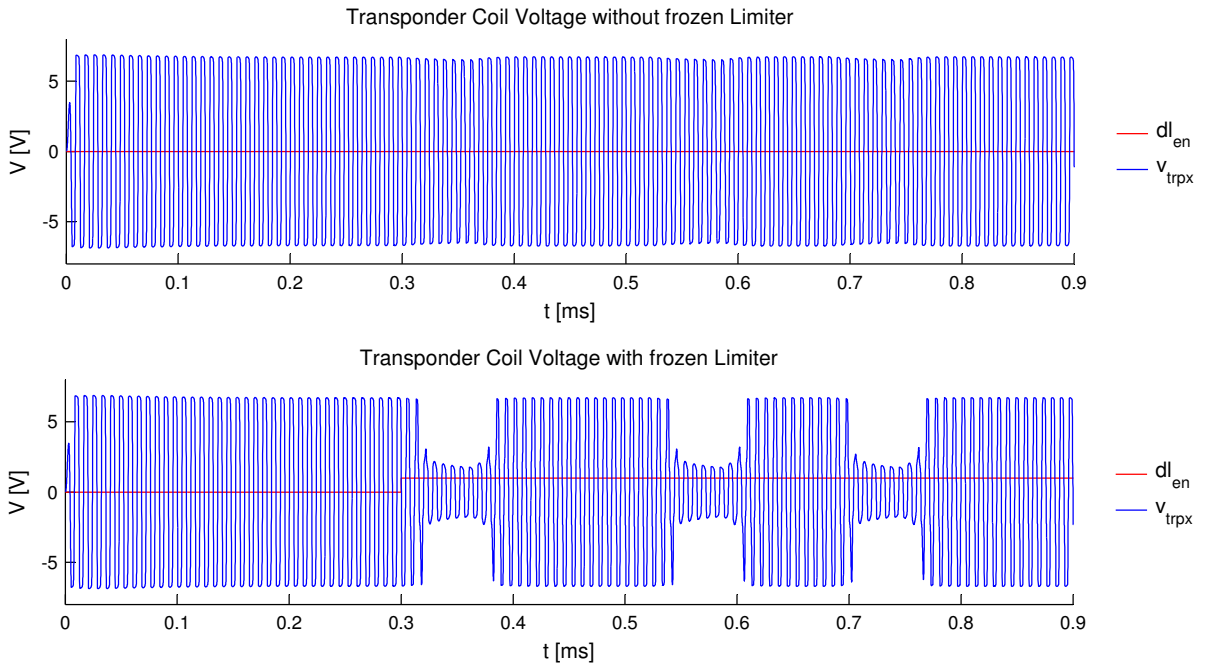


**Figure 3.22:** Simulation output comparison for a transponder with and without frozen limiter enabled.

### Active Transmitter

The active transmitter is responsible for the transponder uplink communication. During this communication, the basestation driver is always turned off. The model is shown in figure 3.23. A controlled current source drives a rectangular BPSK modulation current into the coil. The control signal *trp\_uplink\_current* is generated in the Matlab top level script. Because of the large Q factor, a sinusoidal current appears in the transponder coil. Energy for the current source is directly provided by the support capacitor  $C_{\text{Vddc}}$ . The Correction Factor models non-idealities, which can occur in a real system.

A simulation output of a transmitted BPSK sequence is shown in figure 3.24. The top plot contains the desired baseband signal and the corresponding modulation current. A phase

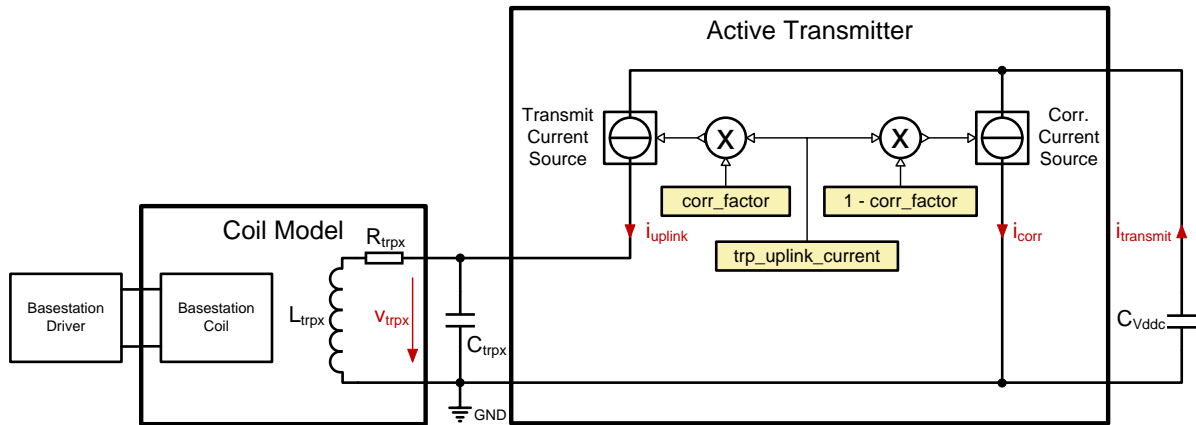


Figure 3.23: Active Transmitter Simulink model.

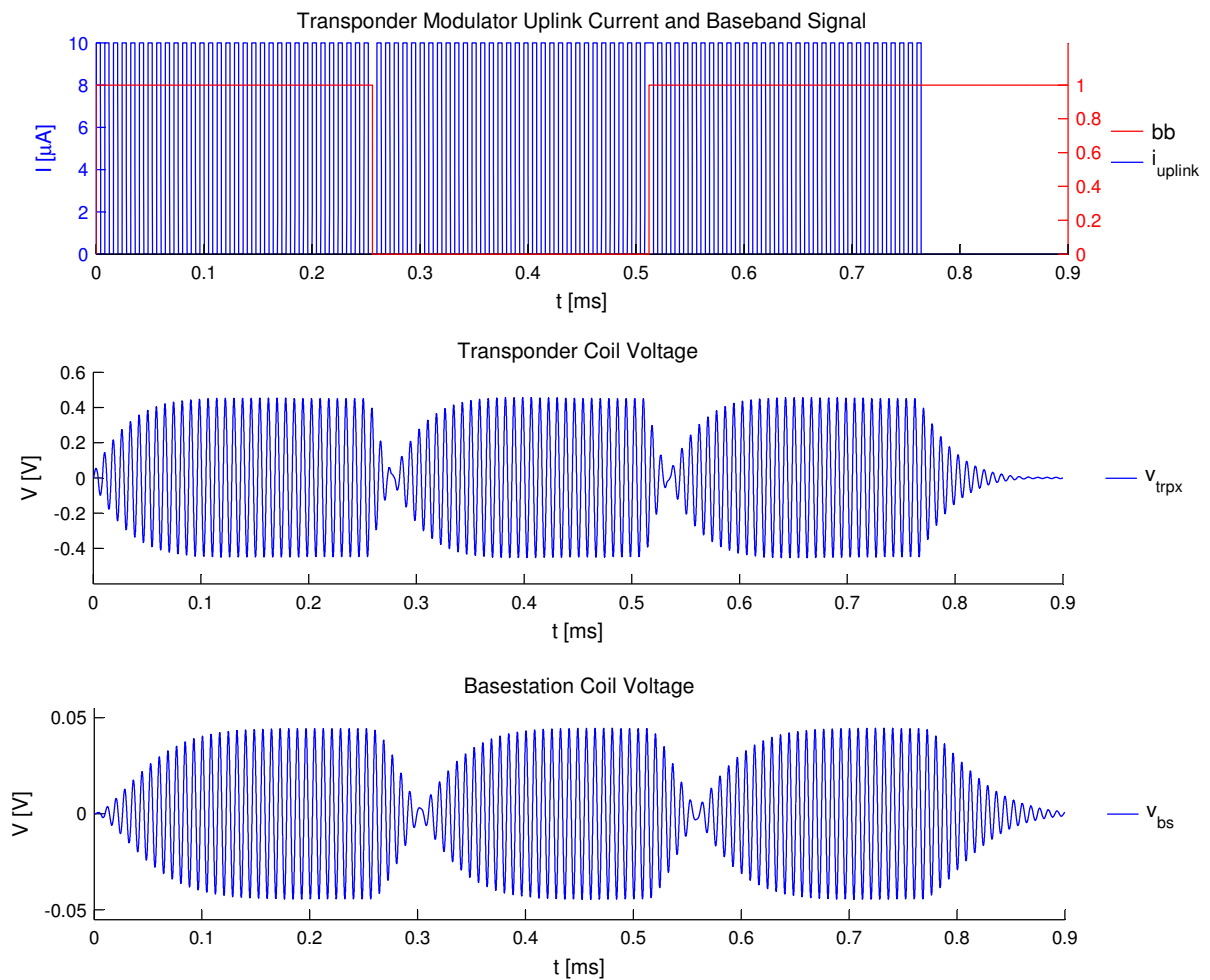


Figure 3.24: Simulation output of a transponder transmitted BPSK sequence.

change is accomplished by changing the phase of the rectangular uplink current carrier. The second plot shows the voltage at the transponder coil and the bottom plot contains the signal

received at the basestation coil for a coupling factor of 4.4%. Due to the Q factors of the coils, no sharp phase change is possible. The phase needs approximately ten carrier cycles to settle to the desired value.

## Demodulator

This block is responsible for demodulating the basestation sent BPLM signal. A discrete square law demodulator with comparator output is implemented (figure 3.25). The basic idea is taken from [12]. The following equations derive the functional principle of how the baseband signal  $m(t)$  is obtained from the modulated signal  $m(t) \cdot \cos(\omega t)$ :

$$mod\_sig = m(t) \cdot \cos(\omega t) \quad (3.17)$$

square the signal,

$$\Rightarrow (m(t) \cdot \cos(\omega t))^2 \quad (3.18)$$

with using trigonometric formulas it follows,

$$= \frac{1}{2}m(t)^2 \cdot (\cos(0) + \cos(2\omega t)) = \frac{1}{2}m(t)^2 \cdot (1 + \cos(2\omega t)) \quad (3.19)$$

next the signal is applied to a sharp low pass filter,

$$\Rightarrow \frac{1}{2}m(t)^2 \quad (3.20)$$

a division by 2 and subsequent squaring produces the baseband signal,

$$bb\_sig = m(t) \quad (3.21)$$

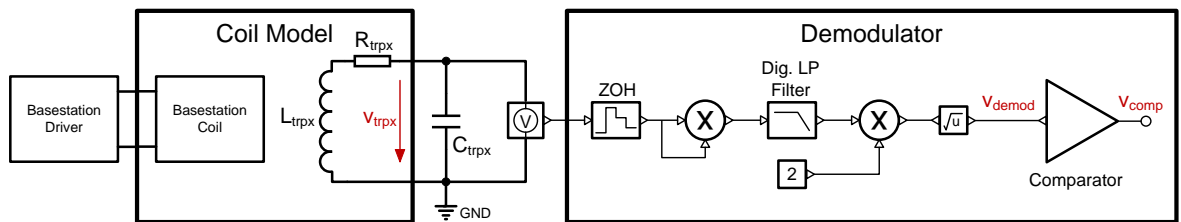


**Figure 3.25:** Demodulator Simulink model.

The demodulator contains only basic Simulink blocks and is implemented discrete to increase the simulation speed. A comparator is used to introduce steep edges, which are necessary for the post processing checks. Figure 3.26 shows a simulation output of the demodulator function. The top plot contains the transponder coil voltage and the bottom plot the demodulated baseband signal and comparator output.

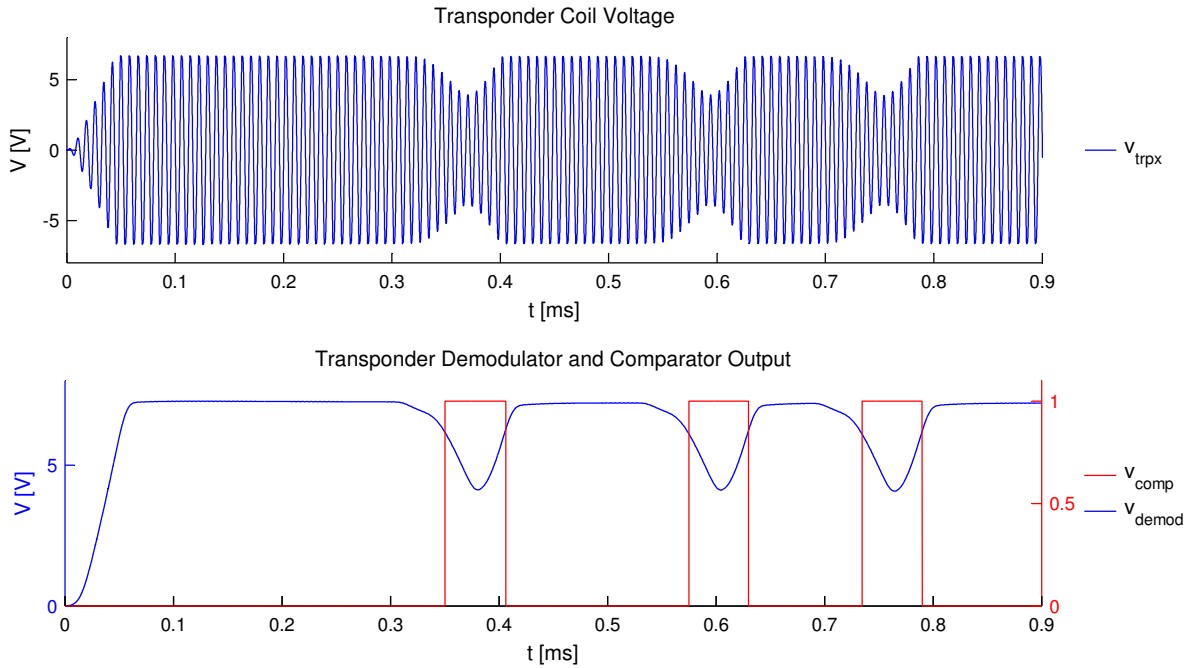


**Figure 3.26:** Simulation output of the transponder demodulation function.

### Counter, POR Detection and Preswitch

These three blocks are necessary for connecting the decoupling capacitor  $C_{\text{fld}}$  with the support capacitor  $C_{\text{Vddc}}$ . For their interconnection, please refer to the model overview in figure 3.16.

The counter is responsible for signaling the preswitch that a constant carrier with sufficient amplitude is available for a specific time (i.e. 2 ms). This time is necessary for the real IC to recognize that the used protocol is intended for an immobilizer communication and not for a Passive Keyless Entry communication. The voltage at  $C_{\text{fld}}$  supplies the analog frontend. If the preswitch would be closed with zero impedance, the small  $C_{\text{fld}}$  capacitor would be shorted with the large  $C_{\text{Vddc}}$  capacitor. As a result, the supply drops to almost zero voltage. To prevent this behavior, the preswitch goes into a soft closing mode after receiving the counter high signal. This means that it is closed with a large series impedance so that the  $C_{\text{fld}}$  voltage remains at a sufficient level while  $C_{\text{Vddc}}$  is loaded.

When the voltage level at  $C_{\text{Vddc}}$  is large enough, the power on reset detection (POR) signals the preswitch to go into a hard closing mode, which means that now  $C_{\text{fld}}$  and  $C_{\text{Vddc}}$  are shorted. From this time on, the support capacitor is directly connected to the rectifier.

The preswitch is modeled as PMOS transistor. Depending on whether the counter signal or the POR detection signal is high, the gate voltage is set to different values. The counter is modeled as simple integrator, which counts the time as long as the  $v_{\text{sense}}$  voltage from the limiter is larger than a specific value. The POR detection is implemented as comparator that switches to high state when the voltage at  $C_{\text{Vddc}}$  is larger than a user definable level (i.e. 2 V).

The simulation output in figure 3.27 shows the behavior of the three blocks. For the whole simulation, the basestation emits a magnetic field with a constant carrier. The top plot

shows the voltage induced at the transponder coil and the bottom one shows the voltages at the capacitors  $C_{\text{fld}}$  and  $C_{\text{Vddc}}$ . At the beginning, only  $C_{\text{fld}}$  is loaded. After  $300\ \mu\text{s}$  constant carrier, the counter activates the preswitch soft mode. From this time on,  $C_{\text{Vddc}}$  is loaded. After  $450\ \mu\text{s}$ , the POR detection activates the preswitch hard mode, which shorts  $C_{\text{Vddc}}$  with  $C_{\text{fld}}$ .

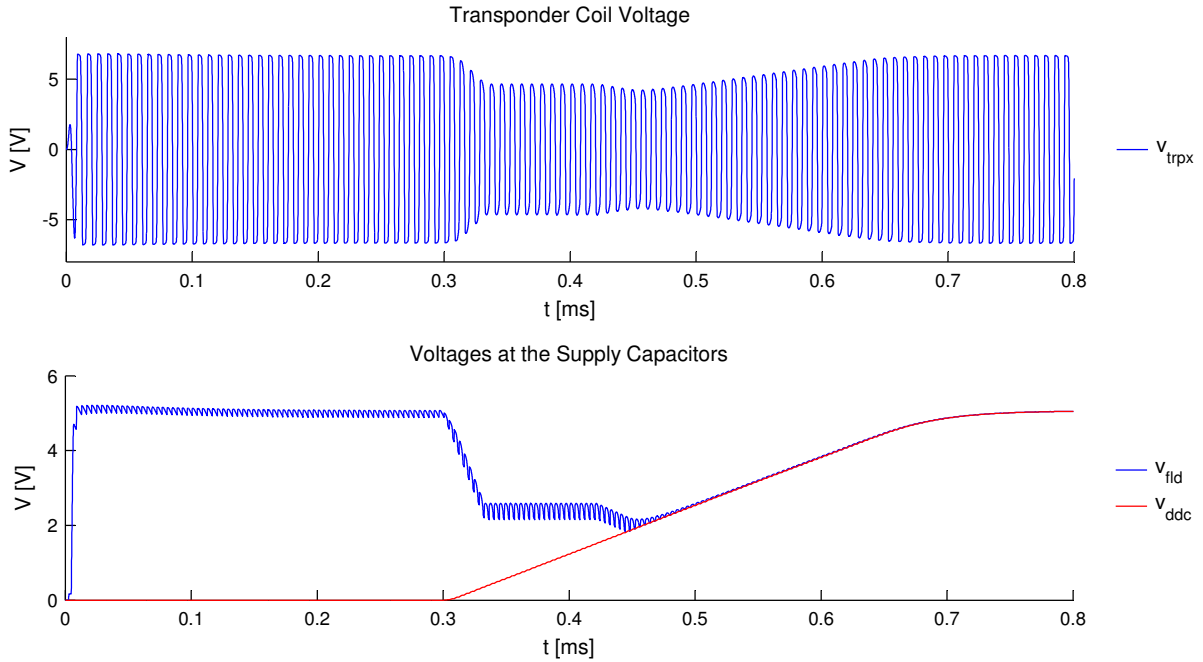


**Figure 3.27:** Simulation output of the supply capacitor voltages.

### Analog Current Consumption

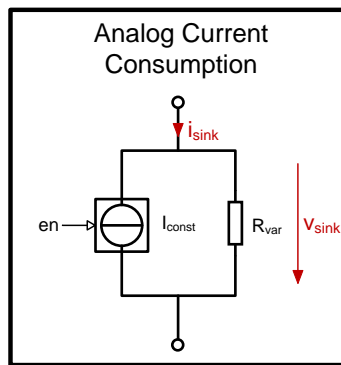


**Figure 3.28:** Analog Current Consumption model.

The analog part of the real IC consists of a frontend and a powermanagement block. Each of these two parts has an almost constant current consumption because the internal circuits are biased. Thus, the analog current consumption model can be implemented as an enabled constant current sink with a resistor in parallel (figure 3.28). In the transponder model overview, it can be seen that each of the two analog blocks is modeled with such a separate

sink. The idea behind the model is that the biased current of the real IC is activated as long as the supply voltage is large enough (i.e. 1 V). When the supply voltage increases, also the consumed current of the internal circuit increases a little bit. This behavior is modeled with the parallel resistor.

### Digital Current Consumption

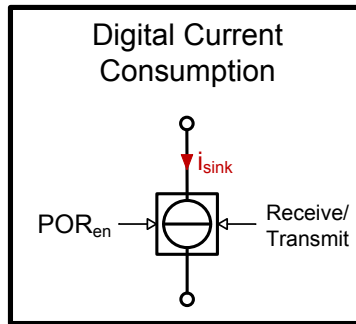


**Figure 3.29:** Digital Current Consumption model.

The digital current consumption models the current consumed by the transponder microcontroller. It is implemented as current sink with different states (figure 3.29). In the real IC, the microcontroller is started, when it gets an OK from the POR detection circuit. At the booting phase, it consumes a large amount of current and then, it falls into an idle state, which consumes only a small constant current. After receiving and before transmitting data, the microcontroller wakes up and configures the appropriate circuit parts such as the AES encryption unit. This produces short current consumption pulses.

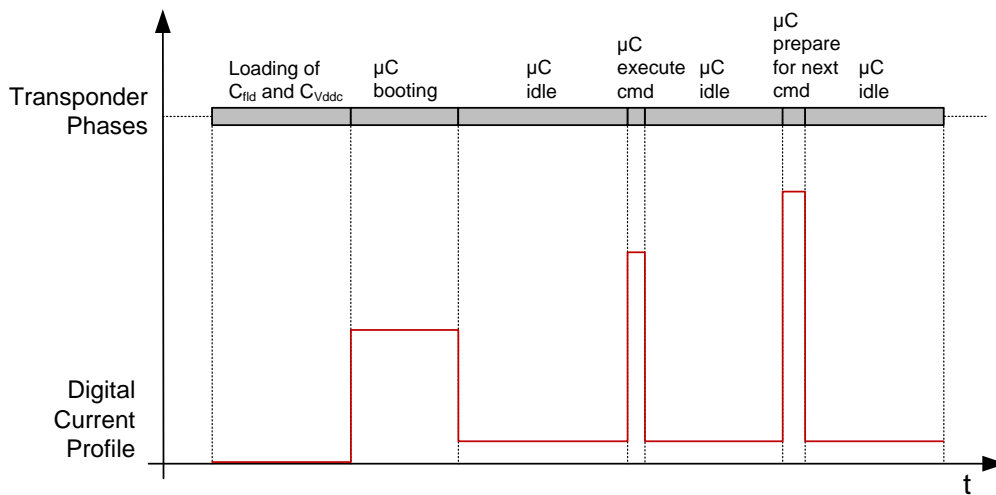


**Figure 3.30:** Diagram of a typical digital current consumption profile.

A typical digital current profile for different phases is shown in figure 3.30. Because the microcontroller is supplied by an LDO regulator, this profile does not depend on the  $C_{Vddc}$  voltage. Of course, the real digital current is not as discrete as in this drawing. But for the voltage drop at the large supply support capacitor, such a discrete current pulse approximation

is valid since only the integral of the current (i.e. the consumed charge) makes a voltage change.

### Simulation Abort Criteria

The Simulink model also contains simulation abort criteria. These are very useful for reducing the simulation time. For example, when the voltage at  $C_{V_{ddc}}$  falls below the power on reset falling threshold after starting the microcontroller, the simulation can be aborted because in a real transponder, the digital part would stop operating with such a low voltage. The following list contains all abort criteria:

1.  $V_{fd} < 0$ .
2. Basestation begins to transmit and microcontroller has not finished booting.
3.  $V_{ddc}$  smaller than power on reset falling threshold and microcontroller is ready.

### 3.3.4 ActiveTX Top Level Model

The activeTX top level Matlab model includes a top level script, function scripts and the Simulink model. A principle diagram of the top level script is shown in figure 3.31.

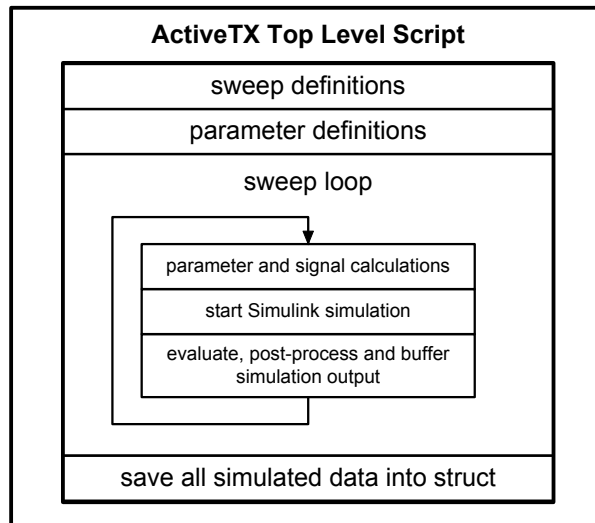


**Figure 3.31:** Principle diagram of the activeTX Matlab top level script.

The *parameter definitions* section contains more than hundred values for configuring the model. Some of the most important parameters are:

- Carrier frequency
- Distance between the coils
- Coil arrangement
- Coil inductances

- Coil detuning
- Value of the support capacitor  $C_{V_{ddc}}$
- Protocol timings
- Current consumption values
- Transponder uplink current amplitude

Each of the parameters can be used as a sweep parameter. For instance, when a distance sweep is desired, the wanted distance values need to be defined in the *sweep definitions* section. The sweep loop uses the values from the *parameter definitions* section and additionally inserts the appropriate sweep value to calculate the needed signals for the Simulink model. Then, the Simulink model is executed. After a successful simulation, the simulation output is post-processed and buffered into the Matlab workspace. With this approach, a maximum of three nested sweeps can be configured. In the last section of the script, the whole simulation data is saved into a data struct.

For example, if a nested sweep with two parameters is simulated, in which the inner loop and the outer loop consist of 10 values, a total amount of 100 simulation outputs is produced. To cope with this large amount of data, a special user interface for a clear visualization is necessary. The implemented GUI and an example simulation output of the activeTX model are presented in section 3.4.

### Signal and Protocol Definitions

This subsection contains a description of the used Simulink model inputs and protocol definitions. In addition to the constant parameters, such as the coil inductance values, also transient signals are needed for the Simulink model input. These are defined below:

- Basestation driver voltage with included downlink communication
- Enable signal for the transponder demodulator
- Enable signal for the transponder modulator
- Transponder uplink transmission current
- Transponder additional digital current consumption signal (execute command and prepare for next command current pulses)

The implemented protocol is a typical communication for unlocking the car. When the key is inserted into the ignition lock and turned around, the basestation sends a request to query the ID of the transponder (GetIDE command). After the transponder responds, a mutual symmetrical authentication, similar to the description in section 2.1.3, follows. The basestation uses BPLM as modulation scheme, while the transponder communicates via a Manchester coded BPSK modulation.

### 3.3.5 Solver

During the implementation phase of the model, it turned out that a careful choice of the Simulink solver is a crucial point for a successful simulation. This section contains considerations for getting reliable and fast simulation results.

Simulink offers fixed step and variable step ordinary differential equation (ODE) solvers for simulating continuous systems. Because the activeTX model has many sources of discontinuities, a very small step size has to be chosen for a fixed step solver in order to guarantee convergence. In contrast, a variable step solver dynamically adjusts the step size. When the model states change rapidly, the step size is decreased, while for slowly changing states, the step size is increased. Due the advantage of a shorter simulation time, a variable step continuous solver is chosen. [15]

The next consideration is whether the solver should be explicit or implicit. An explicit solver directly calculates the next step of a state using an explicit formula as shown in equation 3.22. [14]

$$x_{n+1} = x_n + h \cdot Dx_n \quad (3.22)$$

$x_{n+1}$  – state value of the next time step

$x_n$  – state value of the current time step

$h$  – step size

$Dx_n$  – solver dependent estimation function of the state derivative at current time step

An implicit solver calculates the next time step with the implicit formula in equation 3.23. [14]

$$x_{n+1} - x_n - h \cdot Dx_{n+1} = 0 \quad (3.23)$$

$Dx_{n+1}$  – solver dependent estimation function of the state derivative at next time step

The difference between those two is that the explicit solver directly uses numerical integration (i.e. Euler's Method or Runge-Kutta) for calculating the next time step, while an implicit solver uses a combination between Newton-Raphson method and extrapolation formulas. In general, implicit solvers have more computational overhead per time step, but can use larger time steps for reaching the same accuracy as explicit solvers. For stiff systems, implicit solvers are recommended because they provide faster simulation times and more stability for oscillatory behavior. A stiff system is a model, which includes large and small time constants. The activeTX system is of stiff type and also has oscillatory behavior. These considerations imply the choice of an implicit solver. [14]

Simulink offers four different variable step continuous implicit solvers, whereas only two are recommended for Simscape models. These are `ode23t` and `ode15s`. Through extensive simulations and reading the description of the solvers in [14], the choice fell on `ode23t`. The

substantial reason for this is that the solver produces simulation outputs without numerical damping. This property is very important for the oscillatory behavior of the activeTX model.

A simulation time comparison between the chosen solver and an explicit solver is given in table 3.4. The much faster `ode23t` points out the necessity of the above made considerations.

Solver	Type	Simulation Time in HH:MM:SS
<code>ode23</code>	explicit	22:56:54
<code>ode23t</code>	implicit	00:15:26

**Table 3.4:** Comparison of the simulation time for an explicit and implicit solver

Because signals with very steep edges can lead to a crash of the simulation or an excessive simulation time, also some investigations on preventing sharp signal transitions are necessary. The first step is to implement the model in a way that infinite gradients cannot occur. For example, a switch must smoothly decrease its impedance when it is switched from off to on state (i.e. linearly decrease the impedance from  $10^9 \Omega$  to  $10^{-2} \Omega$  during  $100 \mu\text{s}$ ). Even if all sharp transitions are removed, the simulation can get stuck. To explain this issue, the Simulink's internal algorithm for solving discontinuities needs to be analyzed. It is called Zero-Crossing Detection (ZCD). Each Simulink block, which contains discontinuities in the internal states (i.e. a saturation block), has an included additional zero crossing variable. This variable simply changes sign when a discontinuity occurs. That helps the Simulink solver to quickly identify the discontinuity. The used approach drastically improves the simulation time performance compared to a conventional solution, in which only the step size is extremely decreased. [15]

Although the advantages of the ZCD outweigh, a big disadvantage could be identified during the implementation phase of the model. For example, when a zero crossing variable of a Simulink block oscillates around zero within a very small range (i.e. between  $-1\text{e-}20$  and  $1\text{e-}20$ ), a zero crossing loop can appear. This loop invokes the ZCD every time step and, in the worst case, the simulation gets stuck because of the large amount of computational load. The problem is well known and thus, special solver settings for avoiding such loops exist. These are explained in [15]. For the activeTX model, the zero crossing algorithm is switched from non-adaptive to adaptive. The adaptive algorithm provides a property for specifying a signal threshold, beyond which a zero crossing is not evaluated. With a setting of  $1\text{e-}15$ , zero crossing loops could be avoided for all tested simulations.

### 3.4 Graphical User Interface

As already mentioned, the implemented Graphical User Interface (GUI) is required for analyzing the large amount of simulation output data. Essentially, the GUI is a Matlab function, which is invoked with a simulation output struct as argument. Figure 3.32 shows a picture of the finished implementation. On the right side, there are check boxes for choosing the displayed signals in the plots. These allow the user to identify, if the chosen parameters would work for a real activeTX system.

The description of the signals follows now:

- plot 1:** VbsCoilDL – Basestation coil voltage  
VbsCoilUL – Zoom of the basestation coil voltage when the transponder transmits
- plot 2:** VtrpCoilx,-y,-z – Voltages of the three transponder coil axes
- plot 3:** Vf1d – Voltage at the decoupling capacitor  $C_{fd}$   
Vddc – Voltage at the support capacitor  $C_{Vddc}$
- plot 4:** IQQtrp – Transponder IC current consumption, consisting of analog frontend, powermanagement and digital current  
ItrpCoilx,-y,-z – Current which flows from the respective transponder coil axis into the IC
- plot 5:** TrpDLdig – Transponder demodulator output  
ItrpLimx,-y,-z – Consumed limiter current at the respective transponder coil axis

Because the simulation time is long, compared to a clock cycle of  $8 \mu s$ , some signals appear as solid bars (i.e. VbsCoilDL). Like all Matlab figures, the GUI offers the user a zoom function to zoom in and see each clock cycle.

The top left side of the GUI contains the sweep values and the bottom left side lists important parameter settings. In this particular example, a nested sweep with two sweep parameters is shown. The inner loop contains a distance sweep and the outer loop a sweep over the transponder coil misalignment angle (first outer sweep: coaxial 1D  $z$ -axis arrangement, second outer sweep: coaxial 3D arrangement). By clicking one of the distances, the associated signals appear in the plot region. The color of the arrow specifies if the whole communication procedure finishes successfully (green indicates a passed communication and red or yellow indicate an error). For the coaxial 1D  $z$ -axis arrangement, the shown distance of 112 cm is just enough to allow a sufficient supply for the transponder since  $V_{ddc}$  is always large enough. For 115 cm, an error occurs. Figure 3.33 shows the GUI for this sweep. It is explained in the diagram title that at 107.77 ms, the supply is too small for operating the transponder IC.

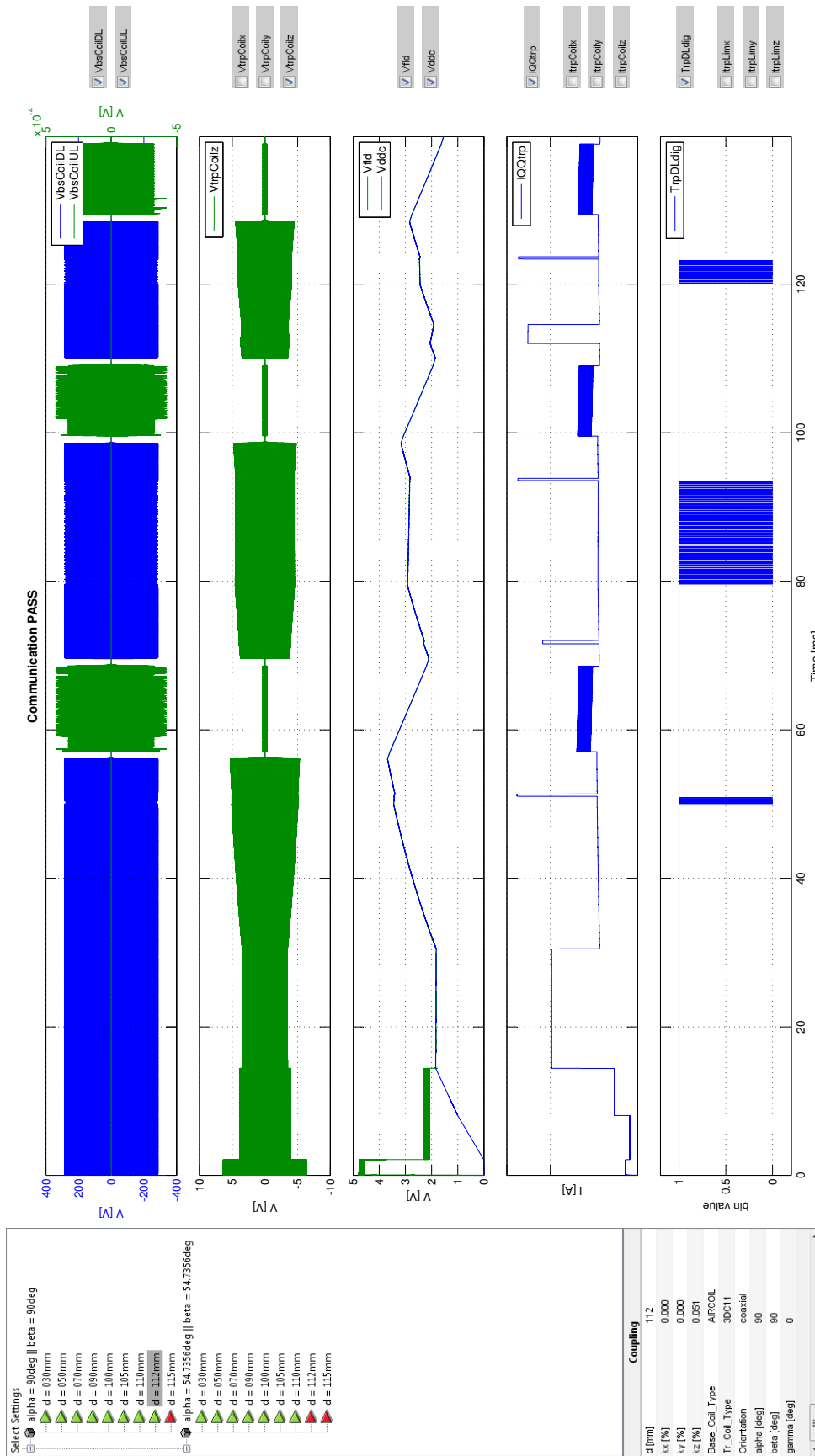


Figure 3.32: GUI for visualizing the activeTX simulation results, containing a passed communication

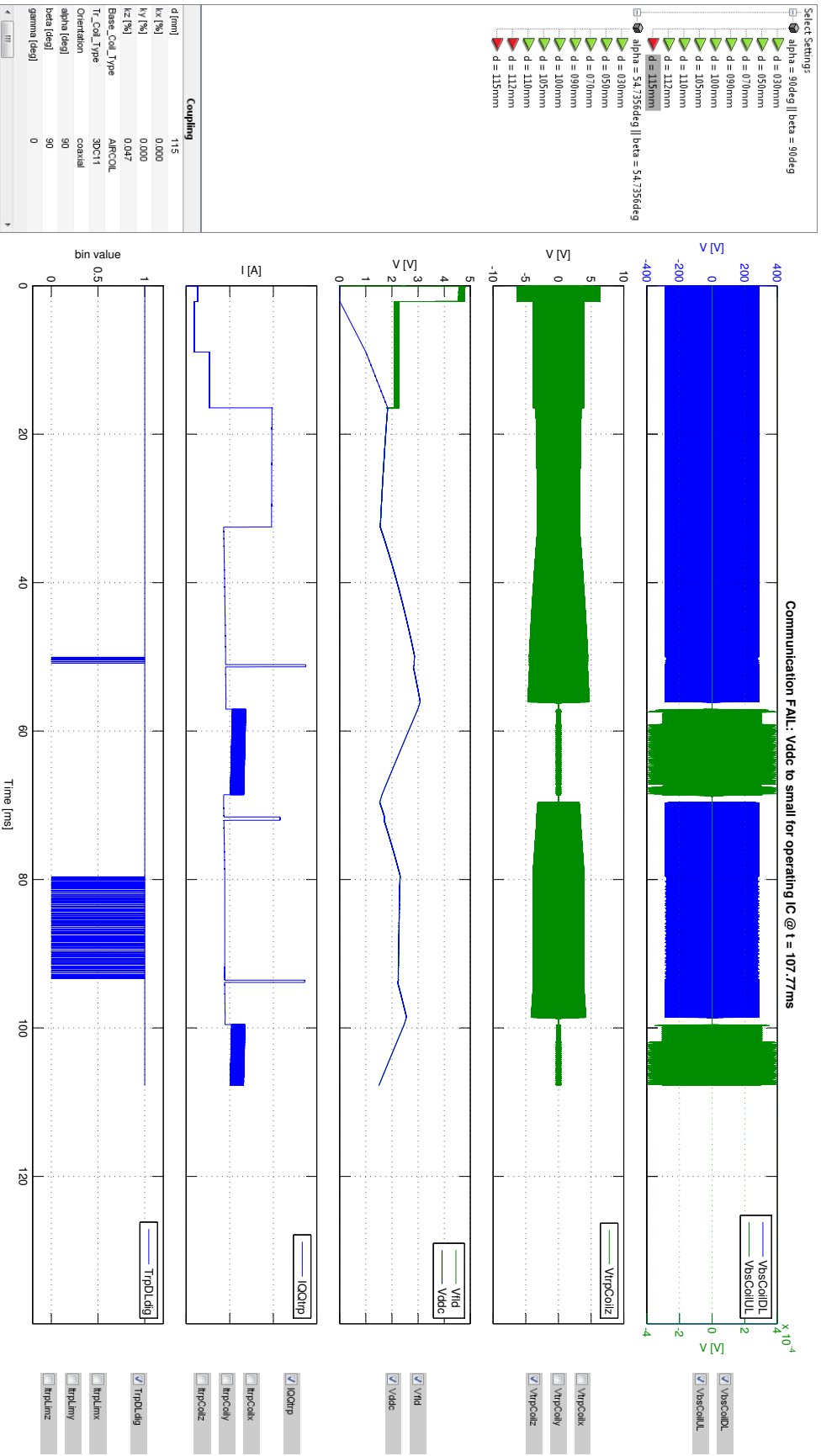


Figure 3.33: GUI for the visualization of a failed communication

# Chapter 4

## Lab Setup

The lab setup fulfills three major goals. First, it is necessary for validating the activeTX Matlab model. The second important goal is to have an activeTX demonstration hardware in place, which is very useful for getting a detailed insight into the whole system. The third goal is to use it as reproducible validation setup for the future ICs.

This chapter begins with the description of the mechanical distance setup in section 4.1. Sections 4.2 - 4.7 cover the implemented electronic setup, containing both hardware and software design.

### 4.1 Mechanical Distance Setup

A reliable comparison between measurement and simulation requires an accurate mechanical setup, which allows different distance and coil arrangement adjustments. Because there is no such setup available at NXP, it is also part of the Master's Thesis to design the necessary mechanical parts. This chapter deals with the considerations and development of the mechanical distance setup.

#### 4.1.1 Requirements

The requirements for the setup are:

- Distance adjustable with an accuracy of at least 1 mm
- Minimum stroke length of 200 mm
- Accurate positioning indicator included
- Coplanar 1D, coplanar 3D, coaxial 1D and coaxial 3D arrangements possible
- Transponder and basestation coils accurately fixable to ensure reproducibility
- Distance adjustable by hand or with stepper motor
- Non-magnetic materials
- Transponder side suitable for thermostream measurements

### 4.1.2 Approaches for the Mechanical Setup

From the requirement of the different coil arrangements, two design approaches can be stated:

1. Every possible misalignment angle and position is freely adjustable. This needs to be realized with three different rotatable axes on transponder side and one rotatable axis on basestation side.
2. The coils are attached to fixed blocks. Different arrangements are reached through switching between these blocks.

Table 4.1 contains a comparison of the two approaches for important properties. The approach with a better suitability for the particular property is provided with a check mark.

Property	Approach 1	Approach 2
Larger coil arrangement freedom	✓	✗
Advantage of a lower design complexity	✗	✓
Better measurement reproducibility	✗	✓
Easier thermostream attachment	✗	✓
Smaller production expenditure	✗	✓
Lower price	✗	✓

**Table 4.1:** Comparison between the two realization approaches for the mechanical setup

This comparison leads to the decision of choosing approach 2. The crucial factors are the better measurement reproducibility due the avoidance of rotating components and an easier possibility for the thermostream attachment. But also the time saving of a lower design complexity and the lower price are important advantages.

### 4.1.3 Implemented Mechanical Setup

For the implemented mechanical setup, it has to be mentioned that the principle design is made within this Master's Thesis, while some parts are re-designed by the manufacturer [10]. This re-designs are necessary due to an easier production.

#### Material Choice

One of the most important considerations is the non-magnetic material requirement. The usage of a thermostream on transponder side makes it even harder to find materials, which have a temperature-resistance for the required automotive temperature range (-40 to +85 °C). A comparison of plastic materials in handbook [9] leads to a choice of Polyoxymethylene (POM) as material for the milled parts. Some important properties of POM are a very good form stability, a good machinability, a high heat stability and an operating temperature from -40 to +110 °C.

All used screws, except for the motor attachment, are made of nylon. The basic component for the setup is a prefabricated linear bearing from [11] with a stroke length of 300 mm. This part

is shown in figure 4.1. As can be seen, all used materials are nonmagnetic. The positioning indicator is mechanical and displays the distance in 0.1 mm steps.

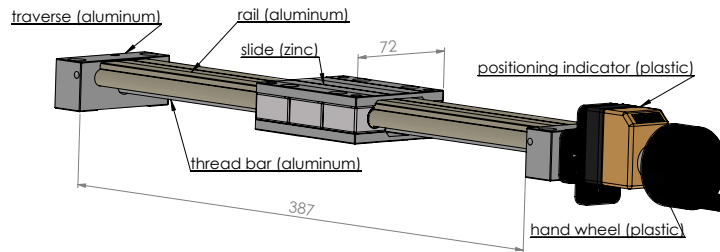


**Figure 4.1:** Linear bearing with included material description. [11]

### Complete Mechanical Setup

A CAD-drawing of the complete mechanical setup is shown in figure 4.2. Specifically, a coaxial 1D z-axis arrangement can be seen. The coils are mounted on PCBs, which are attached to the transponder and basestation blocks with nylon screws. On transponder side, two different blocks are used to reach the required arrangements (1D and 3D block). The centers of the coils are more than 180 mm away from the ground so that a placement of the setup on a magnetically conducting electrostatic-discharge-worktable makes no significant distortion of the field lines. If required, the hand wheel can be replaced by a stepper motor, which allows automatic measurements for a characterization of the future ICs. Of course, a motor always contains magnetic materials. Since it is far enough away from the coils, the influence on the magnetic field lines can be neglected.

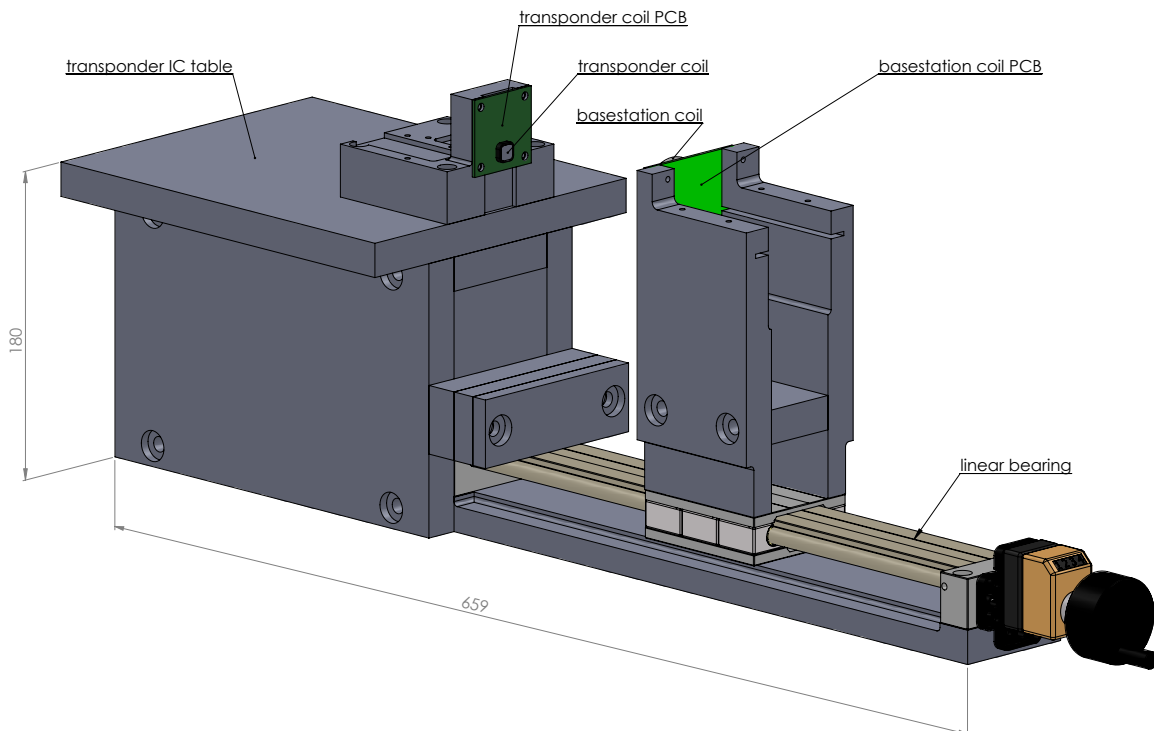


**Figure 4.2:** Mechanical distance setup in 1D z-axis arrangement.

The transponder table is intended as storage space for the transponder application PCB and hence, only short wires are needed for a connection with the coil PCB. The table also allows the attachment of a thermostream head on the transponder PCB. Since in a real application, the basestation is located far away from its coil (i.e. 2m), no table is necessary for the basestation application PCB. It can be placed anywhere next to the setup, with the basestation coil PCB connected via long wires.

The next section describes how the distance setup can be used for different coil arrangements.

### Arrangement Principles

The geometries of the setup and the coil PCBs are constructed in a way that exact coplanar and coaxial arrangements for all 1D and a special 3D case are possible. To change the setup to a different arrangement, only small re-construction work is necessary. The 1D transponder block provides assembly positions for all three antenna axes. If a coaxial 3D z-axis arrangement, as shown in figure 4.3, is desired, simply the 1D block needs to be changed with the 3D block. This can be done very quickly because the blocks are attached with nylon screws. The 3D block is designed for the worst case transponder voltage misalignment angle, where each axis is misaligned exactly  $54.74^\circ$  (see derivation in equation 3.14).

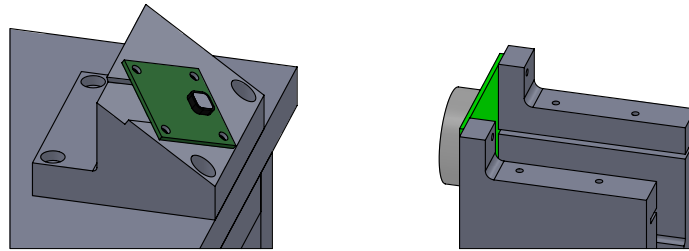


**Figure 4.3:** Distance setup in coaxial 3D arrangement.

The coplanar 1D z-axis arrangement is shown in figure 4.4. For changing to this arrangement, the basestation coil PCB has to be inserted into the designated slot.

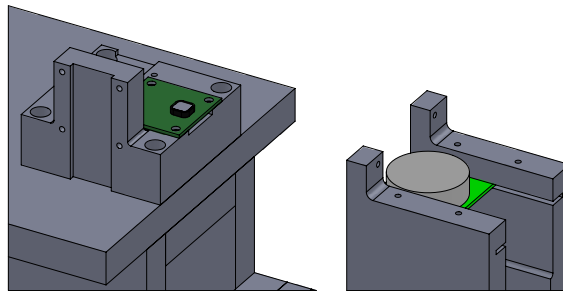


**Figure 4.4:** Distance setup in coplanar 1D z-axis arrangement.

## 4.2 Requirements and Overview of the Electronic Setup

The activeTX electronic setup should behave the same as the Matlab model. To be able to understand the setup, this section contains a description of the requirements and a simple overview of the needed hardware and software parts.

## Transponder Requirements

- 3D-coil with tuning capacitors
- All transponder IC functional components which have been already explained in section 3.3.3. (rectifier & limiter, active transmitter, demodulator, counter, preswitch, power on reset detection)
- External support capacitor  $C_{V_{ddc}}$
- Adjustable current consumption
- Amplifiers with low input capacitance to measure coil voltages without parasitic detuning
- Microcontroller
- Software for generating BPSK signals
- Software for receiving BPLM commands
- Software state machine which implements simple immobilizer protocol

## Basestation Requirements

- Air-coil with high voltage tuning capacitors and high power resistors for Q factor adjustment
- Driver which can drive currents with 1 A amplitude (for a 125 kHz carrier frequency)
- Current probe to measure the coil current
- Amplifier for the received transponder response signal
- Protection circuitry to protect amplifier input from high voltages during the basestation driver is on
- Microcontroller
- Software which implements simple immobilizer protocol
- Software which controls receiver protection circuit and amplifier

## Overview of the needed parts

A block diagram representation of the required hardware parts is illustrated in figure 4.5. The red signals are intended to be measured with an oscilloscope. These signals, which have been already explained in section 3.3.3, are sufficient for the user being able to analyze the activeTX lab setup for different settings (i.e. transponder current consumption).

On the basis of the basestation requirements, it can be noticed that no BPSK demodulator is needed. Since this Master's Thesis focuses on the transponder side, such an implementation is not part of the project. An oscilloscope visualization of the receiver amplifier output should be enough for the user to decide whether the signal quality is good or not.

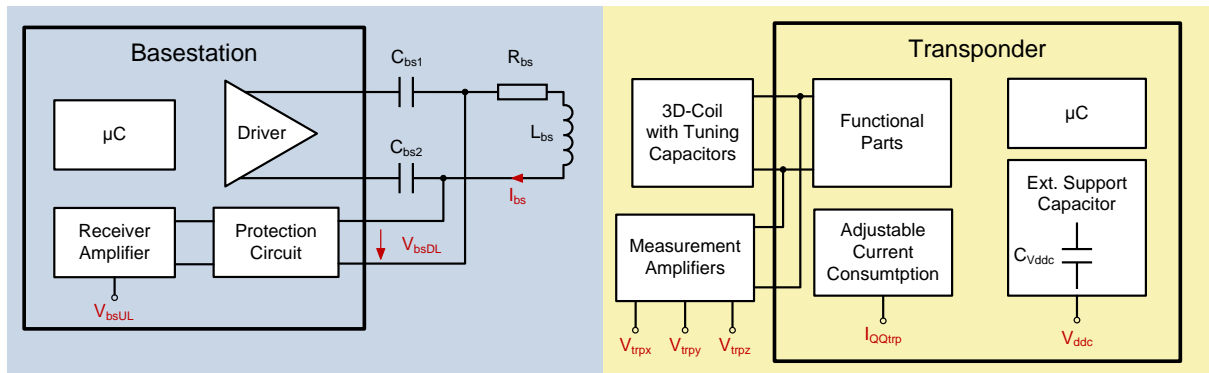


Figure 4.5: Overview of the required hardware setup.

## 4.3 Transponder Hardware

The lab transponder should behave as close as possible like a real future activeTX IC. To be able to find the most suitable solution, this section begins with a discussion of the hardware options. The second part covers a detailed description of the implemented hardware.

### 4.3.1 Transponder Approaches

The two major transponder hardware approaches are:

1. An implementation of all activeTX transponder parts including the functional parts with discrete components.
2. The usage of a load modulation transponder, which is extended with discrete devices to build the activeTX transponder.

An in place available load modulation transponder IC already contains the following necessary parts: rectifier & limiter, demodulator, counter, preswitch, current source for forcing a current into the coil. Because the IC also has an on-board microcontroller, these parts can be directly controlled. The big advantage of approach 2 is that only a small adapter board for the remaining parts is necessary.

The advantage of approach 1 is the freedom to make all possible settings adjustable. For example, the limiter feedback loop can be made in a way that many different limiter profiles can be tested. A big disadvantage of approach 1 is the problem with parasitics. Since each of the coil axes needs at least three full wave rectifiers and one limiter, the corresponding parasitic capacitances of the diodes would result in a much larger coil detuning compared to a real transponder IC. Also a demodulator and active transmitter have to be directly connected to the coil, what would introduce even more large parasitics. Another disadvantage compared to approach 2 is a much higher implementation effort due to a complete discrete transponder development.

The disadvantages of the discrete approach lead to the decision of choosing approach 2. The used load modulation transponder is a newer version of the presented transponder in section 2.1.4. It also has controllable current sources included, what allows to directly drive a current

into the coil. This feature can be used to implement the controlling of the activeTX transponder transmitter in software. Because of the architecture of the embedded microcontroller, the IC's current consumption depends on whether the program is executed from ROM or EROM. A real transponder state machine is implemented in ROM and has a low digital current consumption because the ROM is optimized for low power applications. The only chance to implement the activeTX transponder is to load the appropriate source code into the EROM and execute it from there. Since an EROM execution has a much larger current consumption, some considerations must be made to emulate the required smaller current consumption of a real IC. The possible options are explained now.

### **Variants for the Transponder Current Consumption**

An adjustable transient transponder current consumption is one of the most important requirements. To compensate the large EROM microcontroller current, there basically exist two different options:

1. The design of a current source, which adds an external current into the support capacitor to reach an overall smaller consumption. The added current must be changeable, depending on the actual transponder communication state. The resulting desired current profile, which completely consists of the extracted energy from the basestation magnetic field, is then the difference between the IC consumption and the added current.
2. The used load modulation IC has an option to switch to an external supply for the microcontroller and analog powermanagement. The remaining extracted current from the support capacitor consists then only of the analog frontend current. Because this current is much too low for a real transponder consumption, a current sink, which draws current from the support capacitor, must be designed. The frontend current plus the current of the sink represent then the desired consumption profile.

Approach 1 has the disadvantage that every time, a new sample of the load modulation IC is used, the added current has to be adjusted. This can be explained by the inherent current consumption deviations due to the manufacturing process of the IC. If an accurate current sink is used for approach 2, no such problem exists (only the small frontend current can make a deviation). On the basis of this advantage, approach 2 is chosen for the current consumption emulation.

### **4.3.2 Implemented Hardware**

The implemented transponder lab hardware consists of a load modulation IC, an adapter board and an amplifier board. At first, the adapter board, which contains the controllable current sink and comparators for a threshold voltage detection, is explained. Then, the amplifier board for buffering the coil voltages is described. At the end, the complete transponder hardware is presented.

#### **Transponder Adapter Board**

The main task of the adapter board is to provide a microcontroller controllable current sink for emulating different transponder current consumption profiles. Many possibilities exist for such an implementation. For example, an approach with binary weighed current sources (i.e.

source followers with connected binary weighed resistors), which are switchable with eight microcontroller pins, is one of the options. A second option would be a Digital-to-Analog Converter (DAC), which controls the input of a voltage controlled current source.

Through extensive research, a single IC solution (DAC 08 from Analog Devices [1]) that exactly provides the desired functionality could be found. The IC is a high speed 8-bit multiplying current sink DAC with parallel interface. Its functional block diagram is shown in figure 4.6. An input reference current needs to be fed into the  $V_{ref(+)}$  input. This can be accomplished by connecting a voltage source with a series resistor  $R_{ref}$  at  $V_{ref(+)}$  and connecting the inverting input of the reference amplifier  $V_{ref(-)}$  to ground. Through the gain of the reference amplifier, the potential at  $V_{ref(+)}$  is driven to virtual ground. The reference current is then defined as the voltage across  $R_{ref}$ , divided by the resistance. The output current  $I_{out}$  can be controlled with eight parallel bits ( $I_{out} = DigIn \cdot \frac{I_{ref}}{256}$ ). Since always the same current flows through the binary weighed transistor current sources (either from  $I_{out}$  or  $\overline{I_{out}}$ ), the IC shows a very good linearity and accuracy. A second advantage is a small settling time. [1]

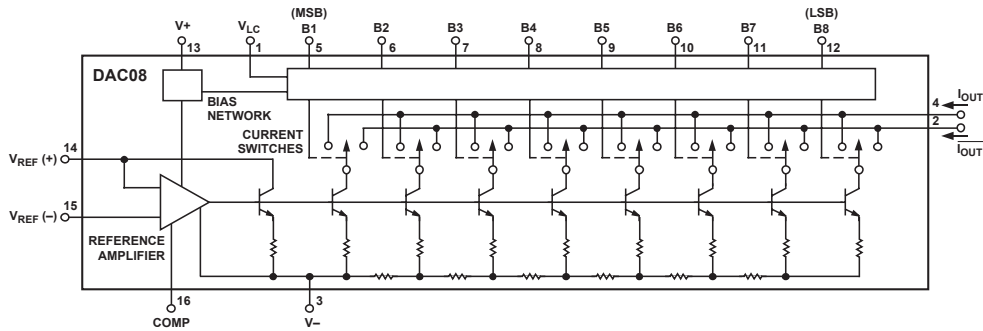


**Figure 4.6:** Functional diagram of the chosen current DAC. [1]

The adapter board is implemented on a prototype PCB. A simplified schematic is illustrated in figure 4.7 (for the full schematic please refer to appendix C). A reference current of  $200 \mu\text{A}$  is used for the DAC. This leads to an LSB of  $0.78 \mu\text{A}$ , which is small enough to accurately emulate the digital transponder current consumption. The non inverting current input  $I_{out}$  is directly connected to the transponder support capacitor. Because the inverting current is not needed, it is connected to a fixed potential of  $3 \text{V}$ . The sink current needs to be measurable with an oscilloscope. This is possible through the voltage drop across the  $1 \text{k}\Omega$  shunt resistor. Due to the very low voltages (1LSB corresponds to  $0.78 \text{mV}$ ), an instrumentation amplifier with a switchable gain between 10 and 100 is used for a signal amplification.

The comparators are required to signal the microcontroller that a certain threshold at the support capacitor is reached. For example, the POR rising comparator signals that the voltage is large enough for enabling the digital booting current consumption, while the POR falling comparator signals that the supply voltage is too small for operating the emulated transponder. By adjusting the potentiometers, the levels of the thresholds can be set between 0 and  $3 \text{V}$ . The NMOS transistor  $M_{\text{short}}$  gives the microcontroller the possibility to fully discharge the support capacitor before the next measurement cycle begins.

A total of 12 microcontroller I/Os are needed for communicating with the adapter board. Since the load modulation IC has 21 general purpose I/Os, this requirement is given.

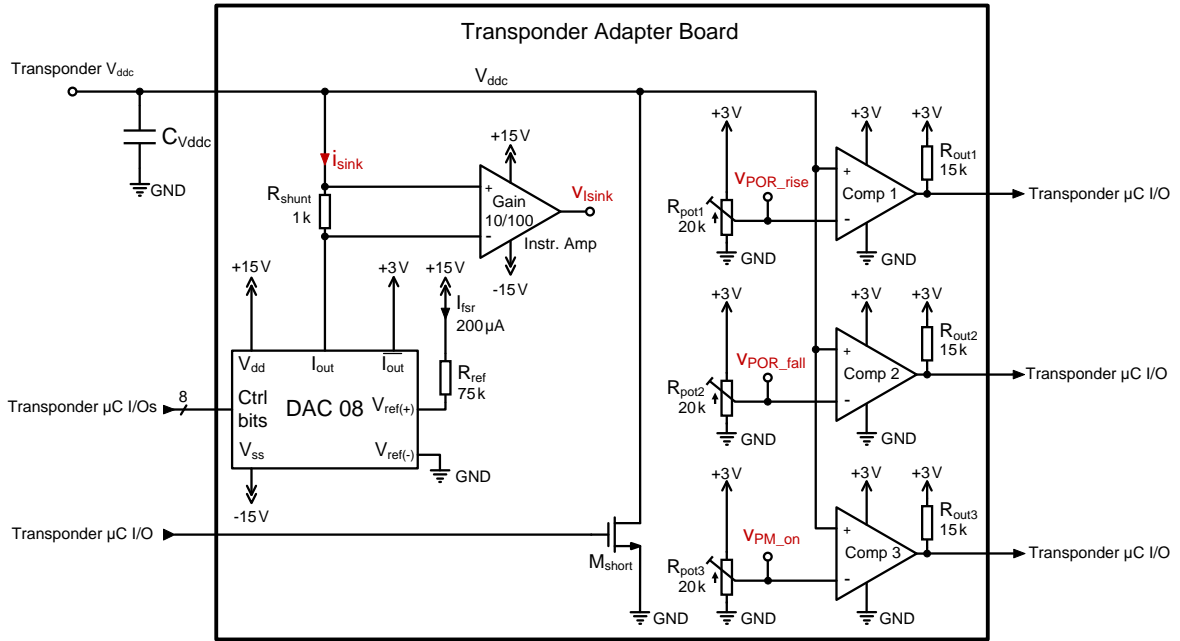


Figure 4.7: Schematic of the transponder adapter board.

## Amplifier Board

The three transponder coil voltages shall be measurable with an oscilloscope. A connection of the probes (10 pF capacitance) is already enough to significantly detune the resonance frequency. Also the voltage has to be measured differentially, what requires two probes per coil axis. To avoid these problems, amplifiers with the following specification are required:

- Differential amplifier
- Low input capacitance
- Low input bias current
- Large differential and common mode input resistance
- Supply voltage at least  $\pm 15$  V (the coil voltages can be up to  $16 V_{pkpk}$ )
- Slew rate minimum  $8 V/\mu s$

The instrumentation amplifier INA111AP [3] meets the requirements. It has an input capacitance of 6 pF differential and 3 pF common mode. This is not much smaller than the capacitance of an oscilloscope probe, but in contrast to the probe, the amplifier is always connected. Thus, the coil can be exactly tuned with the amplifier.

The schematic of the amplifier board with a connected 3D transponder coil is shown in figure 4.8. Because a sampling frequency of 2.5 MegaSamples/s is used for the oscilloscope, an anti-aliasing filter is required to suppress higher frequencies. This is reached by a first order low-pass filter with a cut-off frequency of 590 kHz.

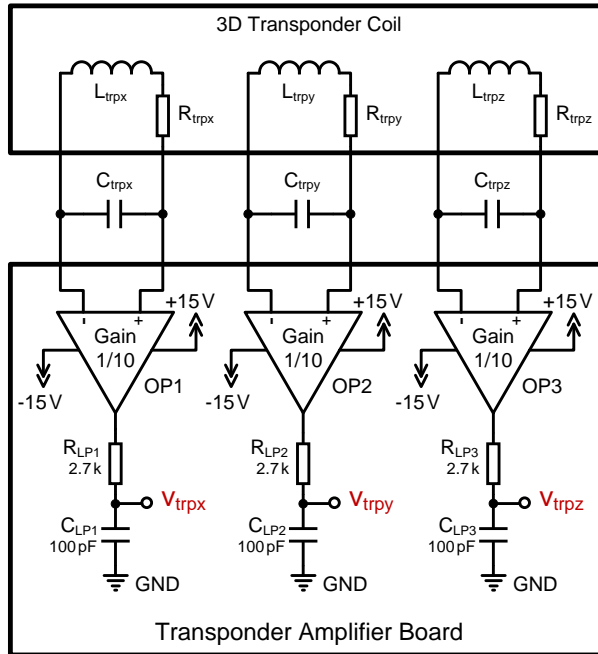


Figure 4.8: Transponder amplifier board with connected 3D coil.

### Complete Transponder Lab Hardware

The complete transponder hardware is shown in figure 4.9. The blue marked blocks are supplied from the basestation magnetic field and all other blocks are supplied from an external DC supply. For example, the microcontroller of the load modulation transponder IC is always on, independent of whether the basestation is emitting or not. Because the active transmitter corresponds to the same power domain as the microcontroller, it is also supplied externally. This has the consequence that also the average consumed transmitter current has to be emulated with the current sink DAC.

With the presented hardware approach, all necessary parts for emulating an activeTX transponder are available. It is now up to the microcontroller program to control the analog frontend and the current sink in a way that the desired behavior can be reached. This software is explained in the next section.

## 4.4 Transponder Software

The embedded microcontroller of the load modulation IC is a 16 bit low power RISC controller [18, 3] and the associated compiler supports both C and assembler language. The activeTX transponder software is written almost completely in C. Only the timing critical active transmitter routine is written in assembler. Figure 4.10 shows a flow diagram representation of the microcontroller program. It is organized in two main parts: *Start Phase* and *activeTX Transponder Emulation*.

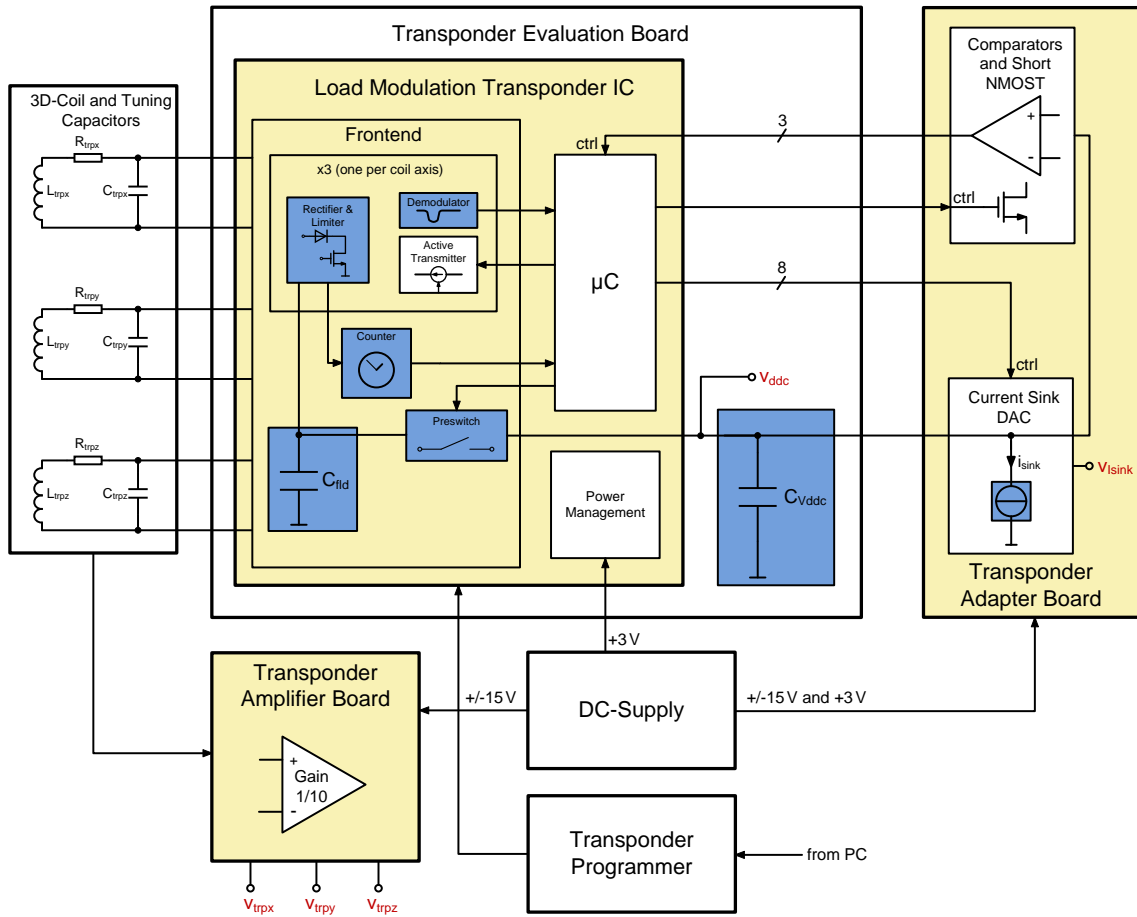


Figure 4.9: Block diagram of the complete transponder hardware.

### Start Phase

The *Start Phase* begins when the external DC supply is enabled. After the boot routine has finished, the user program starts executing. At the beginning, all necessary registers, interrupts, I/Os, peripherals and the clock are initiated. Then, the current sink DAC is initiated to 0 A. Because the DAC has an 8bit parallel interface, it can be controlled with one I/O port register. This has the advantage that the current can be changed within one clock cycle. The last step of the *Start Phase* discharges the support capacitor  $C_{V_{ddc}}$  to 0 V (enable the  $M_{short}$  transistor for a short time and then disable it again). This is very important to guarantee the same start value for  $V_{ddc}$  as in the simulation because due to the large capacitance, it can happen that  $C_{V_{ddc}}$  is still loaded to a small voltage.

During the *Start Phase*, the basestation is not allowed to transmit, because the emulated transponder is not ready till the *activeTX Transponder Emulation* phase begins. Since the *Start Phase* requires less than 2 ms, this constraint can be simply handled by always starting the basestation after the transponder.

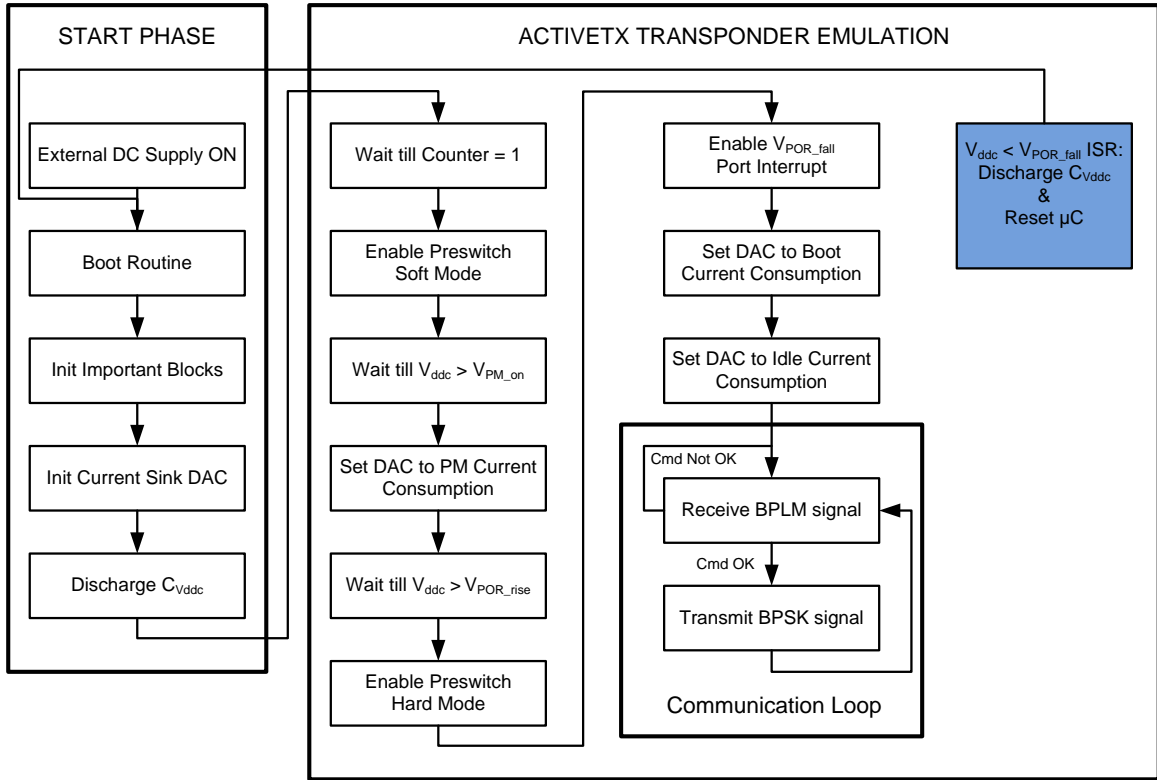


Figure 4.10: Flow diagram of the transponder microcontroller software.

### activeTX Transponder Emulation

The *activeTX Transponder Emulation* part fulfills the task of implementing the complete transponder behavior, which has been already explained in the Simulink model (section 3.3.3). It contains the current consumption emulation (please refer to figure 3.30 for a typical transponder digital current consumption profile) and communication routines.

In the first step, the microcontroller waits till the analog frontend detects a 2 ms constant emitted basestation field (Counter = 1). Then, the preswitch is enabled in soft mode and  $C_{V_{ddc}}$  begins charging from the extracted field energy. Afterwards, it is waited till  $V_{ddc}$  is large enough (i.e 1 V) so that the *powermanagement current consumption* can be emulated. This requires the  $V_{PM\_on}$  comparator from the transponder adapter board to go high. In the next step, the program waits till  $V_{ddc}$  reaches the power on reset threshold (check if  $V_{POR\_fall}$  comparator goes high). From this time on, the preswitch is set to hard mode and a port interrupt is enabled, which senses if  $V_{ddc}$  falls beyond the power on reset falling threshold ( $V_{POR\_fall}$  comparator goes low). With this approach, the microcontroller is able to emulate the behavior of a too small supply voltage. If the interrupt request flag is set during the subsequent program execution, the interrupt service routine immediately shorts  $C_{V_{ddc}}$  for a certain amount of time to ground and then resets the microcontroller. Now the program starts again from the beginning.

After enabling the interrupt, the transponder *booting current consumption* is emulated (i.e. set DAC current to  $70 \mu A$  for 12 ms). Then, the *digital idle current consumption* is set. In the next step, the communication loop, which consists of a receiver and transmitter routine, starts.

The *execute command*, *wait for next command* and *transmit current consumption* emulation is embedded in this two routines. When the loop is entered, the demodulator polls on a basestation sent BPLM commands. If it recognizes a valid command, a response is sent using the active transponder transmitter routine. This function performs the task of controlling the internal current source of the load modulation IC in a way that a BPSK signal is generated at the transponder coil (see figure 3.24 for an example simulation output of such a signal). A BPSK signal can be generated on every coil axis. In the current implementation, the signal is only transmitted on the z-axis because the load modulation IC offers no possibility to find the strongest coupled channel (i.e. the coil axis with the largest coupling to the basestation coil). The routine is very timing critical and is thus completely implemented in assembler language.

When a communication cycle is finished, the basestation stops transmitting. Due to the current consumption of the load modulation IC frontend and the emulated current consumption, at some time  $V_{\text{ddc}}$  falls beyond the power on reset falling threshold. This triggers the  $V_{\text{POR\_fall}}$  interrupt service routine and the starting phase begins again. Shortly after the starting phase, the transponder emulation refreshes to its initial state. Hence, the whole explained emulation concept exactly behaves like a real activeTX transponder.

### activeTX Header File

The transponder software is organized in various source and header files. One header file with the name `activeTX.h` contains all necessary parameters, which are important for the user. These are:

- Current consumption values
- Valid receive commands
- Transmit commands
- User definable timings

For example, when the user wants to see if the transponder also works for a larger digital idle current consumption, he only needs to change the particular value in the header file, compile and then download the program to the load modulation IC.

## 4.5 Basestation Hardware

An in-place available IC, which is capable of driving currents with amplitudes larger than 1 A, is used as basestation driver. It has also an embedded microcontroller that can be programmed in C language. Because the IC is designed for a load modulation system, it has no included activeTX BPSK receiver. One of the requirements on basestation side is the visualization of the received transponder signal. To be able to measure the small signal, an amplifier chain and a separate protection board is necessary. These two parts are explained below.

## Basestation Protection Board

In normal operation, the voltage appearing at the basestation coil is larger than  $500 V_{\text{pkpk}}$ . The same voltage level appears at the differential tuning capacitors, where the receiver amplifier chain is connected. To protect the amplifiers during the driver on state, the protection board, illustrated in figure 4.11, is used.

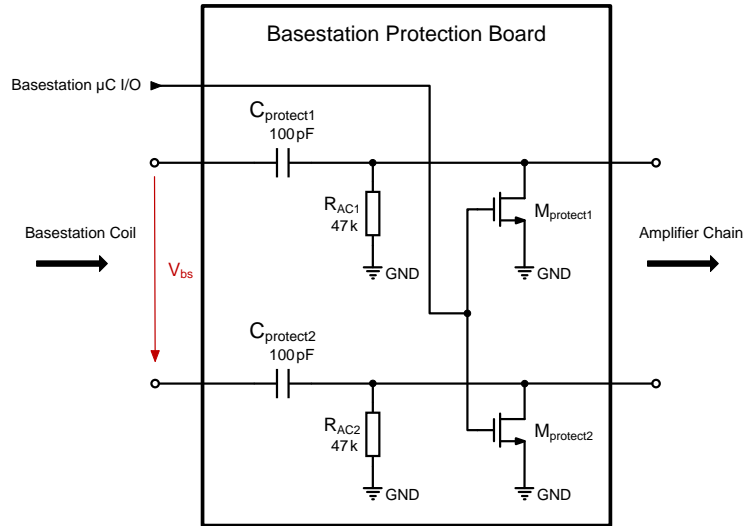


**Figure 4.11:** Schematic of the basestation protection board.

Since the basestation coil signal is differential, also the protection is carried out differentially. During the basestation driver ON-time, the microcontroller I/O pin is set to high (5 V). Thus, the transistors are switched on and the nodes, which protect the amplifier inputs, are pulled low ohmic to ground. The large coil voltage drops completely at the 100 pF high voltage capacitors. It is very important for the transistors to have a low on resistance. The used transistors [6] have a typical on resistance of  $3.1 \Omega$  for a gate source voltage of 4.5 V. This is sufficient to protect the amplifier input.

Although there exist larger transistors with much lower on resistance, another consideration is taken into account for choosing exactly this type of transistor. When the driver is turned off, also the transistors are switched to off state so that the received transponder signal can pass through to the amplifier chain. A larger transistor has a large drain source capacitance  $C_{\text{ds}}$ . This introduces a parasitic capacitive voltage divider between the 100 pF capacitor and  $C_{\text{ds}}$ , what lowers the signal. The chosen transistor has only a typical  $C_{\text{ds}}$  of 6 pF and thus shows a good trade off between on resistance and output capacitance.

The AC coupling resistors in combination with the 100 pF capacitors are used for filtering low frequency components (cut-off frequency = 34 kHz).

## Basestation Receiver Amplifier Chain

The received transponder signal varies between  $1 mV_{\text{pkpk}}$  and  $100 mV_{\text{pkpk}}$ , depending on the distance between basestation and transponder coil and the transponder transmit current amplitude. This requires a dynamic range of 40dB for the amplifier chain. To ensure that the amplifiers are not driven into clipping for large input signals, a gain control is necessary. For

the lowest possible input signal, the gain should be high and for the largest input signal, it should be low (i.e.  $\text{Gain} = 1000$  for  $V_{\text{in}} = 1 \text{ mV}_{\text{pkpk}}$  and  $\text{Gain} = 10$  for  $V_{\text{in}} = 100 \text{ mV}_{\text{pkpk}}$ ). To achieve this, a feedback loop for gain controlling is required. The passive keyless entry block of the presented IC in section 2.1.4 includes a receiver amplifier, which shows exactly the desired behavior. Only a small microcontroller program (see section 4.6.2) is needed to configure some internal test switches so that the amplifier can directly be used as first gain stage of the receiver chain.

The schematic of the amplifier chain is shown in figure 4.12. A gain controlling is achieved by generating a rectified signal from the output of the IC amplifier, which is fed back to regulate the input attenuator, consisting of  $R_{\text{in}}$  and  $M_{\text{atten}}$ . The basestation microcontroller I/O is intended for enabling the amplifier. An external instrumentation amplifier makes a differential to single ended conversion so that the received amplified signal can be measured at the anti-aliasing filter output by only using one oscilloscope probe.

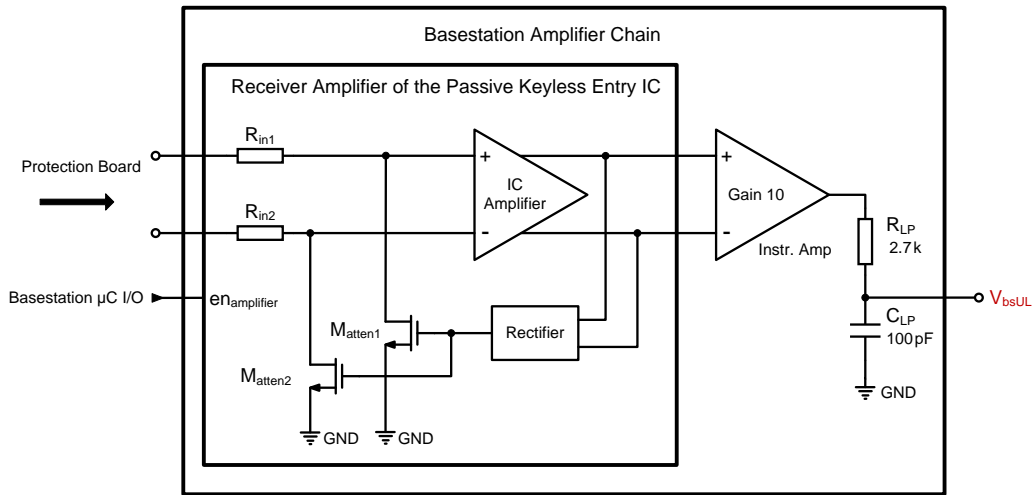


**Figure 4.12:** Schematic of the basestation amplifier chain.

## Complete Basestation Lab Hardware

The complete basestation hardware is shown in figure 4.13. An additional tuning capacitor and Q factor board, which consists of high voltage capacitors and high power resistors, is used for the basestation coil tuning. Both protection board and amplifier chain are controlled by one single microcontroller I/O. Due to the large driving currents, the basestation IC requires a high power DC supply (i.e. a maximum output current of at least 2 A).

## 4.6 Basestation Software

The master control of the hardware is done by the basestation IC microcontroller, but also a separate software is necessary for configuring the gain control of the passive keyless entry IC in the amplifier chain. Both are programmed in C language.

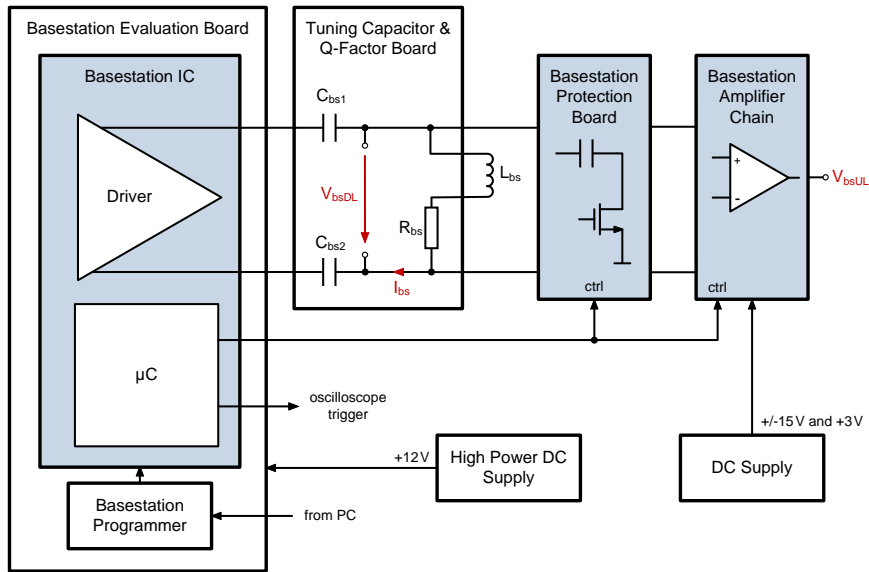


Figure 4.13: Block diagram of the complete basestation hardware.

#### 4.6.1 Driver Software

According to the flow diagram in figure 4.14, the basestation driver software is divided into two parts: *Start Phase* and *Transmit Loop*. In the *Start Phase*, the microcontroller is booted and the necessary parts are initiated. Because the used IC has no EROM for storing the program, it is loaded into the RAM and executed from there.

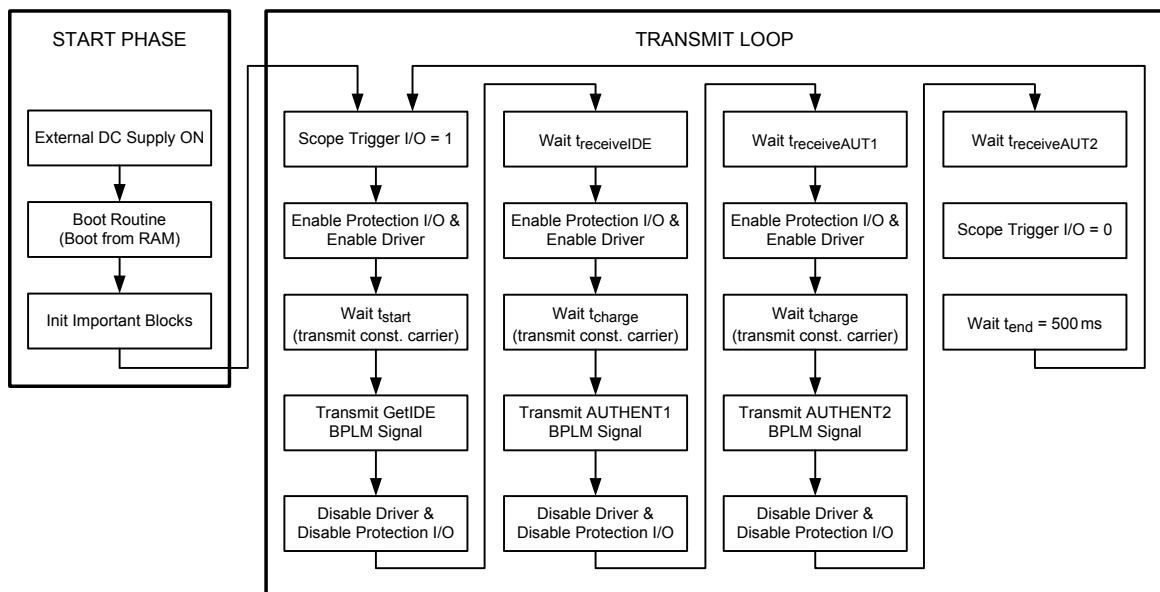


Figure 4.14: Flow diagram of the basestation driver microcontroller software.

A typical immobilizer communication sequence, optimized for the activeTX system, is implemented in the *Transmit Loop*. This sequence includes a command to request the transponder ID and two authentication commands. In a real application, the basestation would only begin

with the authentication when it receives the right transponder ID. Since no BPSK demodulator is available in the lab setup, a transponder response cannot be recognized. Thus, the commands AUTHENT1 and AUTHENT2 are always transmitted, regardless whether the transponder responds or not. The correct transponder behavior can only be validated with an oscilloscope.

The first step in the *Transmit Loop* is to set the I/O pin for triggering the oscilloscope. This has the advantage that the scope's starting point is always the beginning of the communication sequence. In the next step, the I/O for closing the protection NMOST is set and afterwards, the driver is enabled. It is very important that the protection for the receiver amplifier is enabled before the driver starts operating, otherwise the amplifier input can be destroyed immediately. The consecutive state starts the constant carrier for loading the transponder support capacitor, followed by a GetIDE command transmission. Then, the driver is turned off for a user definable time  $t_{\text{receiveIDE}}$  for receiving the transponder ID. Afterwards, the same procedure follows for the AUTHENT1 and AUTHENT2 commands.

At the end, the oscilloscope trigger is set to low and it is waited 500 ms till the loop starts all over again. With this approach, the user is able to increase the distance between basestation and transponder coil during the loop execution, whereby a real-time evaluation of the transponder behavior is possible. For example, at some distance, the harvested transponder energy is too small for operating the IC. The user can directly track on the scope screen at which phase of the communication sequence, the supply drops below the power on reset falling threshold.

As for the transponder microcontroller, also the basestation IC has to be reprogrammed if a setting (i.e. driving current) is changed. To make such a change comfortable for the user, all important settings are organized in the header of the software.

#### 4.6.2 Receiver Amplifier Software

The basestation receiver amplifier software makes it possible to use the controllable gain amplifier of the PKE IC. The flow diagram of the microcontroller software is shown in figure 4.15.

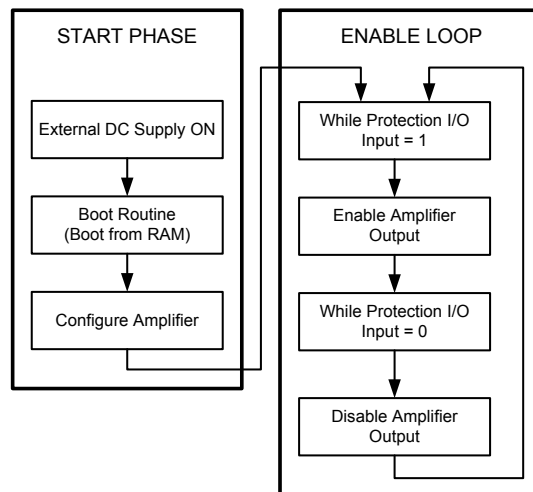


**Figure 4.15:** Flow diagram of the basestation receiver amplifier microcontroller software.

In the *Start Phase*, the microcontroller is booted and afterwards, the amplifier is configured. Because the amplifier output of the IC is only used internally in normal operation, some test switches and test registers have to be set so that the voltage is switched through to an analog test pin.

The *Enable Loop* starts with a wait state, at which the program execution waits as long as the I/O for enabling the protection circuit is high. In the next state, the amplifier output is enabled. Before the output is disabled again, it is waited for the protection I/O to go high. Since the protection I/O is only low during the transponder response, this loop ensures that just the uplink is shown on the amplifier output pin. During the basestation driver ON-time, the amplifier is deactivated because it is not needed.

## 4.7 Complete Lab Setup

The full lab setup meets all requirements from section 4.2. It consists of the following components:

- Mechanical distance setup
- Basestation hardware
- Transponder hardware
- High power DC-supply
- DC-supply
- PC
- Oscilloscope

The block diagram in figure 4.16 shows the location and interconnection of the lab setup parts. Because in a real application, the transponder IC is on the same PCB as the 3D-coil, it must be ensured that also the activeTX transponder boards are connected with short wires. Thus, all transponder parts are located on the distance setup table, where the 3D-coil is attached. The basestation boards are placed outside the distance setup, connected via a long wire with the coil. This is allowed because in a real application, the basestation can also be far away from the coil (i.e. 2m).

The oscilloscope probes are connected to the red marked pins. In the actual setup, it is only possible to measure four signals since this is the number of scope channels. For almost all measurements, four visualized signals are enough because after configuring the basestation, only the transponder signals and the received signal on basestation side are of interest (i.e. connect the scope probes to  $V_{\text{ddc}}$ ,  $V_{\text{trpz}}$ ,  $V_{\text{Isink}}$  and  $V_{\text{bsUL}}$  for a coaxial 1D z-axis coil arrangement). The basestation coil current  $I_{\text{bs}}$  is large enough to be measured accurately with a current probe.

Both basestation and transponder programmer are connected via USB cable to the PC. The scope is externally triggered by the basestation driver microcontroller. An Ethernet connection to the PC allows a remote control of the scope. This ensures that all necessary parts are controllable via PC.

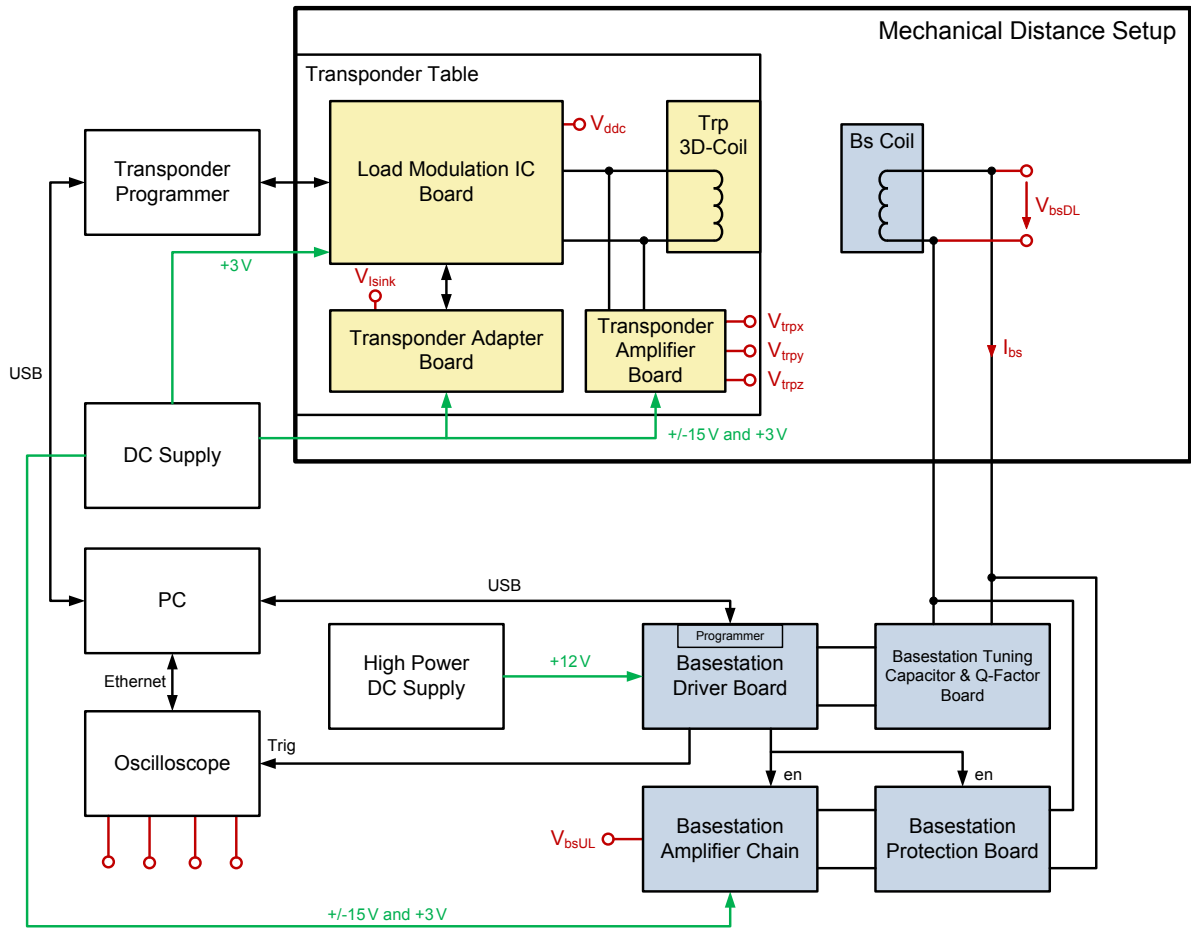


**Figure 4.16:** Block diagram of the complete activeTX lab setup.

### 4.7.1 Configuration Principle of the Lab Setup

If all hardware parts are connected as illustrated in figure 4.16, the lab setup can be started with the following steps:

1. Connect the oscilloscope probes to the wanted signal pins.
2. Set the desired transponder settings in the transponder microcontroller program header.
3. Compile the source code and download it to the load modulation IC. This brings the IC immediately into the activeTX transponder emulation state.
4. Set the desired basestation settings in the basestation driver microcontroller program header.
5. Compile the source code and download it to the basestation driver IC. Now the basestation driver outputs the communication sequence in an endless loop.
6. From this time on, the distance between transponder and basestation coil can be adjusted using the hand wheel of the mechanical distance setup. As the scope is always triggered

at the start of the communication sequence, the transponder behavior can be evaluated in real time during the distance adjustment.

7. To stop the setup, the basestation driver needs to be set into its initial state by pressing a reset button on the basestation evaluation board.

#### 4.7.2 Transponder Current Consumption Measurement Principle

The transponder current consumption consists of the emulated DAC sink current and the frontend current of the load modulation IC. As already explained in section 4.3.2, the emulated current appears as voltage signal on a  $1\text{ k}\Omega$  resistor, which is additionally amplified by an instrumentation amplifier with a gain of 100. Hence, the resulting current can be determined by dividing the measured voltage through  $10^5$ .

Since it is not possible to measure the frontend current consumption during the communication sequence, a special setup is needed to determine the values. The setup uses a pico-ammeter to get the current for a specific supply voltage range in steady state (i.e. vary  $V_{\text{ddc}}$  between 2 and 5 V).

After a communication sequence measurement, these current values have to be added to get the full transponder current consumption. A Matlab post-processing function is implemented for that. The function uses a voltage dependent current source approximation of the real frontend current, similar to the Analog Current Consumption model in section 3.3.3. Of course, a small error results from this approach because the real frontend current is not exactly linearly voltage dependent. Comparison measurements show that the approximation is very accurate up to a certain supply voltage level. A detailed discussion of the deviation at high supply voltages is given in section 5.1.1.

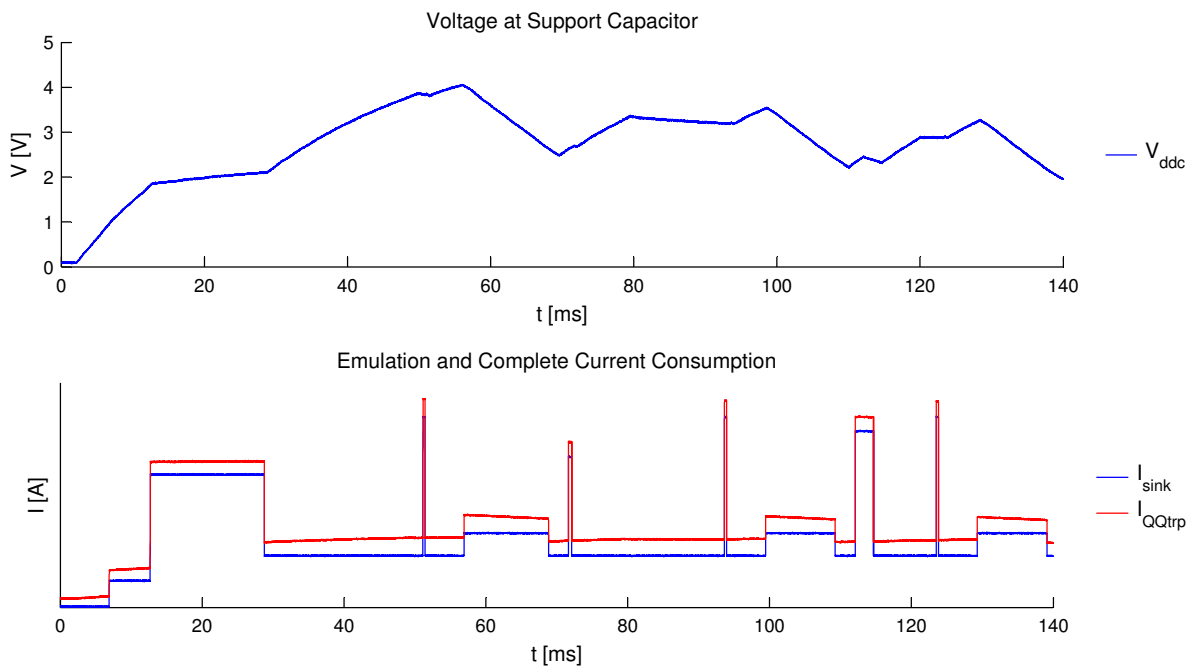


**Figure 4.17:** Signals which explain the complete current consumption principle.

Figure 4.17 illustrates the principle of the complete transponder current consumption determination for a typical communication sequence.  $V_{\text{ddc}}$  and  $I_{\text{sink}}$  (emulated current) are measured with the oscilloscope. Through the post-processing function, the full current consumption  $I_{\text{QQtrp}}$  with included voltage dependent frontend current approximation is generated. It can be seen that  $I_{\text{QQtrp}}$  is slightly dependent on  $V_{\text{ddc}}$ .

### 4.7.3 Measurement GUI

A special Matlab GUI is implemented to visualize the measured lab setup results. This GUI is an adapted version of the presented simulation GUI in section 3.4. To use it, the measurement results need to be saved into a special data struct. When the GUI is invoked with the struct as argument, a visualization of the measured signals, as shown in figure 4.18, is generated. If the struct also contains the simulation results, a direct comparison between model and lab setup is possible by switching on the appropriate check boxes on the right side. In this particular plot, only the measured signals are shown. Please refer to section 3.4 for the meaning of the signals.

Because the struct contains a large amount of measured data, a trade of between oscilloscope sample rate and consumed memory space has to be made. A reasonable sample rate is 2.5 MegaSamples/s. This low sample rate value explains the necessity of the anti aliasing low pass filters for the hardware parts.

Select Settings

- alpha = 90deg || beta = 90deg
- d = 93mm
- d = 95mm
- d = 97mm
- d = 99mm
- d = 100mm
- d = 105mm
- d = 110mm
- d = 112mm
- d = 115mm

alpha = 54.7356deg || beta = 54.7356deg

Coupling	
d (mm)	110
k <sub>x</sub> (%)	0.000
k <sub>y</sub> (%)	0.000
k <sub>z</sub> (%)	0.053
Base_Coil_Type	AIRC01L
Tc_Coil_Type	30C11
Orientation	coaxial
alpha (deg)	90
beta (deg)	90
gamma (deg)	0

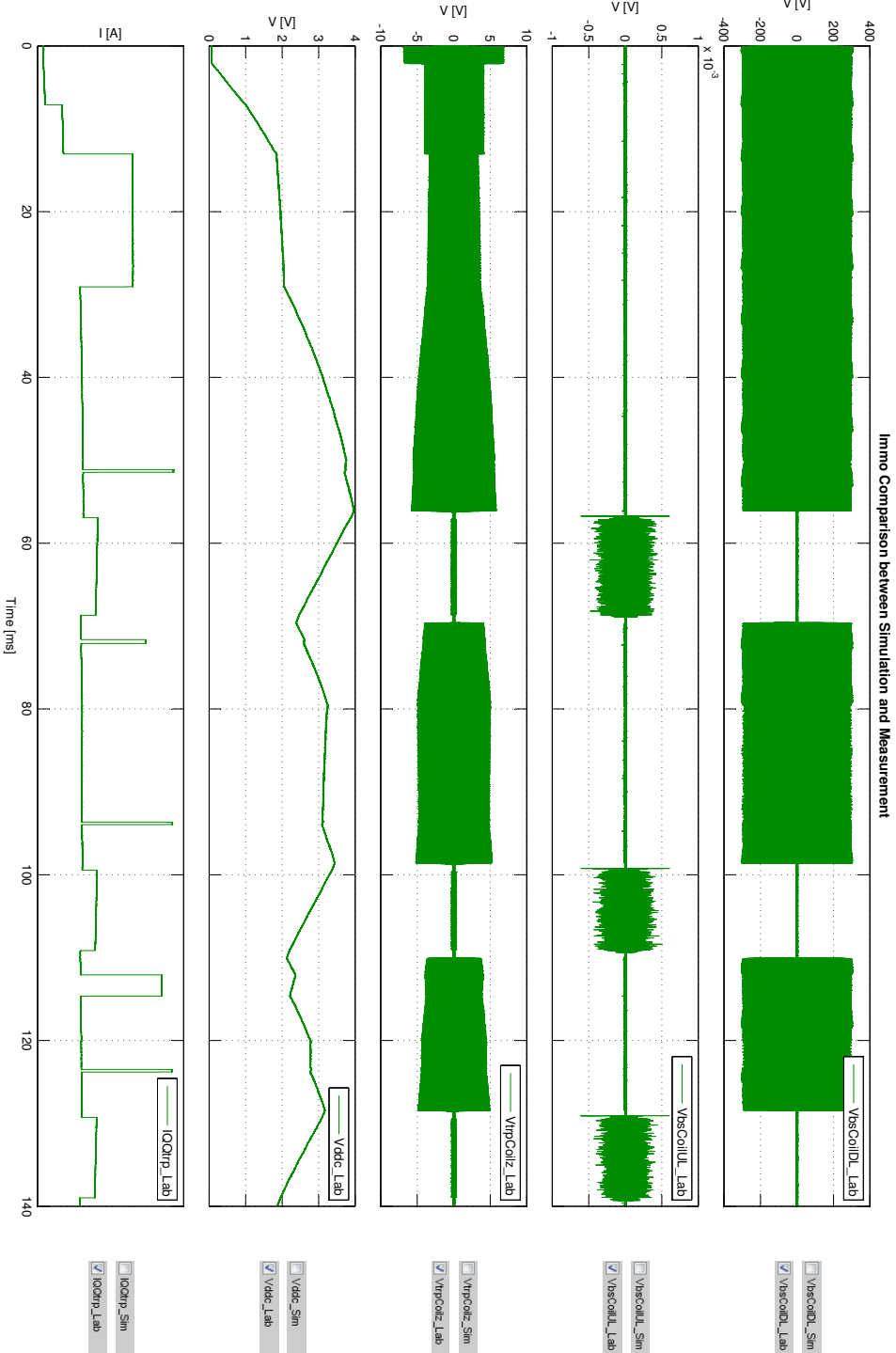


Figure 4.18: GUI for the visualization of the activeTX measurement results

# Chapter 5

## Results

Chapter 5 starts with a comparison between lab setup and Matlab model in section 5.1. The proof that both are consistent is one of the most important goals of this Master's Thesis. Because then, the Matlab model can be used for reliable predictions of the activeTX performance parameters without the need of setting up complicated measurements in the lab (i.e. for checking the effect of coil detuning).

Section 5.2 gives a design example of an activeTX system and shows how the Matlab model is utilized to obtain a specification.

### 5.1 Comparison between Lab Setup and Matlab Model

Using the very accurate mechanical distance setup, the first measurement results showed the required reproducibility and were consistent at first glance. But precise comparisons with the simulation results showed some differences due either parasitics of the lab setup or inaccuracies in the model. All of these differences are discussed in detail in subsection 5.1.1.

After most of the non-idealities could be included in the model, selected comparison plots are shown in subsection 5.1.2.

#### 5.1.1 Explanation of the Differences

The six identified differences between lab setup and model are explained below. At the end, a table follows, which indicates whether the particular non-ideality could be included in the model or not.

##### Transponder 3D Coil Parasitic Coupling

The 3D transponder coil has a parasitic inductive coupling between the three axes with coupling factors up to 3%. Due to the construction type, the coupling between the x- and y-axis shows the largest value. This results from the fact that the coils are located on top of each other. For an ideal case, the coils are arranged in an angle of  $90^\circ$ , what leads to a coupling factor of zero. Inherent inaccuracies of the manufacturing process can easily result in typical coupling factors between  $-1\%$  and  $1\%$ . This corresponds to an arrangement angle of the coils between  $89.4^\circ$  and  $90.6^\circ$ . Even when the coil axes are exactly aligned orthogonally,

a small inductive cross coupling is possible since all of the three axes share the same ferrite core.

The coupling factors differ from coil to coil and thus cannot be determined with the coupling factor model presented in section 3.2.3. The only possibility to get the values for  $k_{xy}$ ,  $k_{xz}$  and  $k_{yz}$  is a determination via an adapted version of the measurement setup from section 3.2.4. For example, a voltage is applied at the x-axis and the coupling factor can be calculated through measuring the induced voltage at the y-axis.

The activeTX 3D-coil Simulink model (see section 3.3.1) already has the parasitic coupling factors included. Hence, the influence of these factors can be demonstrated with a simulation output. Specifically, a coaxial 3D coil arrangement, where each transponder coil axis has the same coupling with the basestation, is simulated. Figure 5.1 shows the loading phase of the support capacitor  $C_{V_{ddc}}$  for a distance of 100 mm with and without parasitic coupling of the transponder coil axes. In case  $k_{xy}=k_{xz}=k_{yz}=1.5\%$ , all axes influence each other, resulting in a parasitic coil detuning. As can be seen in figure 5.1, this is manifested through a flatter loading curve of  $C_{V_{ddc}}$ .

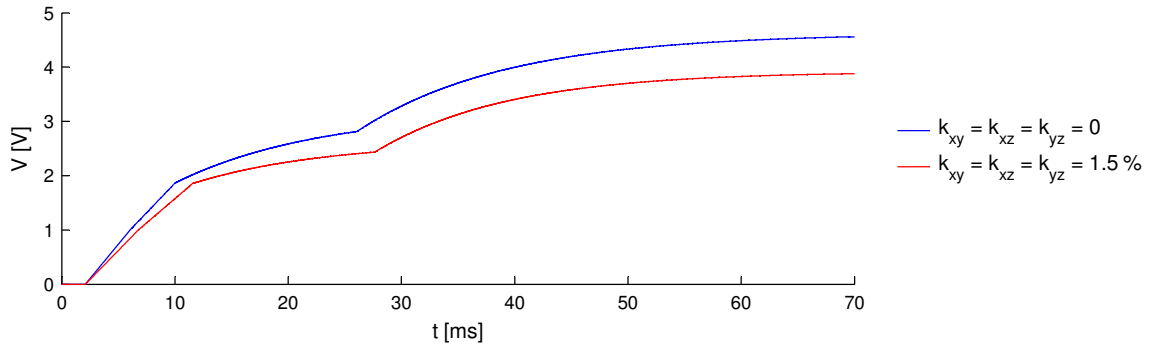


**Figure 5.1:** Simulation output of  $V_{ddc}$  for two different transponder coil cross coupling values.

### Basestation to Transponder Coupling Factor

The implemented basestation to transponder coupling factor model (see section 3.2.3) shows inaccuracies for very small distance values. This can be explained by the assumed simplification of a homogenous field at the complete transponder coil surface, which is not true for small distances.

For distances smaller than 30 mm, a maximum relative error of 3% between measurement and model is possible. Since in this region, the transponder has anyway enough energy, the error is not significant for the purpose of the model. The much more interesting distances are those, which are larger than 100 mm. Here, the error is bounded to 1% and can be neglected because the effective distance error is even smaller due to the relationship:  $k \propto \frac{1}{d^3}$ . For example, at 100 mm, the effective distance error is only 0.33% for a 1% coupling error. Equation 5.1 represents the calculation of this value.

$$\frac{k_1}{k_2} = \left(\frac{d_2}{d_1}\right)^3$$

$$\Rightarrow d_2 = d_1 \cdot \sqrt[3]{\frac{k_1}{k_2}} = 100 \text{ mm} \cdot \sqrt[3]{1.01} = 100.33 \text{ mm} \quad (5.1)$$

$$\Rightarrow \text{error} = \frac{d_2 - d_1}{d_1} = \frac{100.33 \text{ mm} - 100 \text{ mm}}{100 \text{ mm}} = 0.33 \%$$

$d_1$  – ideal distance

$d_2$  – erroneous distance

$k_1$  – ideal coupling factor

$k_2$  – erroneous coupling factor

## Transponder Rectifier Diodes

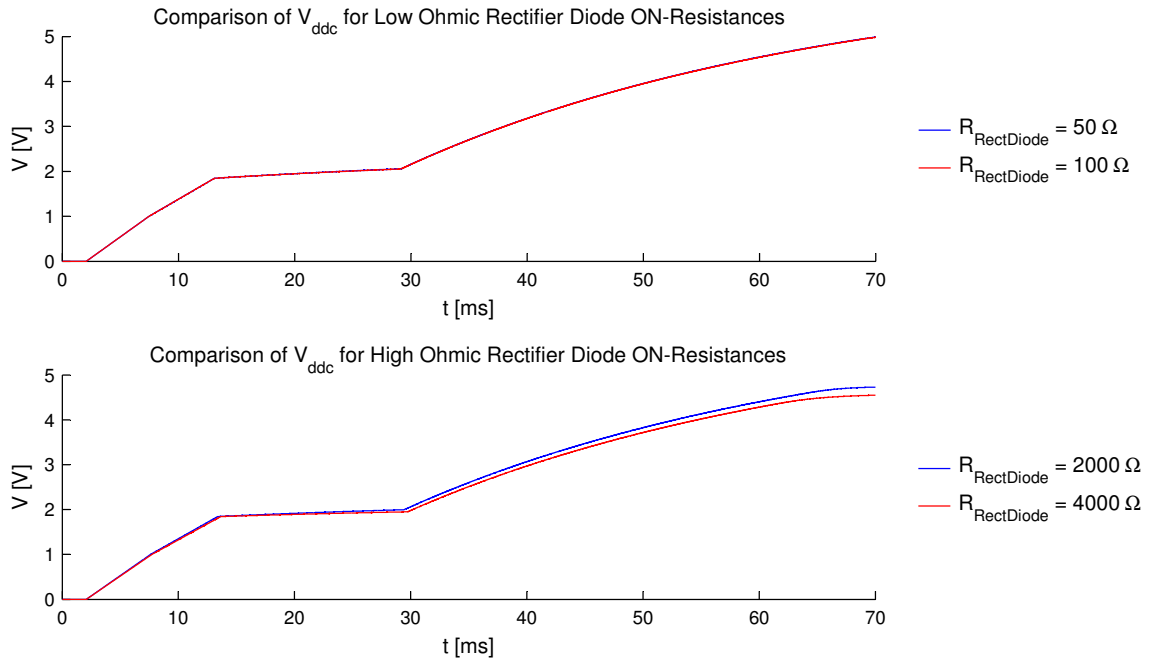


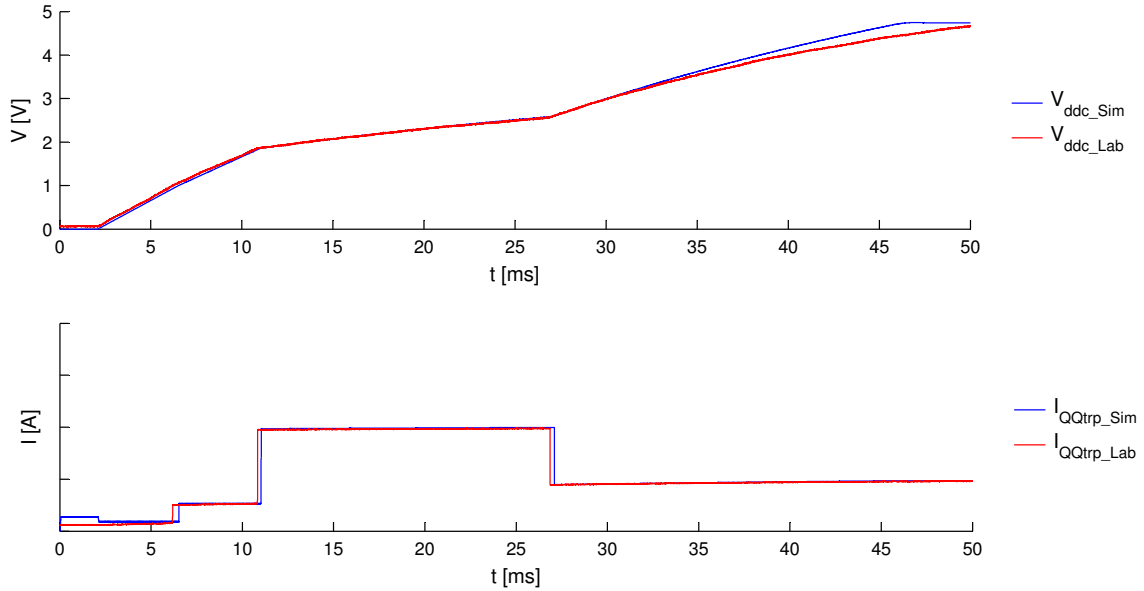
**Figure 5.2:** Simulation comparison of the support capacitor voltage  $V_{ddc}$  for four different rectifier diode on-resistances.

The rectifier diodes of the used load modulation IC are diode-connected MOS transistors, whereas the Simulink model uses a piecewise-linear diode model with a constant resistance in the on-state. If both MOS diode and the modeled diode have a low ohmic on-resistance, the error referred to the harvested energy in the support capacitor  $C_{V_{ddc}}$  is very small, regardless if the on-resistances of model and IC are exactly matched. This is due to the fact that  $C_{V_{ddc}}$  is always loaded immediately when the time constant ( $\tau = R_{RecDiode} \cdot C_{V_{ddc}}$ ) is small enough. Since model and load modulation IC meet this requirement, the error is negligible.

The explained fact can be demonstrated with a simulation. Figure 5.2 shows the harvested transponder supply voltage  $V_{\text{ddc}}$  for four different rectifier diode resistances. The signals for the low ohmic resistances  $50\ \Omega$  and  $100\ \Omega$  do not vary significantly, whereas the signals for the high ohmic resistances  $2000\ \Omega$  and  $4000\ \Omega$  show a difference. Although for both plots, the resistances differ by a factor of 2, only the high ohmic simulation shows a variation of  $V_{\text{ddc}}$  and the above explanation is proven.

### Transponder Limiter Current

In contrast to the model, the limiter of the load modulation IC already begins to decrease the Q factor when the supply voltage is below the limiter threshold level. For example, both model and IC have a limiter clipping value of 5 V (referred to  $V_{\text{ddc}}$ ). Then, due to the internal architecture of the IC, the limiter already begins to draw a small current at 4 V. This reduces the loading of  $C_{\text{Vddc}}$  compared to the model because the modeled limiter current starts not before  $V_{\text{ddc}}$  reaches 5 V.



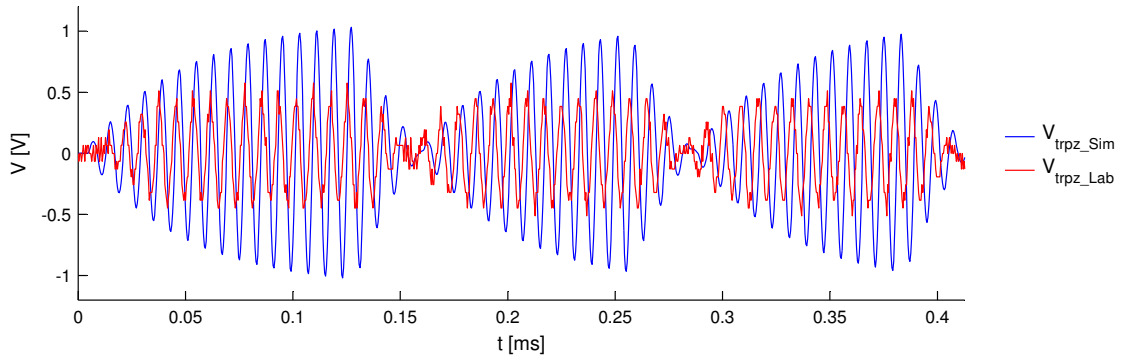
**Figure 5.3:** Demonstration of the inaccuracy of the lab setup limiter current when the supply voltage rises above 4 V

Figure 5.3 shows a comparison between measurement and simulation for  $V_{\text{ddc}}$  and the consumed transponder current  $I_{\text{QQtrp}}$ . Although the currents look the same, the fact that the limiter current is not exactly accurate causes a difference in  $V_{\text{ddc}}$  after 35 ms. After this time, the mentioned condition of a supply voltage level larger than 4 V is met.

### Transponder Active Transmitter

The active transponder transmitter, which is a test feature on the load modulation IC, is implemented as controlled current source that drives a current into one side of the coil, whereas the other side is shorted to ground. This concept is similar to the implemented active transponder transmitter Simulink model explained in section 3.3.3.

The frequency of the applied rectangular current is equal to the transponder coil resonance frequency and the coil voltage reaches its maximum after a few cycles . Because one side of the coil is shorted to ground, the voltage of the other side oscillates around 0 V. Hence, during the negative half cycle, the voltage level is lower than zero. Exactly here is the problem of the inaccuracy between model and lab setup. For voltages lower than -0.3 V, the substrate diode of the transponder begins to conduct. This damps the oscillation, resulting in a smaller emitted magnetic transponder field as in the ideal case.



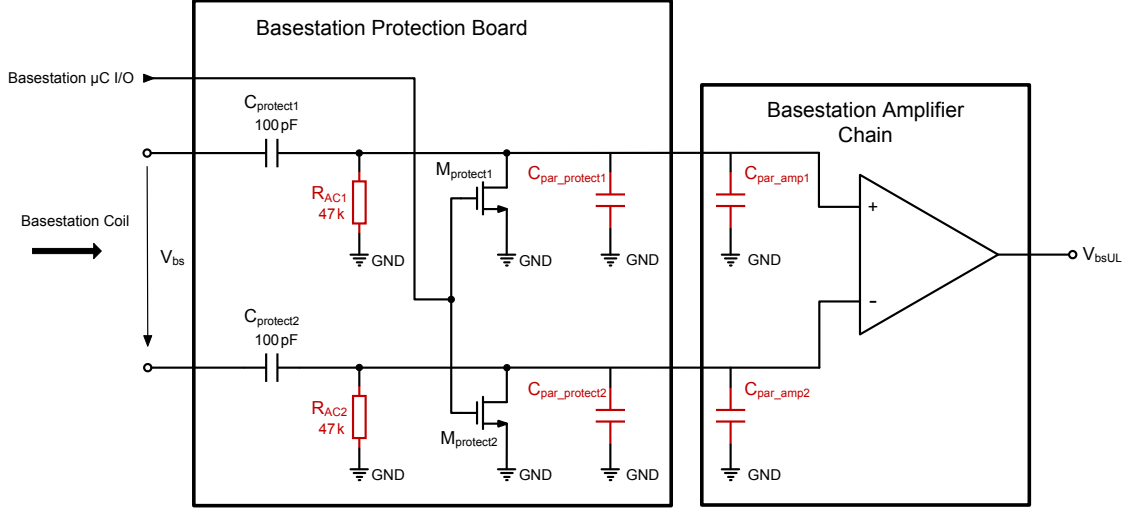
**Figure 5.4:** Demonstration of the load modulation IC substrate diode damping effect, during a typical transponder uplink BPSK communication.

Figure 5.4 illustrates a comparison between simulation and lab setup of the transponder coil voltage for a typical uplink communication. The simulated signal represents the ideal case, while the measured signal shows a smaller amplitude due to the damping of the substrate diode. To include this inaccuracy also in the model, a correction factor is implemented in the active transmitter Simulink model (see figure 3.23). It depends on the used transponder uplink current if the oscillation is damped or not. For example, if the uplink current is small enough so that a theoretical coil voltage amplitude smaller than 0.3 V is generated, the damping can be neglected.

### Basestation Amplifier Chain

For distances larger than 100 mm, the received uplink signal on basestation side is small enough so that the controlled gain feedback loop of the basestation amplifier chain is not active. This means that the gain is at its maximum and thus well known from measurements. To calculate back to the received basestation coil uplink signal, the measured voltage on the amplifier chain output simply needs to be divided by the gain. However, the first comparison showed that the lab setup signal is about a factor of two smaller than the simulated basestation coil uplink signal. Hence, there has to be a parasitic attenuator somewhere in the basestation receiver chain (protection board + amplifier chain).

During the debugging measurements, it was found out that a parasitic voltage divider exists between the 100 pF protection circuit and the amplifier input. Figure 5.5 shows the differential receiver chain with the parasitic impedance components marked in red.



**Figure 5.5:** Schematic of the basestation receiver chain with the parasitic attenuator components marked in red.

These are:

- $R_{AC}$ : Required AC-coupling resistance for suppressing low frequency components
- $C_{par\_protect}$ : Parasitic output capacitance of the protection board. Since the drain source capacitance of the chosen NMOS transistor is only 6 pF, the main contribution to this parasitic is the board capacitance.
- $C_{par\_amp}$ : Amplifier input capacitance, consisting of board and IC input capacitance.

With an impedance analyzer, a value of 60 pF was measured for the parasitic capacitance  $C_{par\_protect} + C_{par\_amp}$  at 125 kHz. Together with the AC coupling resistance, the attenuation is calculated in the following equations:

$$X_{par} = \frac{R_{AC} \cdot \frac{1}{j\omega (C_{par\_protect} + C_{par\_amp})}}{R_{AC} + \frac{1}{j\omega (C_{par\_protect} + C_{par\_amp})}} = 19.34 \cdot e^{-j \cdot 1.15} \text{ k}\Omega \quad (5.2)$$

$$Gain = \left| \frac{X_{par}}{X_{par} + \frac{1}{j\omega C_{protect}}} \right| = 0.62 \quad (5.3)$$

Based on this calculation, an attenuation with a gain of 0.62 occurs on the amplifier input. As the attenuation is a systematic error, it can be included in the comparison by simply multiplying the gain of the receiver chain with this value.

Another difference between lab setup and model appears when the amplifier chain input signal is large enough so that the gain controlling feedback loop starts to decrease the gain. Then, the gain depends on the voltage level of the input signal and is not exactly known. Figure 5.6 shows the case, where the simulated signal, with the gain controlling loop not included in the model, is larger than the measured signal. This results from the fact that the measurement GUI simply divides the measured signal by the maximum gain. As this behavior occurs only for small distance values, the error is not really critical because it is out of the main focus of the model purpose. But it should be kept in mind that the measurement GUI will show a too small received uplink signal for short distances between basestation and transponder coil.

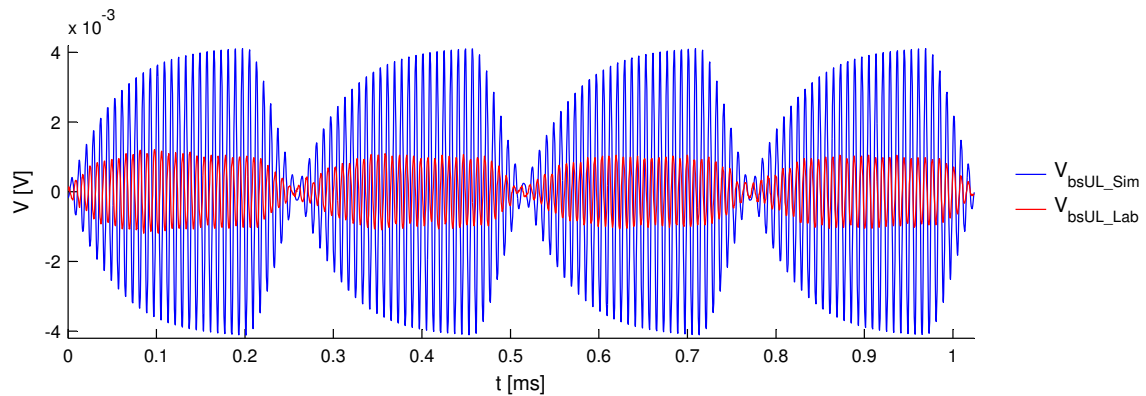


**Figure 5.6:** Demonstration of the basestation receiver chain gain controlling effect for larger amplifier input voltages.

### Summary Table

Table 5.1 indicates whether the identified inaccuracy could be included in the Matlab model or not. If the parasitic is not included, the *Influence* column specifies how the particular inaccuracy affects the consistence between model and lab setup.

Inaccuracy	Included in Model	Influence
Transponder 3D Coil Parasitic Coupling	yes	-
Basestation to Transponder Coupling Factor	no	little influence for small distances
Transponder Rectifier Diodes	no	negligible
Transponder Limiter Current	no	influence if $V_{ddc} > 4\text{ V}$
Transponder Active Transmitter	yes	-
Basestation Amplifier Chain Parasitic Voltage Divider	yes	-
Basestation Amplifier Chain Gain Control Loop	no	Matlab model shows correct value (inclusion of controllable gain is not desired in model)

**Table 5.1:** Summary of the found differences between model and lab setup

### 5.1.2 Comparison Plots

With the mentioned parasitics included in the Matlab model, comparison plots between lab setup and model can be shown. Specifically, a coaxial 1D  $z$ -axis arrangement at a distance of 110 mm is compared. Some important simulation settings are listed in table 5.2. The first plot shows the comparison GUI for the complete communication sequence and the subsequent plots show a zoom into a downlink and uplink communication.

Setting	Symbol	Value
distance between basestation and transponder coil	$d$	110 mm
coupling factor between basestation and transponder coil	$k_z$	0.053 %
basestation inductance	$L_{bs}$	370 $\mu\text{H}$
basestation quality factor	$Q_{bs}$	10
transponder $z$ -axis inductance	$L_{trpz}$	7.37 mH
transponder $z$ -axis quality factor	$Q_{trpz}$	18.5

**Table 5.2:** Settings for the comparison plots

## Complete Communication Sequence

Figure 5.7 shows the measurement GUI for a complete communication sequence comparison. Because of the long protocol timings, the signals  $V_{bsCoilDL}$ ,  $V_{bsCoilUL}$  and  $V_{trpCoilz}$  appear as solid bars. When the user zooms in, each cycle of the 125 kHz carrier can be seen. The most important outcome of this comparison is the fact that the support voltage  $V_{ddc}$  and the transponder current consumption  $I_{QQtrp}$  match very accurately. A perfect matching is of big importance since it is possible to predict the transponder energy distance with these two signals.

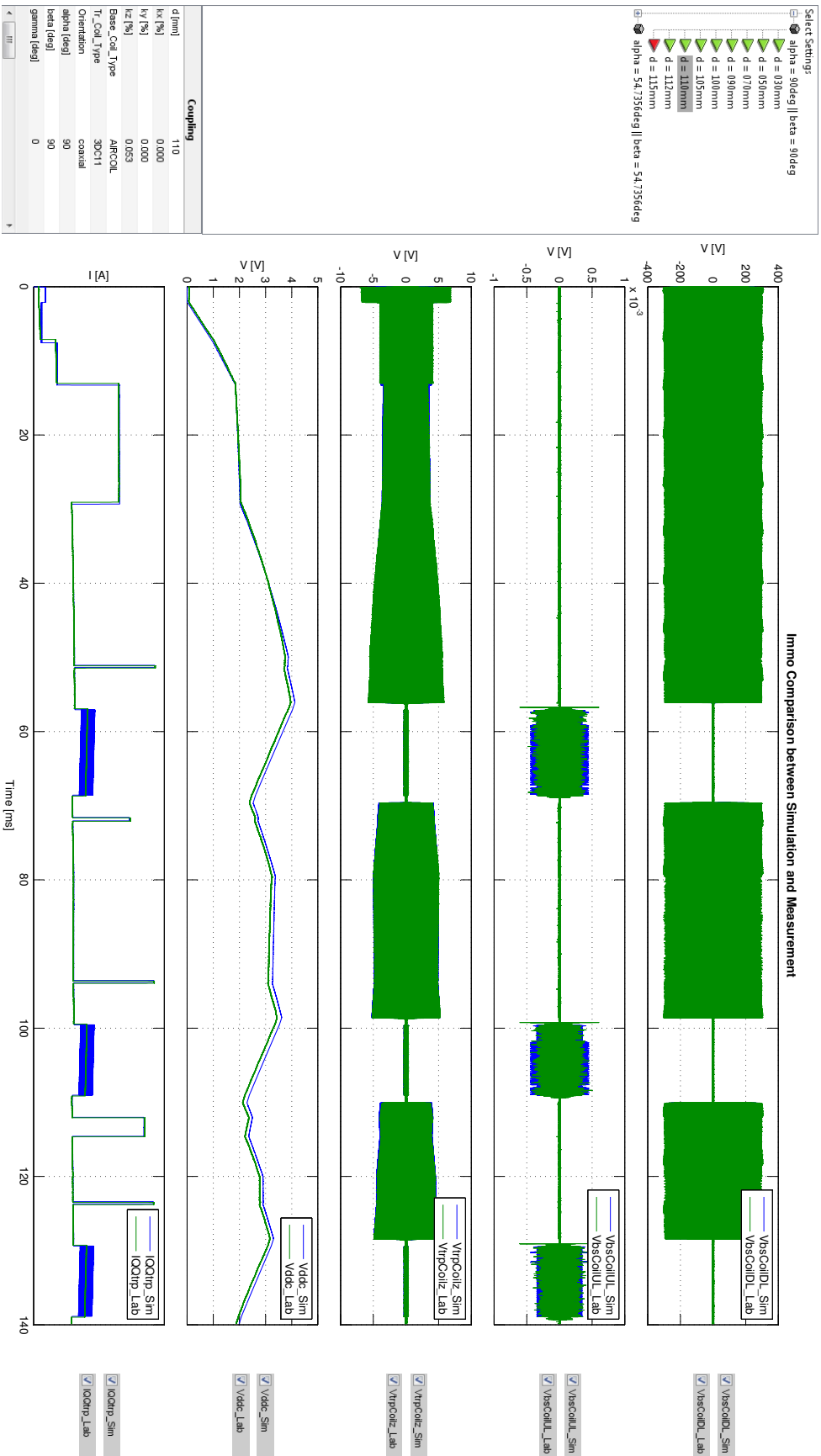
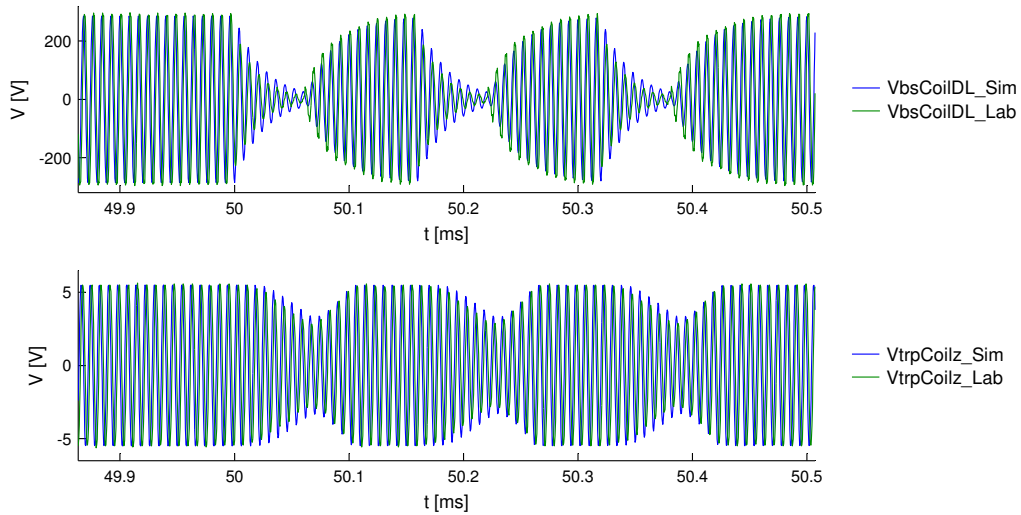


Figure 5.7: Comparison between lab setup and simulation of a complete communication sequence

### Zoom into a Downlink Communication

Figure 5.8 shows a zoom into a downlink communication (i.e. a zoom of figure 5.7 in the interval 49.86 to 50.51 ms). In this case, for both transponder ( $V_{trpCoilz}$ ) and basestation coil voltage ( $V_{bsCoilDL}$ ), a very accurate matching between simulation and lab setup is given.



**Figure 5.8:** Comparison of a downlink communication. (zoom of figure 5.7)

### Zoom into an Uplink Communication

A zoom of an uplink communication (i.e. a zoom of figure 5.7 in the interval 57.07 to 57.87 ms) can be seen in figure 5.9. The actively transmitted transponder signal ( $V_{trpCoilz}$ ) shows a good matching between simulation and lab setup, while the comparison of the received basestation signal ( $V_{bsCoilUL}$ ) shows slightly some deviations. This is due to the additional circuit noise on the very small signal.

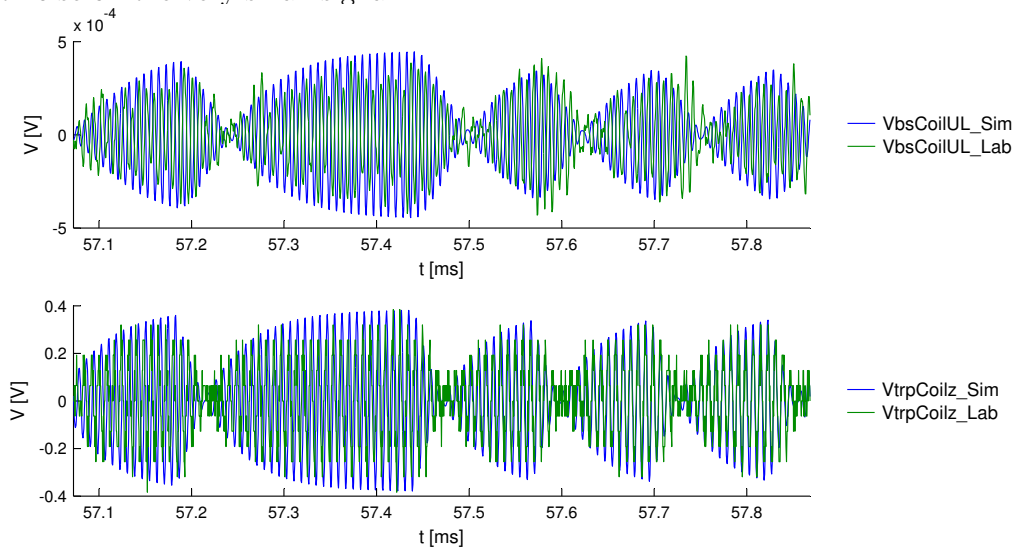


**Figure 5.9:** Comparison of an uplink communication. (zoom of figure 5.7)

### 5.1.3 Discussion

The comparisons were also made for a coaxial 3D arrangement and a different operating point of the system, which includes other transponder current consumption and protocol settings. All of these comparisons show a reliable correspondence between model and lab setup. As now the most important requirement of this Master's Thesis is proven, the activeTX Matlab model can be used for a determination of important system parameters. The example in section 5.2 demonstrates how such a process could look like.

## 5.2 Use Case of the ActiveTX Model

This section contains a design example of a hypothetical 50 kHz activeTX system. Since the lab setup allows only a 125 kHz carrier, the activeTX Matlab model has to be used to analyze the system and to determine the required performance parameters.

In section 5.2.1, the optimum inductances on basestation and transponder side are calculated. A starting value for the transponder support capacitance is determined in section 5.2.2. The system optimization, using the activeTX Matlab model, is explained in section 5.2.3. Finally, a possible specification of the most important performance parameters is given in section 5.2.4.

### 5.2.1 Coil Inductance Calculation

#### Basestation

It is assumed that a basestation driver is available, which is capable of generating a sinusoidal voltage of  $30 V_{pk}$  and a maximum current of  $2 A_{pk}$ . When the series resonance circuit is perfectly tuned, the impedances of the coil and the tuning capacitance cancel each other out. Thus, the current is defined only by the ohmic resistance. To have enough bandwidth for transmitting a BPLM downlink command, the Q factor shall be smaller than 10.

The conditions for maximizing the basestation field are:

1. Use the maximum available driver current since it is proportional to the magnetic field.
2. Use the maximum possible inductance because the magnetic field is proportional to the square root of the inductance.

The formula for the quality factor of the basestation series resonance circuit is given in equation 5.4.

$$Q_{bs} = \frac{\omega L_{bs}}{R_{bs}} \Rightarrow L_{bs} = \frac{Q_{bs} \cdot R_{bs}}{\omega} \quad (5.4)$$

This leads to the conclusion that the basestation inductance can be increased by maximizing both quality factor and resistance. The maximum allowed Q factor of 10 is used. In order to maximize the ohmic resistance of the resonance circuit, also the maximum driver output voltage has to be applied. The final values for the coil inductance ( $L_{bs}$ ), resistance ( $R_{bs}$ ) and tuning capacitor ( $C_{bs}$ ) are calculated in equation 5.5.

$$\begin{aligned}
R_{bs} &= \frac{V_{driver\_max}}{I_{driver\_max}} = \frac{30 \text{ V}}{2 \text{ A}} = 15 \Omega \\
L_{bs} &= \frac{Q_{bs} \cdot R_{bs}}{\omega} = \frac{10 \cdot 15 \Omega}{2\pi \cdot 50 \text{ kHz}} = 477 \mu\text{H} \\
C_{bs} &= \frac{2}{\omega^2 \cdot L_{bs}} = \frac{2}{(2\pi \cdot 50 \text{ kHz})^2 \cdot 477 \mu\text{H}} = 21.2 \text{ nF}
\end{aligned} \tag{5.5}$$

### Transponder

The optimum transponder inductance for energy transfer is calculated with a steady state representation of the system, where only one transponder coil axis is considered. The associated equivalent circuit is shown in figure 5.10.

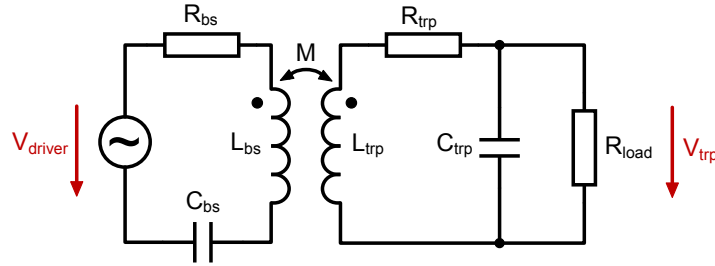


**Figure 5.10:** Steady state equivalent circuit diagram for the determination of the optimum transponder coil inductance.

When the distance between basestation and transponder is large (i.e. more than 70 mm), the mutual inductance is small enough so that the parasitic detuning of the resonance circuits (due to the magnetic coupling) can be neglected. This approximation is valid because the transponder inductance has to be optimized only for large distances. For a perfect tuning, the relation between basestation driver voltage ( $V_{driver}$ ) and transponder coil voltage ( $V_{trp}$ ) can be given with the following formulas.

$$V_{trp} = k \cdot V_{driver} \cdot Q_{bs} \cdot \sqrt{\frac{L_{trp}}{L_{bs}}} \cdot Q_{trp} \tag{5.6}$$

with,

$$Q_{trp} = \frac{R_{load} \cdot Q_{trp\_unloaded}}{R_{load} + \omega L_{trp} \cdot Q_{trp\_unloaded}} \tag{5.7}$$

resulting in,

$$V_{trp} = k \cdot V_{driver} \cdot Q_{bs} \cdot \sqrt{\frac{L_{trp}}{L_{bs}}} \cdot \frac{R_{load} \cdot Q_{trp\_unloaded}}{R_{load} + \omega L_{trp} \cdot Q_{trp\_unloaded}} \tag{5.8}$$

- $k$  – coupling factor between basestation and transponder coil
- $R_{load}$  – transponder average load
- $Q_{trp\_unloaded}$  – unloaded transponder coil Q factor
- $Q_{trp}$  – transponder coil Q factor with included load resistance

The transponder current consumption is approximated with an average load resistance  $R_{load}$  of 100 k $\Omega$ . This value comes from the assumption of an average transponder current consumption of 30  $\mu$ A at 3 V ( $\frac{3V}{30\mu A} = 100\text{ k}\Omega$ ). Figure 5.11 shows a sweep over  $L_{trp}$  by using formula 5.8 with a transponder coil unloaded Q factor of 15.

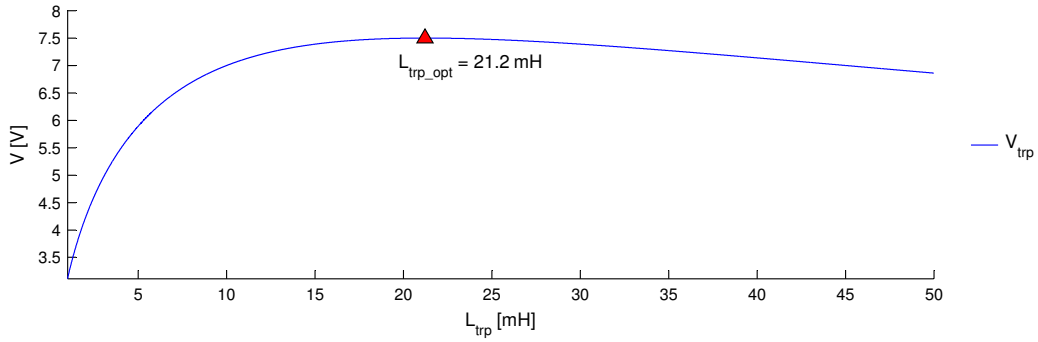


**Figure 5.11:** Sweep over the transponder coil inductance for the determination of the optimum value.

The plot shows a global maximum for  $V_{trp}$  at 21.2 mH. This inductance value has to be used to optimize the transponder energy distance. Finally, the remaining values for  $R_{trp}$  and  $C_{trp}$  are calculated in the following equations..

$$R_{trp} = \frac{\omega L_{trp}}{Q_{trp\_unloaded}} = \frac{2\pi \cdot 50\text{ kHz} \cdot 21.2\text{ mH}}{15} = 444\ \Omega \quad (5.9)$$

$$C_{trp} = \frac{1}{\omega^2 \cdot L_{trp}} = \frac{1}{(2\pi \cdot 50\text{ kHz})^2 \cdot 21.2\text{ mH}} = 477\text{ pF}$$

## 5.2.2 Calculation of the Transponder Support Capacitance

When the transponder transmits a BPSK command, the basestation magnetic field is turned off. During this time, the transponder supplies itself only from the energy stored in the support capacitor  $C_{V_{ddc}}$ . With the requirement of a maximal voltage drop at  $V_{ddc}$  of 1.5 V ( $V_{drop\_max}$ ) during the uplink and four additional requirements (see table 5.3), the minimum capacitance value of  $C_{V_{ddc}}$  can be calculated.

Additional Requirement	Symbol	Value
transponder idle current consumption	$I_{QQtrp\_idle}$	$30 \mu\text{A}$
average transmit current	$I_{trp\_ul}$	$10 \mu\text{A}$
uplink baudrate	$BR_{ul}$	3125 Bd
maximum number of transmit bits	$num_{ul\_bits\_max}$	45

**Table 5.3:** Settings for the comparison plots

The used approximation formula (see equation 5.10) for the capacitance calculation assumes a constant drawn current from  $C_{V_{ddc}}$  during the uplink. With the maximum allowed voltage drop and 2 ms extra margin for the maximum transmission time,  $C_{V_{ddc}}$  has to be at least 437 nF. Referring to the E6 capacitance table, the closest larger value is 470 nF.

$$\begin{aligned}
t_{ul\_max} &= \frac{1}{BR_{ul}} \cdot num_{ul\_bits\_max} = \frac{1}{3125} \cdot 45 = 14.4 \text{ ms} \\
C_{V_{ddc\_min}} &= \frac{(I_{QQtrp\_idle} + I_{trp\_ul}) \cdot (t_{ul\_max} + 2 \text{ ms})}{V_{drop\_max}} \\
&= \frac{(30 \mu\text{A} + 10 \mu\text{A}) \cdot (14.4 \text{ ms} + 2 \text{ ms})}{1.5 \text{ V}} = 437 \text{ nF}
\end{aligned} \tag{5.10}$$

A value of 680 nF for  $C_{V_{ddc}}$  would indeed result in a lower voltage drop. But the big disadvantage is a longer protocol duration due to longer charge times. Thus, a capacitance value of 470 nF will be used for the further investigations.

### 5.2.3 System Optimization

With the needed inductance and capacitance values defined above, the activeTX Matlab model is simulated to find out the maximum transponder operating distance for certain protocol definitions. A coaxial 1D z-axis arrangement is used as reference configuration for the basestation and transponder coil. The first distance sweep simulation with the charge times listed in table 5.4 predicts a maximum transponder operating distance of 105 mm. Figure 5.12 shows the corresponding basestation coil voltage ( $V_{bsDL}$ ), induced transponder coil voltage ( $V_{trpz}$ ), support capacitor voltage ( $V_{ddc}$ ) and transponder current consumption ( $I_{QQtrp}$ ) with an included definition of the charge times. A simulation for a distance of 110 mm predicts that the transponder will stop operating at a time of 158 ms because  $V_{ddc}$  is too small.

Charge Time Setting	Symbol	Value
starting charge time	$t_{\text{start}}$	50 ms
charge time after downlink communication	$t_{\text{charge1}}$	3 ms
charge time after uplink communication	$t_{\text{charge2}}$	5 ms

**Table 5.4:** Charge time settings for the simulation output shown in figure 5.12

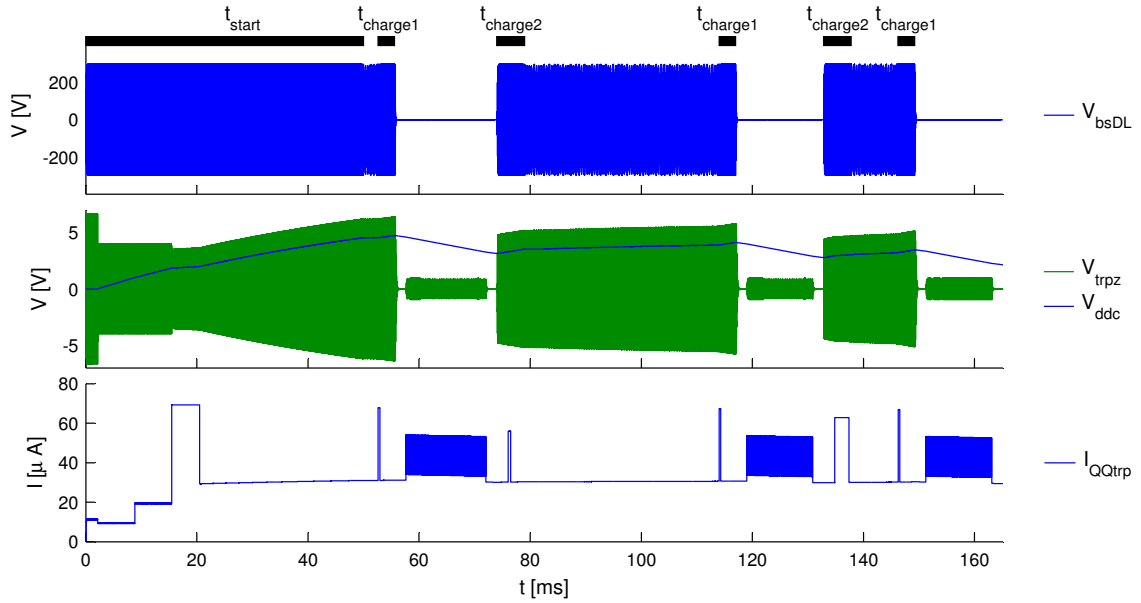


**Figure 5.12:** Simulation output of the 50 kHz system at a distance of 105 mm between basestation and transponder coil.

In the next step, the charging times are increased to the values shown in table 5.5. This results in a total protocol duration of 272 ms, which is very long, but still suitable for an immobilizer application.

Charge Time Setting	Symbol	Value
starting charge time	$t_{\text{start}}$	100 ms
charge time after downlink communication	$t_{\text{charge1}}$	12 ms
charge time after uplink communication	$t_{\text{charge2}}$	20 ms

**Table 5.5:** Charge time settings for the second distance sweep

With the new charge times, the outcome of the distance sweep is a transponder operating distance of 115 mm, which is 10 mm larger compared to the first simulation. Another in-

vestigation can be made with an increase of the transponder Q factor from 15 to 20 and a decrease of the average transponder uplink current by 25 %. A Q factor increase results in a bandwidth decrease on transponder side. Thus, it has to be shown via simulation that the received downlink signal on transponder side can be demodulated for the whole distance range. Since the model also includes a transponder demodulator, such an investigation is possible. A distance sweep shows a regular transponder reception for all simulated distances. The transponder operating distance increases to 120 mm for the new settings.

Another interesting question is, how much the transponder operating distance can be increased, if a better basestation with a maximum driver current ( $I_{bs}$ ) of 3 A and a better transponder with half of the average current consumption ( $I_{QQtrp\_idle}$ ) would be available. The simulation output shows an operating distance of 160 mm. Because such a large basestation driver current and small transponder current consumption are technically very hard to realize, this distance value is more of theoretical interest.

Table 5.6 shows a summary of all above explained simulations. It includes the used simulation settings and two important specification values: transponder operating distance ( $d_{trp\_op}$ ) and amplitude of the received uplink signal on basestation side at the operating distance ( $V_{bsUL\_pk}$ ). The technically realistic system settings of **Sim 3** are now analyzed in more detail in the next section.

	charge times	$Q_{trp}$	$I_{trp\_ul}$	$I_{QQtrp\_idle}$	$I_{bs}$	$d_{trp\_op}$	$V_{bsUL\_pk}$
<b>Sim 1</b>	from table 5.4	15	10 $\mu$ A	30 $\mu$ A	2 A	105 mm	820 $\mu$ V
<b>Sim 2</b>	from table 5.5	15	10 $\mu$ A	30 $\mu$ A	2 A	115 mm	630 $\mu$ V
<b>Sim 3</b>	from table 5.5	20	7.5 $\mu$ A	30 $\mu$ A	2 A	120 mm	490 $\mu$ V
<b>Sim 4</b>	from table 5.5	20	7.5 $\mu$ A	15 $\mu$ A	3 A	160 mm	210 $\mu$ V

**Table 5.6:** Summary table of the 50 kHz simulations

#### 5.2.4 System Specification

The given operating distance of the **Sim 3** settings (see table 5.6) assumes an ideal 1D z-axis arrangement and no parasitic coil detuning. To give a feasible specification, also a 3D arrangement and the worst case coil detuning have to be simulated. For the 3D arrangement, the case with each coil having the same misalignment angle is simulated since this is the worst case for the induced transponder coil voltages. A detuning value of +/-5 % is assumed for both coil's resonance frequency. The outcome shows the worst case operating distance occurring for a 3D arrangement with -5 % transponder coil detuning (the basestation coil detuning has no effect). The worst case received basestation uplink voltage amplitude occurs also in the 3D case, but for a basestation coil detuning of -5 % and a transponder coil detuning of 5 %.

By using the activeTX Matlab model for an evaluation of the 50 kHz system, the following important worst case parameters can now be specified for the **Sim 3** settings in table 5.6:

- transponder operating distance: **110 mm**
- smallest received basestation uplink signal amplitude: **150  $\mu$ V<sub>pk</sub>**



# Chapter 6

## Conclusion

This document presents a model for a new immobilizer concept, called *activeTX*. In cooperation with *NXP Semiconductors Austria*, a Matlab- and fully functional lab model were developed. Through an exact comparison between model and lab setup, it is proven that both are consistent. This allows the usage of the model as reliable prediction tool for the future basestation and transponder development process at NXP. The results have shown that a larger operating distance of the system, which is the most important advantage compared to the currently available *Load Modulation* concept, can be reached.

The lab setup is already in use as first demonstration hardware of the whole system. Also the development of the setup helped a lot in determining possible problems for the future design. The proven accuracy of the Matlab model is of incomparably more importance since this allows a valuable prediction of the system's efficiency. To give an example, the document also contains an analysis of a 50 kHz *activeTX* system by using the Matlab model.

Although all project goals have been fulfilled, some future tasks for an improvement of the model can be defined. These are outlined in the outlook.

### 6.1 Outlook

The configuration of different protocol settings in the lab setup requires the basestation and transponder microcontroller to be reprogrammed using the associated programming tool. To make a protocol change more comfortable, an automation is desirable. A possible approach would be an automation with the software *LabVIEW* from *National Instruments*, which should provide the user a simple graphical user interface for a protocol reconfiguration. This requires also changes in the basestation and transponder software so that the LabVIEW program is able to communicate with the ICs (i.e. via Serial Peripheral Interface (SPI)).

With the current basestation lab implementation, the received transponder response can only be visualized with an oscilloscope because no BPSK demodulator is available on basestation side. A second future task would be the development of such a demodulator. Because the required analog receiver amplifier chain was already implemented in this Master's Thesis, the simplest approach would be the implementation of an all-digital demodulator on either a Digital Signal Processor (DSP) or an FPGA. The integration of the demodulator in the LabVIEW automation would improve the setup to a complete *activeTX* immobilizer system solution with both communication directions included.

# List of Figures

2.1	Block diagram of an inductively coupled RFID system. . . . .	6
2.2	Diagram of FDX, HDX and SEQ over time. [7, p. 40] . . . . .	7
2.3	Block diagram of a circuit for a load modulation signal generation. [7, p. 44] . . . . .	7
2.4	Baseband signal of a pulse pause coding sequence. [7, p. 181] . . . . .	8
2.5	Implementation of a mutual symmetrical authentication. [7, p. 227] . . . . .	9
2.6	Block diagram of an automotive transponder IC developed by <i>NXP Semiconductors</i> . [18] . . . . .	10
2.7	Block diagram of an automotive basestation IC developed by <i>NXP Semiconductors</i> . [17] . . . . .	11
2.8	Basic diagram of an immobilizer system. [4] . . . . .	12
2.9	Simplified diagram of the activeTX immobilizer system. . . . .	13
2.10	Voltage behavior at the external support capacitor of the activeTX transponder during different communication phases. . . . .	14
3.1	Simulink basic block model versus Simscape toolbox model. . . . .	18
3.2	Reference coils. . . . .	20
3.3	Coaxial 1D z-axis arrangement. . . . .	20
3.4	Coplanar 3D arrangement. . . . .	21
3.5	Basic diagram of coupled coils. [7, p. 67] . . . . .	22
3.6	Circuit diagram of coupled coils. . . . .	23
3.7	Parameter illustration for the inductance approximation formula. [19] . . . . .	24
3.8	Coil equivalent circuit. . . . .	24
3.9	Basestation magnetic field z-component in coaxial and coplanar direction. . . . .	26
3.10	RMS z-component of the emitted basestation magnetic field in coaxial direction with $I_{bs} = 1 A_{pk}$ . . . . .	26
3.11	Misalignment angle between transponder and basestation coil. . . . .	26
3.12	Vector interpretation for the derivation of equation 3.13. . . . .	28
3.13	k-factor plot of the coaxial 1D z-axis arrangement. . . . .	29
3.14	Block diagram of the k-factor measurement setup. . . . .	29
3.15	Coupling factor comparison between measurement and model. . . . .	30
3.16	Overview of the activeTX Simulink model . . . . .	33
3.17	3D-coil Simscape model. . . . .	34
3.18	Basestation Simulink model. . . . .	35
3.19	Simulated basestation driver and coil voltages for the component values defined in table 3.2. . . . .	35
3.20	Rectifier & Limiter Simulink model. . . . .	36
3.21	Simulation output comparison for a transponder with and without limiter. . . . .	37

3.22	Simulation output comparison for a transponder with and without frozen limiter enabled. . . . .	38
3.23	Active Transmitter Simulink model. . . . .	39
3.24	Simulation output of a transponder transmitted BPSK sequence. . . . .	39
3.25	Demodulator Simulink model. . . . .	40
3.26	Simulation output of the transponder demodulation function. . . . .	41
3.27	Simulation output of the supply capacitor voltages. . . . .	42
3.28	Analog Current Consumption model. . . . .	42
3.29	Digital Current Consumption model. . . . .	43
3.30	Diagram of a typical digital current consumption profile. . . . .	43
3.31	Principle diagram of the activeTX Matlab top level script. . . . .	44
3.32	GUI for visualizing the activeTX simulation results, containing a passed communication . . . . .	49
3.33	GUI for the visualization of a failed communication . . . . .	50
4.1	Linear bearing with included material description. [11] . . . . .	53
4.2	Mechanical distance setup in 1D z-axis arrangement. . . . .	53
4.3	Distance setup in coaxial 3D arrangement. . . . .	54
4.4	Distance setup in coplanar 1D z-axis arrangement. . . . .	54
4.5	Overview of the required hardware setup. . . . .	56
4.6	Functional diagram of the chosen current DAC. [1] . . . . .	58
4.7	Schematic of the transponder adapter board. . . . .	59
4.8	Transponder amplifier board with connected 3D coil. . . . .	60
4.9	Block diagram of the complete transponder hardware. . . . .	61
4.10	Flow diagram of the transponder microcontroller software. . . . .	62
4.11	Schematic of the basestation protection board. . . . .	64
4.12	Schematic of the basestation amplifier chain. . . . .	65
4.13	Block diagram of the complete basestation hardware. . . . .	66
4.14	Flow diagram of the basestation driver microcontroller software. . . . .	66
4.15	Flow diagram of the basestation receiver amplifier microcontroller software. . . . .	67
4.16	Block diagram of the complete activeTX lab setup. . . . .	69
4.17	Signals which explain the complete current consumption principle. . . . .	70
4.18	GUI for the visualization of the activeTX measurement results . . . . .	72
5.1	Simulation output of $V_{\text{ddc}}$ for two different transponder coil cross coupling values. . . . .	74
5.2	Simulation comparison of the support capacitor voltage $V_{\text{ddc}}$ for four different rectifier diode on-resistances. . . . .	75
5.3	Demonstration of the inaccuracy of the lab setup limiter current when the supply voltage rises above 4 V . . . . .	76
5.4	Demonstration of the load modulation IC substrate diode damping effect, during a typical transponder uplink BPSK communication. . . . .	77
5.5	Schematic of the basestation receiver chain with the parasitic attenuator components marked in red. . . . .	78
5.6	Demonstration of the basestation receiver chain gain controlling effect for larger amplifier input voltages. . . . .	79
5.7	Comparison between lab setup and simulation of a complete communication sequence . . . . .	82
5.8	Comparison of a downlink communication. (zoom of figure 5.7) . . . . .	83
5.9	Comparison of an uplink communication. (zoom of figure 5.7) . . . . .	83

5.10 Steady state equivalent circuit diagram for the determination of the optimum transponder coil inductance. . . . . 85

5.11 Sweep over the transponder coil inductance for the determination of the optimum value. . . . . 86

5.12 Simulation output of the 50 kHz system at a distance of 105 mm between basestation and transponder coil. . . . . 88

# List of Tables

2.1	Comparison between activeTX and load modulation concept . . . . .	15
3.1	Inductance and winding values of the reference coils . . . . .	25
3.2	Settings for the simulation output in figure 3.19 . . . . .	35
3.3	Settings for the simulation output in figure 3.21 . . . . .	38
3.4	Comparison of the simulation time for an explicit and implicit solver . . . . .	47
4.1	Comparison between the two realization approaches for the mechanical setup . . . . .	52
5.1	Summary of the found differences between model and lab setup . . . . .	80
5.2	Settings for the comparison plots . . . . .	80
5.3	Settings for the comparison plots . . . . .	87
5.4	Charge time settings for the simulation output shown in figure 5.12 . . . . .	88
5.5	Charge time settings for the second distance sweep . . . . .	88
5.6	Summary table of the 50 kHz simulations . . . . .	89
A.1	Measured and modelled coupling factor values for a coaxial z-axis arrangement . . . . .	99
B.1	Milled parts . . . . .	101



# Bibliography

- [1] Analog Devices. *DAC 08*, 11 2004. Rev. C.
- [2] Univ.-Prof. Dipl.-Ing. Dr.techn. Oszkar Biro. *Theorie der Elektrotechnik (engl.)*. Institut für Grundlagen und Theorie der Elektrotechnik, 2014.
- [3] Burr-Brown Corporation. *INA111AP*, 3 1998. PDS-1143E.
- [4] MITSUBISHI ELECTRIC. Immobilizer system. [http://www.mitsubishielectric.com/bu/automotive/products/safety\\_and\\_security2/safe10.html](http://www.mitsubishielectric.com/bu/automotive/products/safety_and_security2/safe10.html), 09 2014.
- [5] Wikipedia: The Free Encyclopedia. Immobiliser. <http://en.wikipedia.org/wiki/Immobiliser>, 09 2014.
- [6] Fairchild Semiconductor. *FDV301N*, 6 2009. Rev. F1.
- [7] Klaus FINKENZELLER. *RFID Handbook: Fundamentals and Applications in Contactless Smart Cards, Radio Frequency Identification and Near-Field Communication*. John Wiley & Sons, 3 edition, 2010.
- [8] Michael Gebhart. *Vorlesung RFID Systems, VO: Einige Grundlagen der magnetischen Nahfeld-Kopplung*. Graz University of Technology, 2009.
- [9] EGGGER Handels GmbH. *TECHNISCHE KUNSTSTOFFE*.
- [10] Manfred Pauritsch GmbH. , 8054 Graz, Glesingerstraße 44.
- [11] igus. <http://www.igus.at/>, 10 2014.
- [12] Philippe DONDON-J.M MICOULEAU-J. LEGALL-P.KADIONIK. Design of a low cost bpsk modulator/demodulator for a practical teaching of digital modulation techniques. *Engineering Education, Agios Nicholas : Greece*, version 1:6, 2008.
- [13] MathWorks. *Simscape<sup>TM</sup> User's Guide*, 3.3 edition, March 2010.
- [14] MathWorks. Choosing a solver. <http://www.mathworks.nl/help/simulink/ug/choosing-a-solver.html>, 10 2014.
- [15] MathWorks. Simulating dynamic systems. [http://www.mathworks.nl/help/simulink/ug/simulating-dynamic-systesim\\_matlams.html](http://www.mathworks.nl/help/simulink/ug/simulating-dynamic-systesim_matlams.html), 10 2014.
- [16] MathWorks. Simulink product description. <http://www.mathworks.nl/help/simulink/gs/product-description.html>, 09 2014.

- [17] NXP Semiconductors. *PJF7992A Advanced Base Station IC 2nd Gen. (ABIC 2)*, 01 2012.
- [18] NXP Semiconductors. *NCF2971 KEyLink Lite 3D*, 01 2013. Rev. 03.
- [19] University of Surrey. An introduction to the air cored coil. [http://info.ee.surrey.ac.uk/Workshop/advice/coils/air\\_coils.html](http://info.ee.surrey.ac.uk/Workshop/advice/coils/air_coils.html), 10 2014.
- [20] Eugen Philippow. *Grundlagen der Elektrotechnik*. Verlag Technik Berlin, 200.
- [21] PREMO. <https://www.grupopremo.com/>, 10 2014.
- [22] Behzad Razavi. *Design of Analog CMOS Integrated Circuits*. McGAW-HILL, international edition, 2001.
- [23] K. Simonyi. *Theoretische Elektrotechnik*. Barth Verlagsgesellschaft mBh, 1993.

# Appendix A

## Coupling Factor Values

The measured and modeled coupling factors over distance for a coaxial z-axis arrangement are shown in table A.1. For the plotted curve, please refer to figure 3.15.

d [mm]	k <sub>meas</sub> [%]	k <sub>model</sub> [%]	d [mm]	k <sub>meas</sub> [%]	k <sub>model</sub> [%]
5	12.1640	11.7537	100	0.0713	0.0704
10	8.7727	8.7165	105	0.0621	0.0610
15	5.9246	5.8728	110	0.0544	0.0533
20	3.8719	3.8547	115	0.0476	0.0468
25	2.5721	2.5573	120	0.0420	0.0413
30	1.7676	1.7403	125	0.0373	0.0366
35	1.2337	1.2196	130	0.0330	0.0326
40	0.8946	0.8795	135	0.0294	0.0292
45	0.6553	0.6511	140	0.0263	0.0262
50	0.5022	0.4935	145	0.0238	0.0236
55	0.3884	0.3818	150	0.0216	0.0214
60	0.3054	0.3009	155	0.0195	0.0194
65	0.2447	0.2409	160	0.0178	0.0177
70	0.2002	0.1957	165	0.0163	0.0161
75	0.1659	0.1610	170	0.0149	0.0148
80	0.1363	0.1339	175	0.0138	0.0135
85	0.1148	0.1126	180	0.0126	0.0125
90	0.0980	0.0955	185	0.0116	0.0115
95	0.0840	0.0817	190	0.0106	0.0106

**Table A.1:** Measured and modelled coupling factor values for a coaxial z-axis arrangement



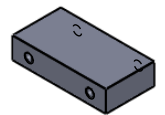
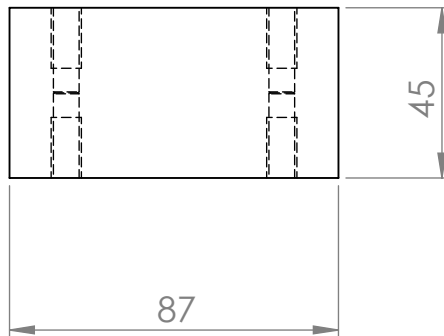
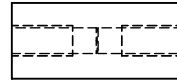
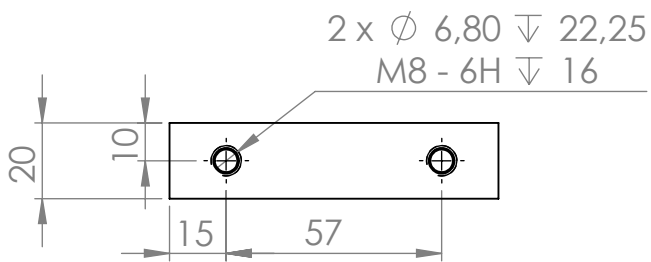
## Appendix B

# Mechanical Distance Setup Drawings

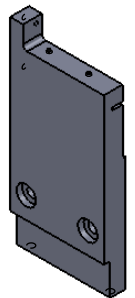
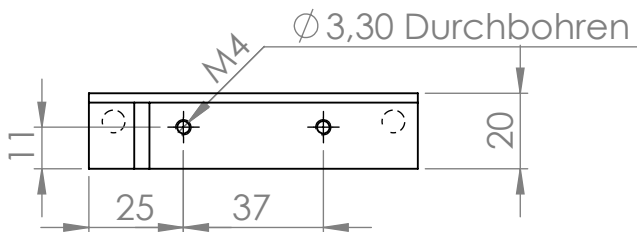
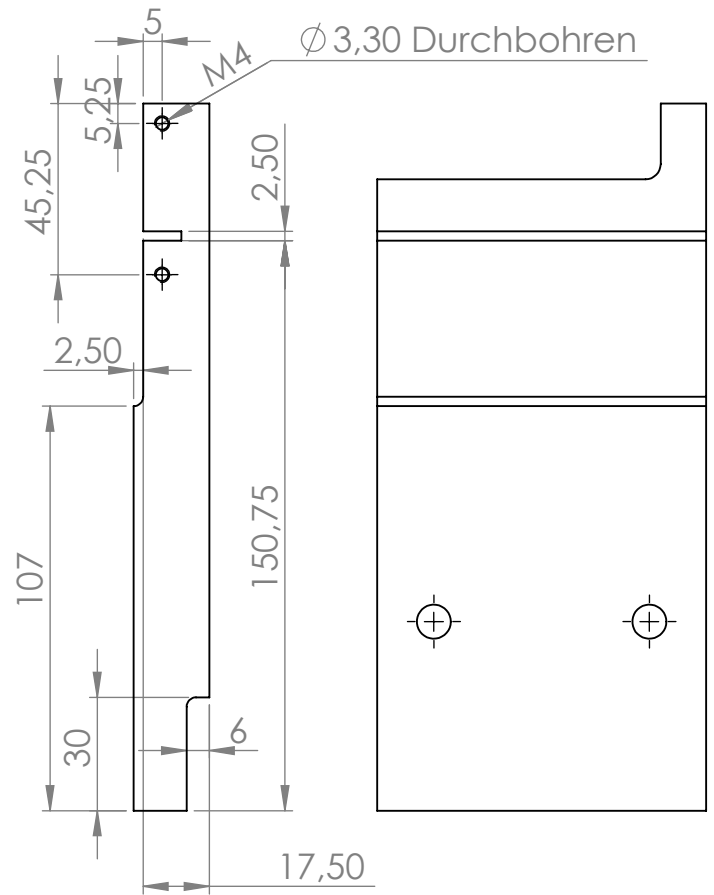
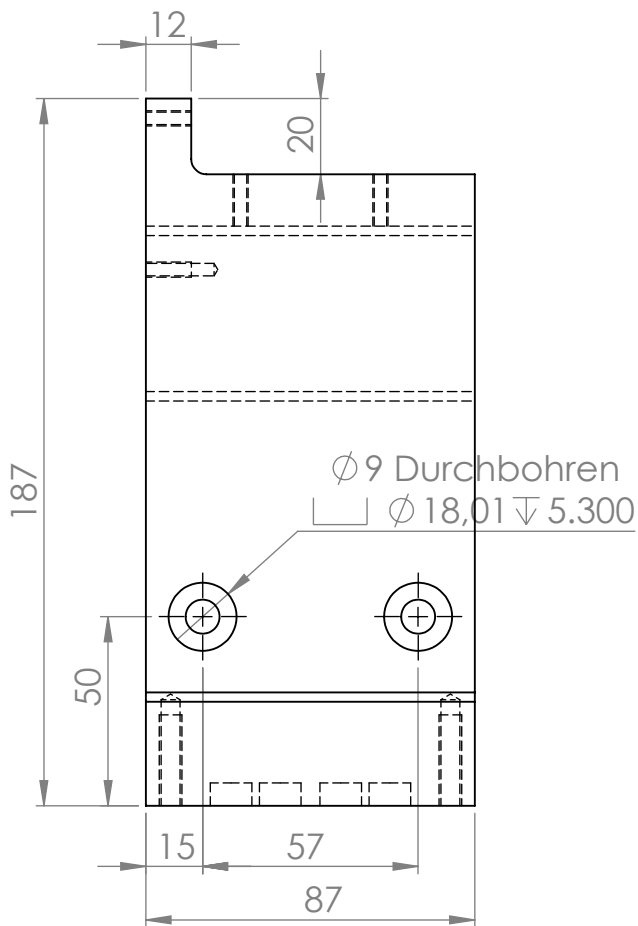
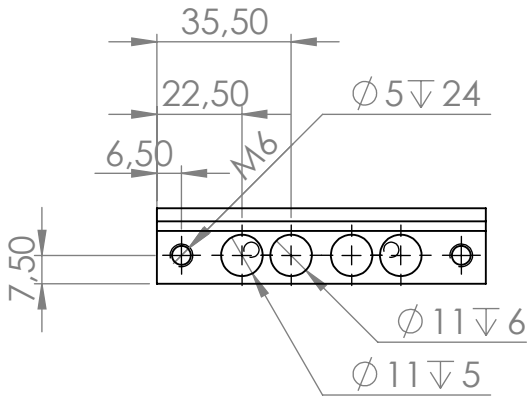
The manufacturing drawings of the milled parts, listed in table B.1, were created by [10]. The linear bearing (Spindel-Lineartisch) is a prefabricated component from [11].

No.	Name
1	Slide_center
2	Slide_left_side
3	Slide_right_side
4	Socket
5	Stop_10
6	Stop_15
7	Stop_20
8	Table_left_side
9	Table_right_side
10	Table_socket
11	Table_top
12	Transponder_Block_1D
13	Transponder_Block_3D

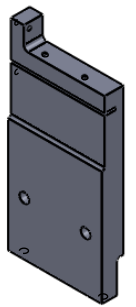
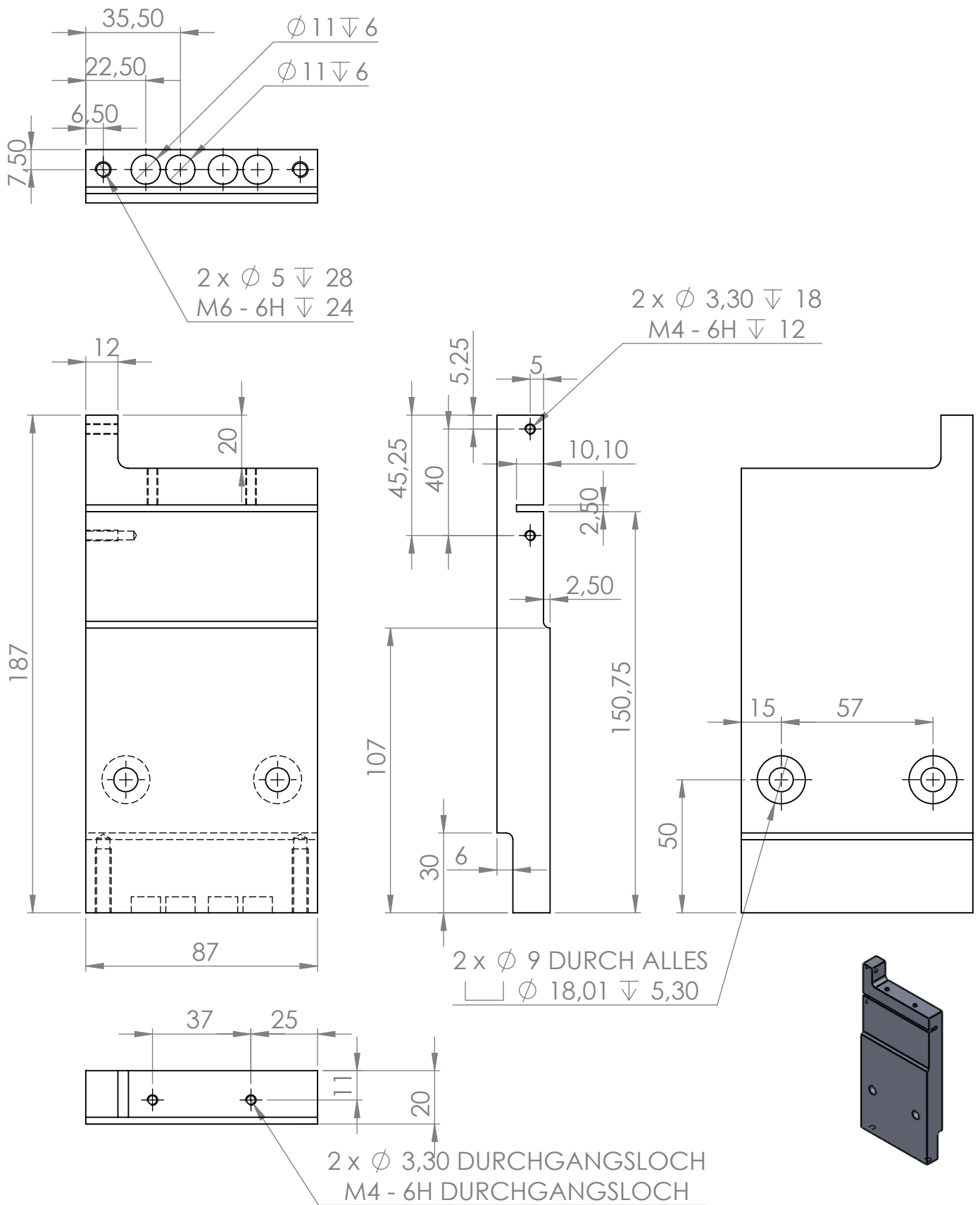
**Table B.1:** Milled parts



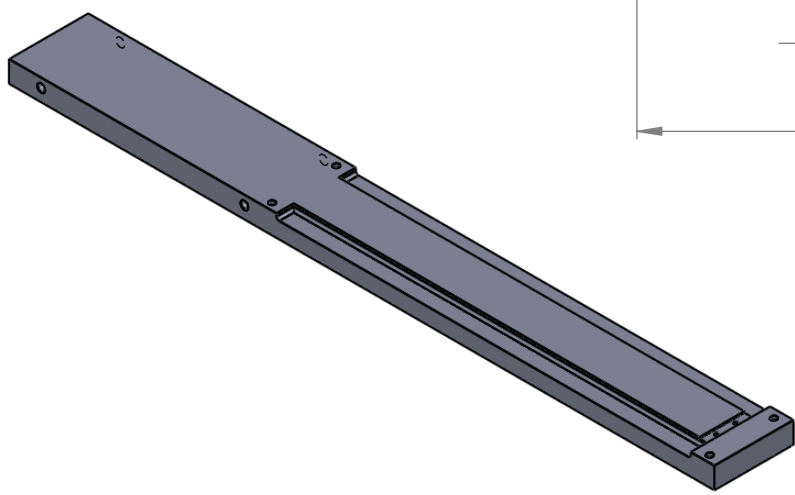
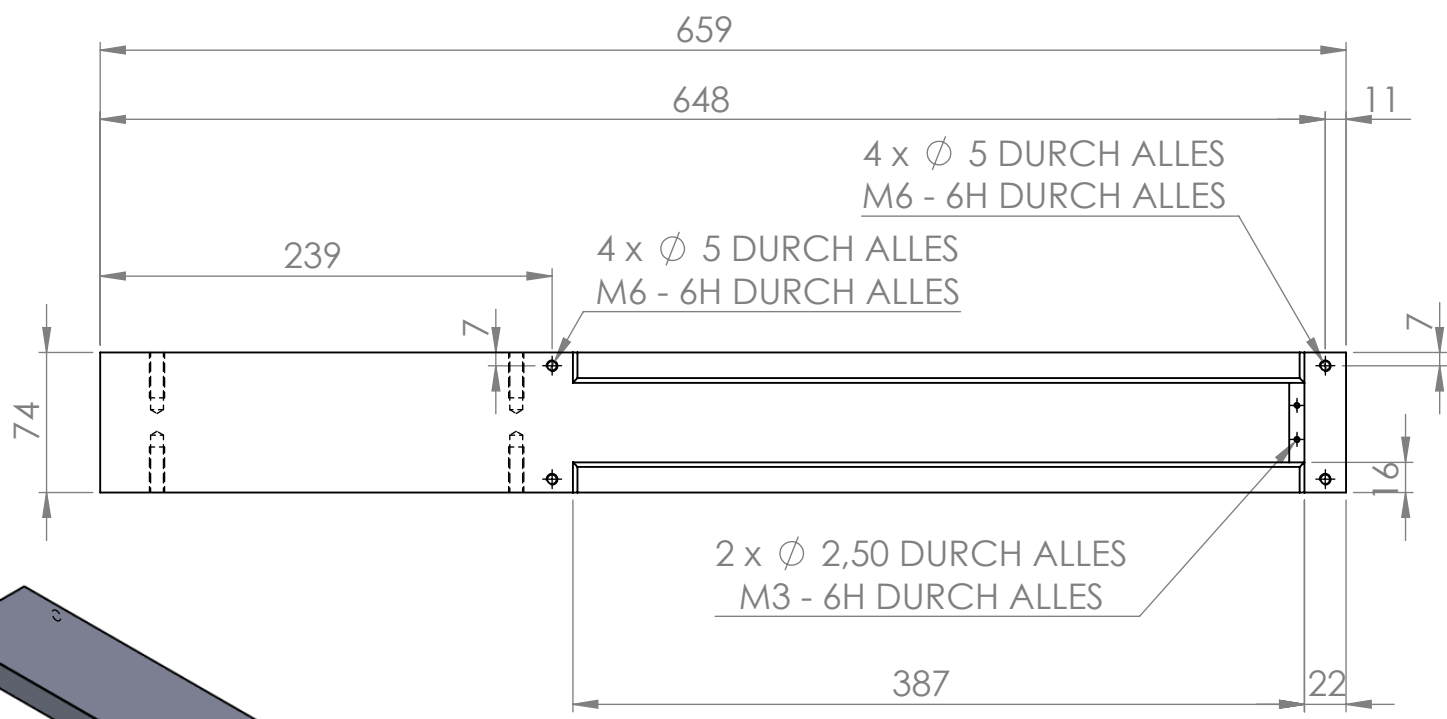
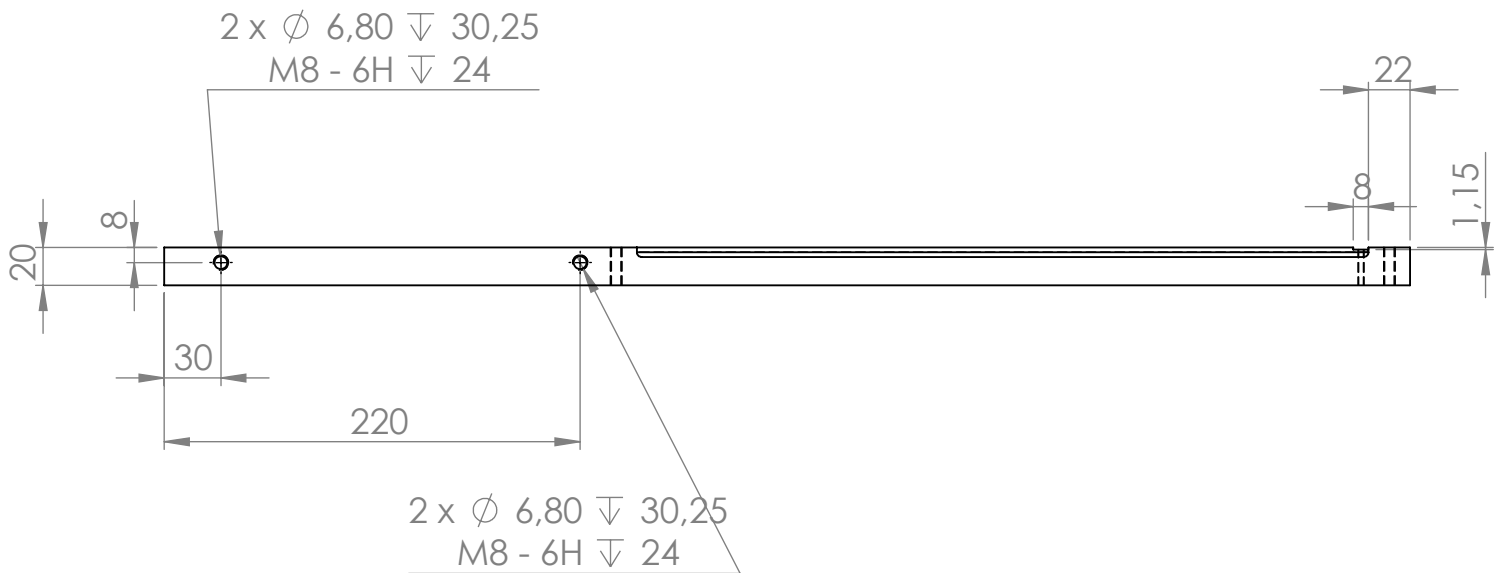
WENN NICHT ANDERS DEFINIERT: BEMASSUNGEN SIND IN MILLIMETER	WERKSTOFF	ENTGRATEN UND SCHARFE KANTEN BRECHEN	
	POM-C		MASSTAB:1:2
			TEIL
			Slide_center
			BLATT 1 VON 1



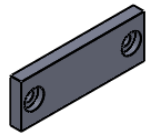
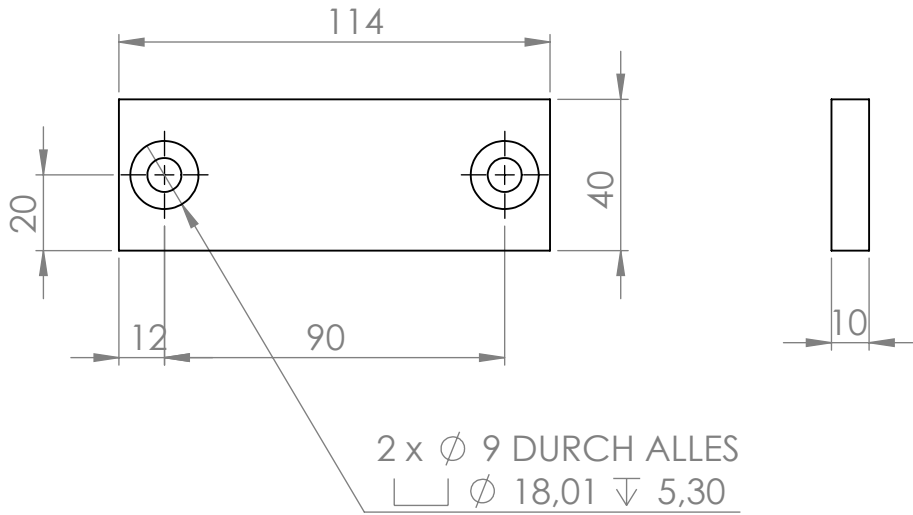
WENN NICHT ANDERS DEFINIERT: BEMASSUNGEN SIND IN MILLIMETER	WERKSTOFF	ENTGRATEN UND SCHARFE KANTEN BRECHEN	
	POM-C		MASSTAB:1:2
			TEIL
			Slide_left_side
			BLATT 1 VON 1



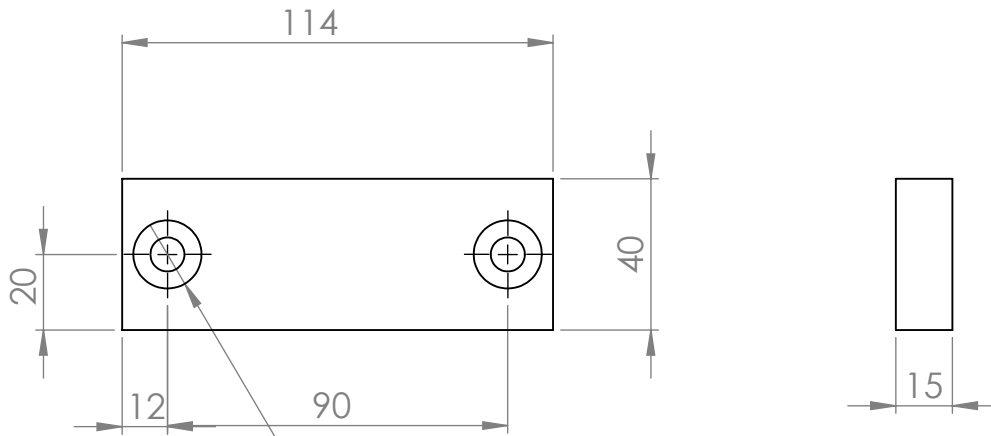
WENN NICHT ANDERS DEFINIERT: BEMASSUNGEN SIND IN MILLIMETER	WERKSTOFF POM-C	ENTGRATEN UND SCHARFE KANTEN BRECHEN	MASSTAB:1:2
			TEIL Slide_right_side
			BLATT 1 VON 1



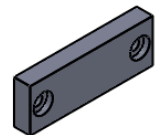
WENN NICHT ANDERS DEFINIERT: BEMASSUNGEN SIND IN MILLIMETER	WERKSTOFF	POM-C	ENTGRATEN UND SCHARFE KANTEN BRECHEN	MASSTAB:1:4
				TEIL
				Socket
				BLATT 1 VON 1



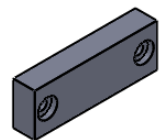
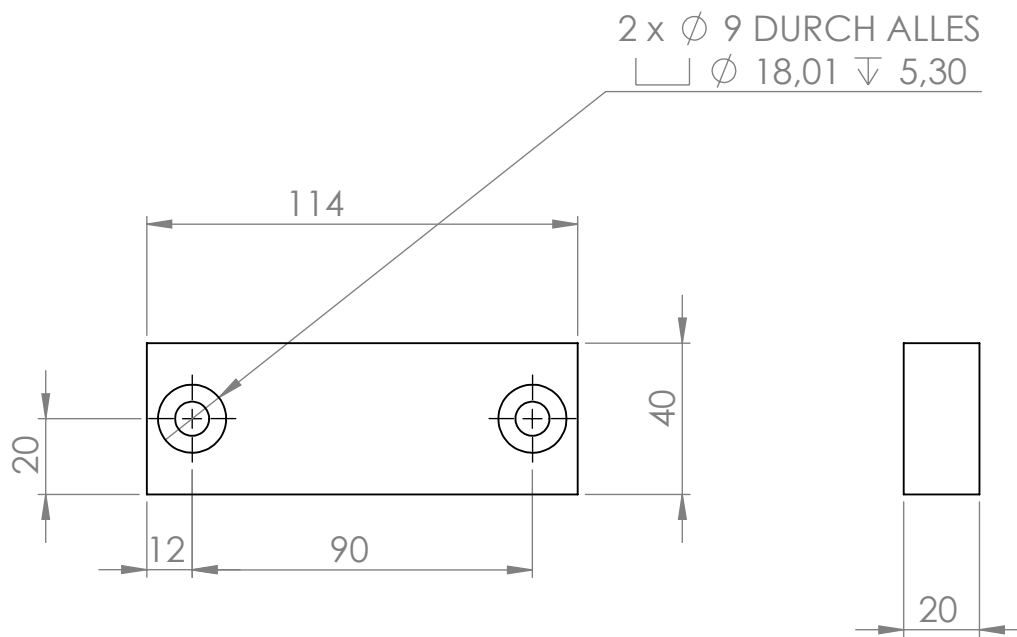
WENN NICHT ANDERS DEFINIERT: BEMASSUNGEN SIND IN MILLIMETER	WERKSTOFF  POM-C	ENTGRATEN UND SCHARFE KANTEN BRECHEN	
			MASSTAB:1:2
			TEIL
			Stop_10
			BLATT 1 VON 1



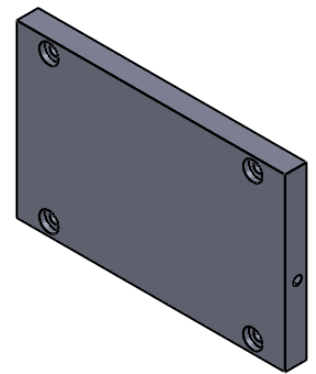
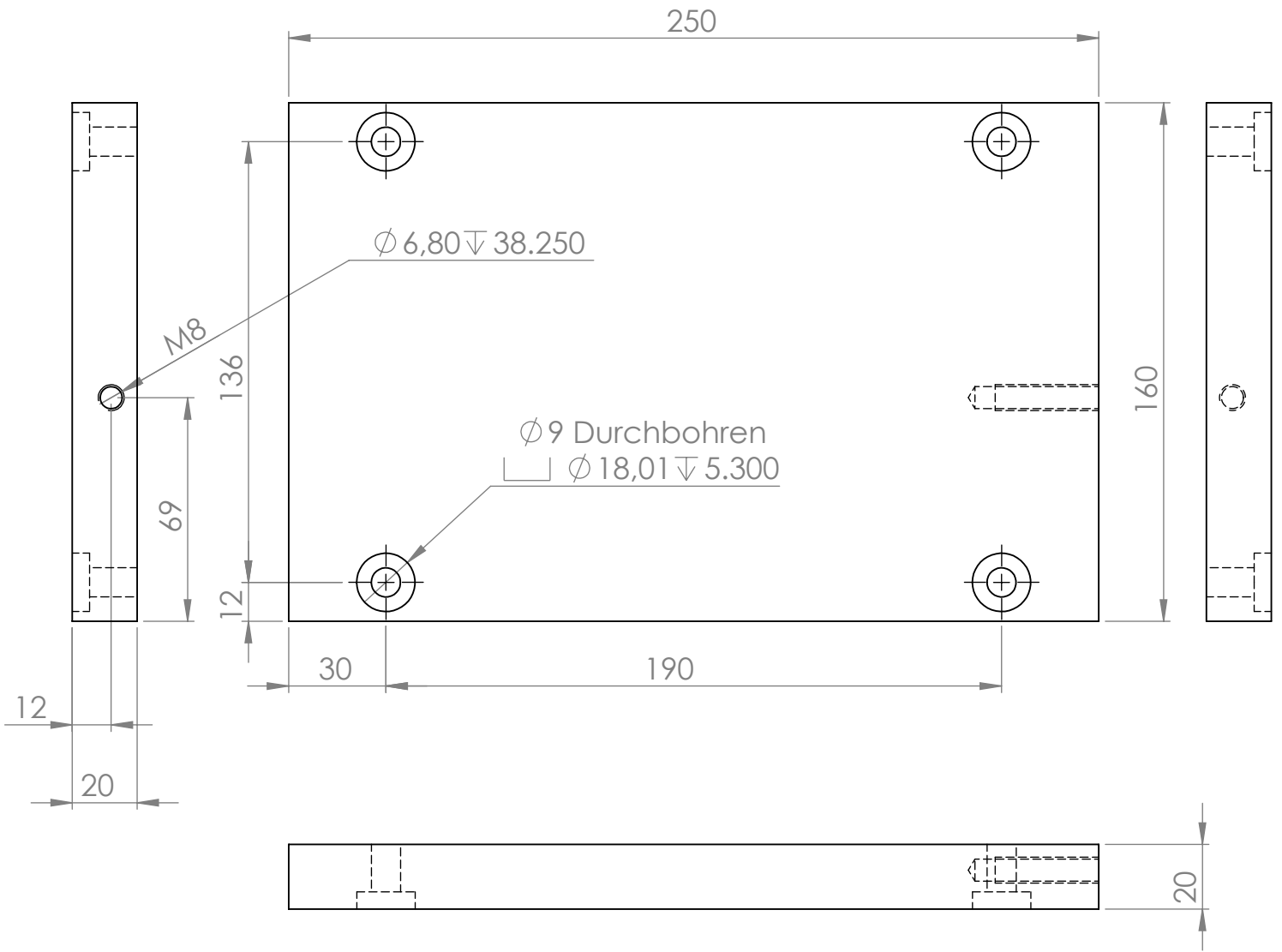
2 x  $\varnothing$  9 DURCH ALLES  
 $\square$   $\varnothing$  18,01  $\nabla$  5,30



WENN NICHT ANDERS DEFINIERT: BEMASSUNGEN SIND IN MILLIMETER	WERKSTOFF  POM-C	ENTGRATEN UND SCHARFE KANTEN BRECHEN	
			MASSTAB:1:2
			TEIL
			Stop_15
			BLATT 1 VON 1



WENN NICHT ANDERS DEFINIERT: BEMASSUNGEN SIND IN MILLIMETER	WERKSTOFF  POM-C	ENTGRATEN UND SCHARFE KANTEN BRECHEN	
			MASSTAB:1:2
			TEIL
			Stop_20
			BLATT 1 VON 1



WENN NICHT ANDERS DEFINIERT:  
BEMASSUNGEN SIND IN MILLIMETER

WERKSTOFF

POM-C

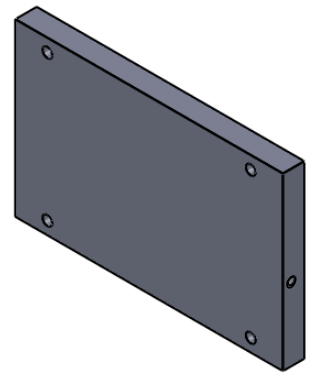
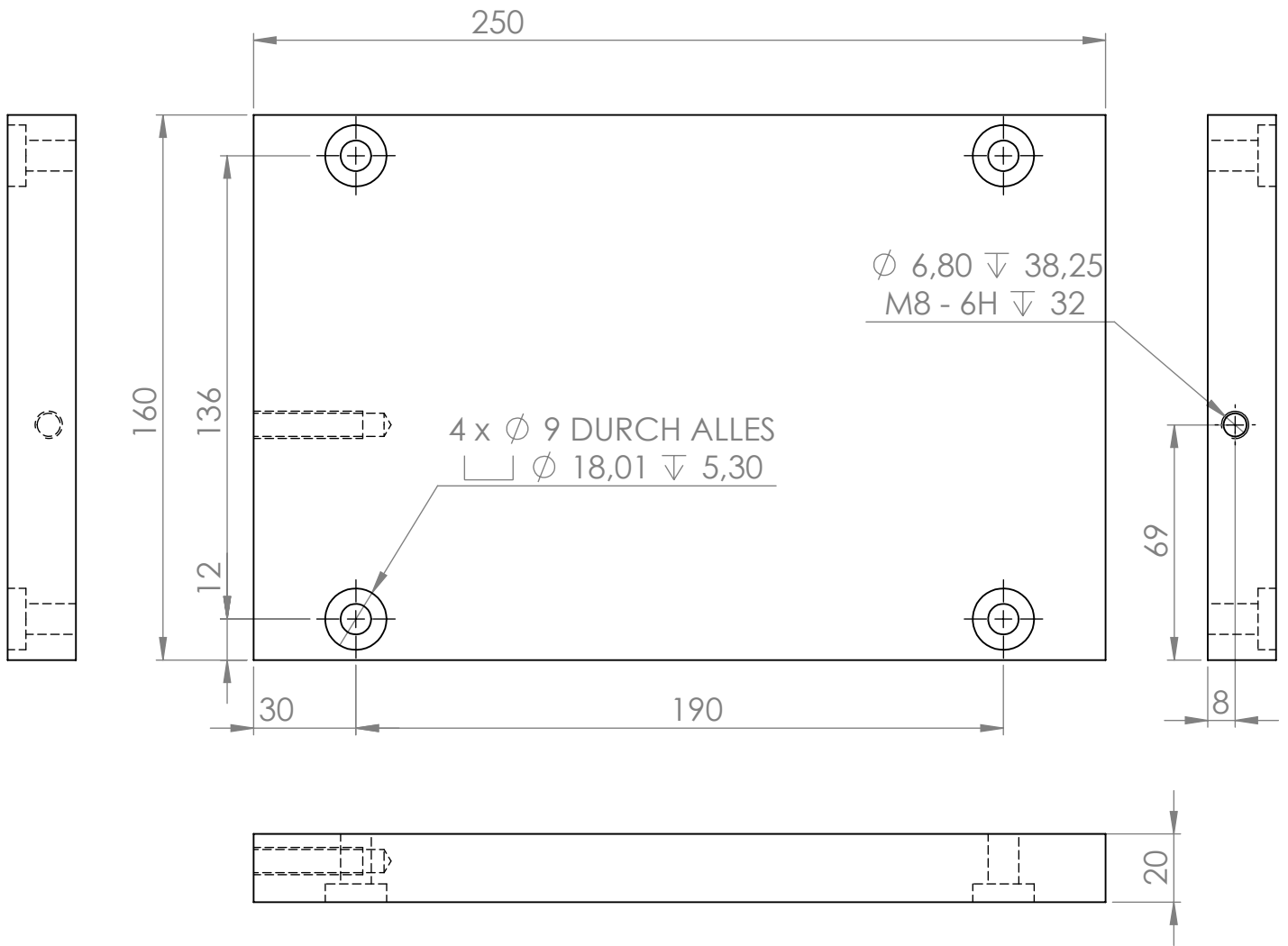
ENTGRATEN  
UND SCHARFE  
KANTEN  
BRECHEN

MASSTAB:1:2

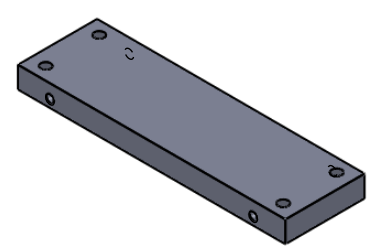
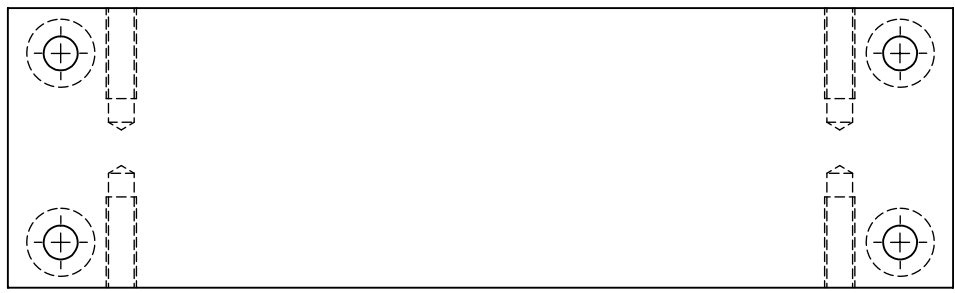
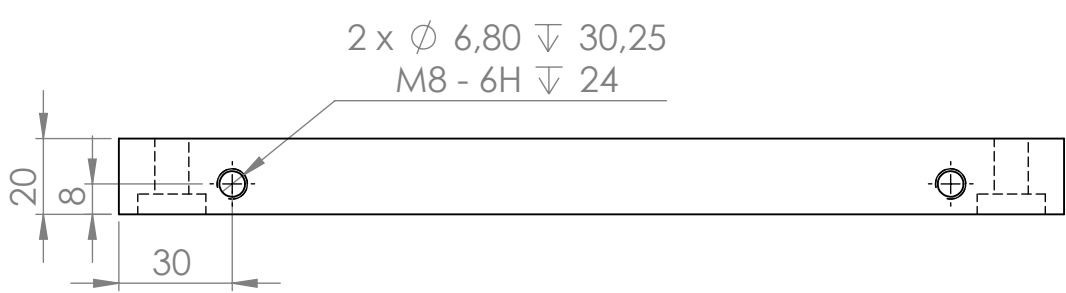
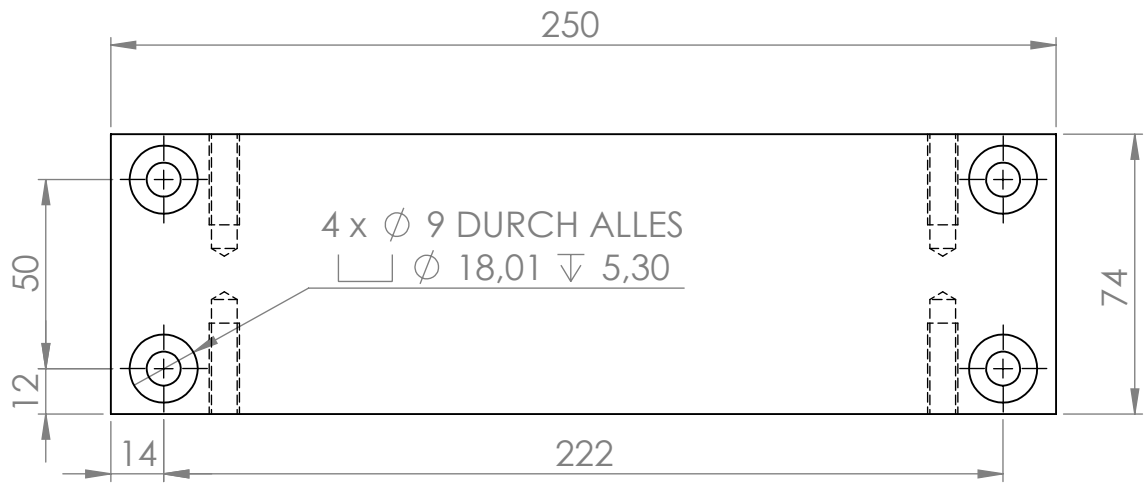
TEIL

Table\_left\_side

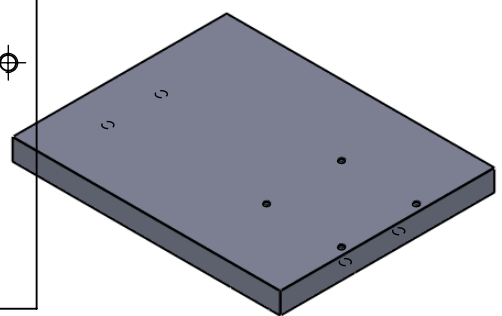
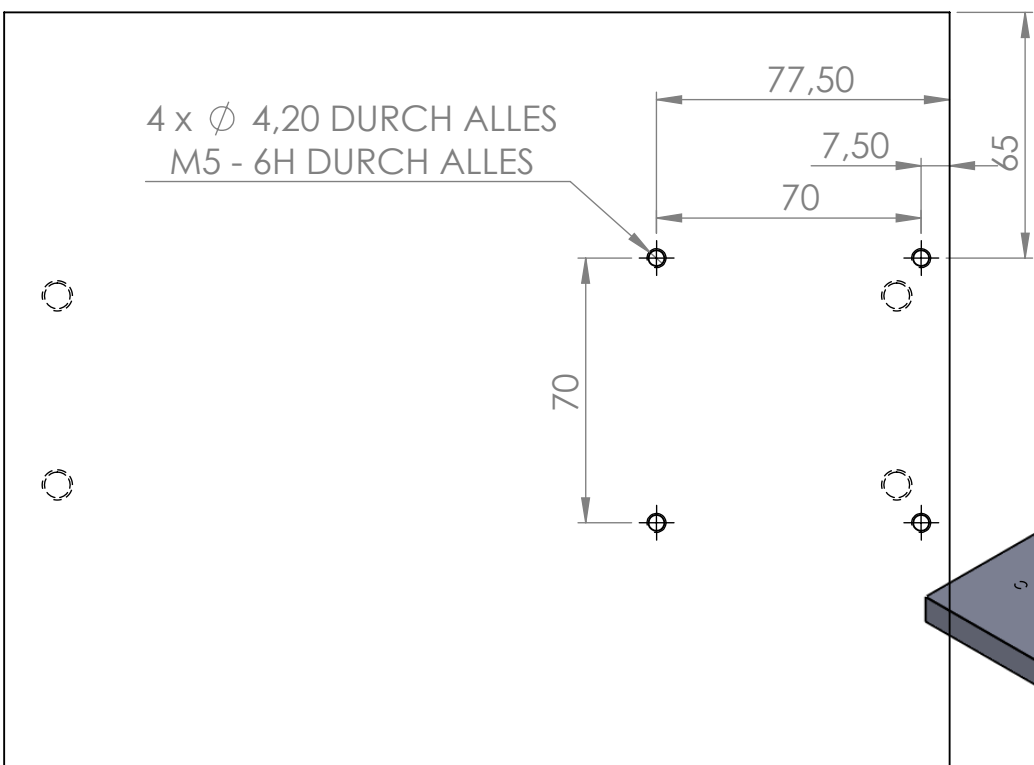
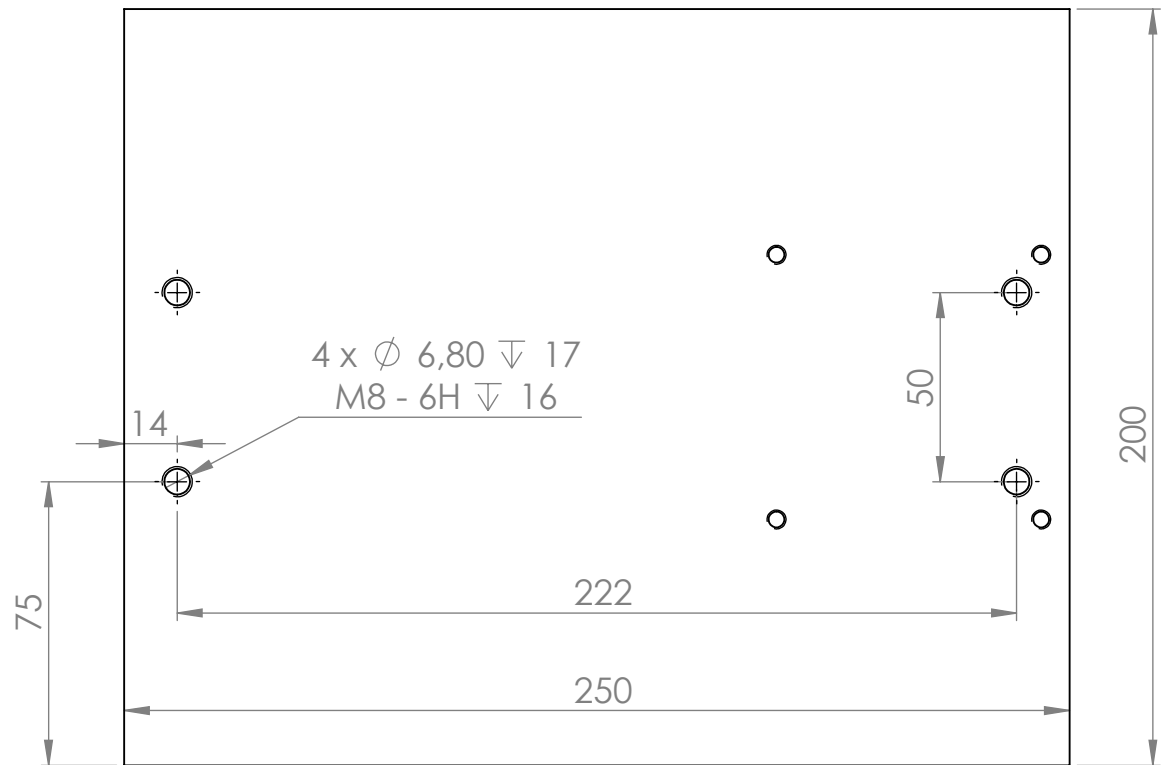
BLATT 1 VON 1



WENN NICHT ANDERS DEFINIERT: BEMASSUNGEN SIND IN MILLIMETER	WERKSTOFF	ENTGRATEN UND SCHARFE KANTEN BRECHEN	
	POM-C		MASSTAB:1:2
			TEIL
			Table_right_side
			BLATT 1 VON 1

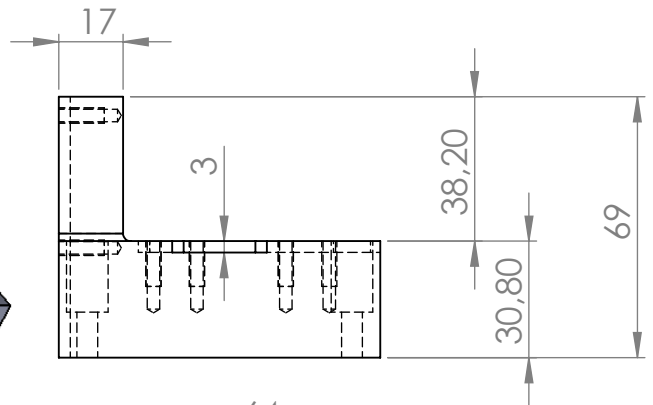
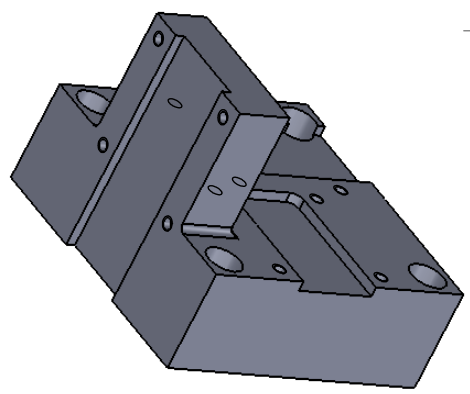
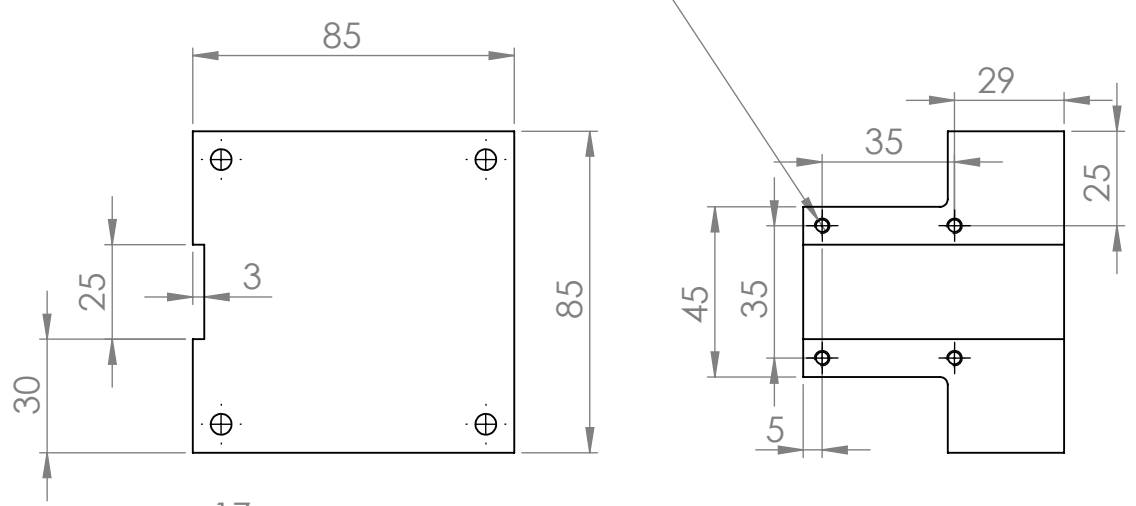


WENN NICHT ANDERS DEFINIERT: BEMASSUNGEN SIND IN MILLIMETER	WERKSTOFF	ENTGRATEN UND SCHARFE KANTEN BRECHEN	
	POM-C		MASSTAB:1:2
			TEIL
			Table_socket
			BLATT 1 VON 1

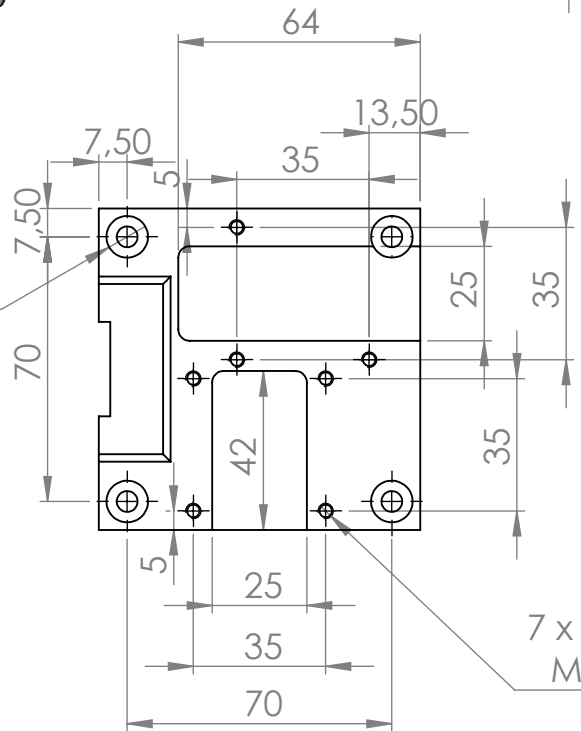


WENN NICHT ANDERS DEFINIERT: BEMASSUNGEN SIND IN MILLIMETER	WERKSTOFF  POM-C	ENTGRATEN UND SCHARFE KANTEN BRECHEN	MASSTAB:1:2
			TEIL  Table_top
			BLATT 1 VON 1

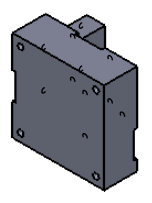
4 x  $\varnothing$  3,30  $\nabla$  15,50  
M4 - 6H  $\nabla$  12



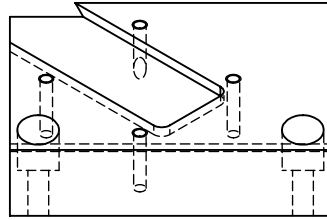
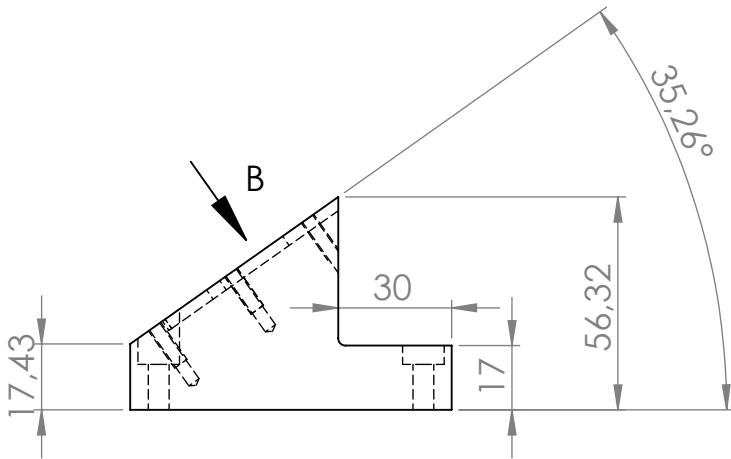
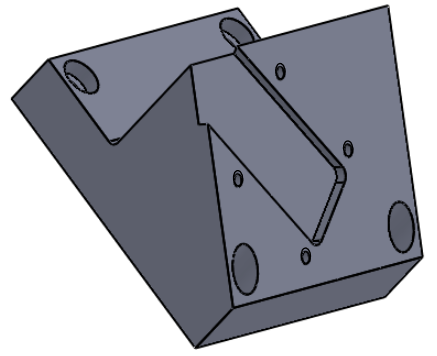
2 x  $\varnothing$  5,50 DURCH ALLES  
 $\sqsupset$   $\varnothing$  11  $\nabla$  57



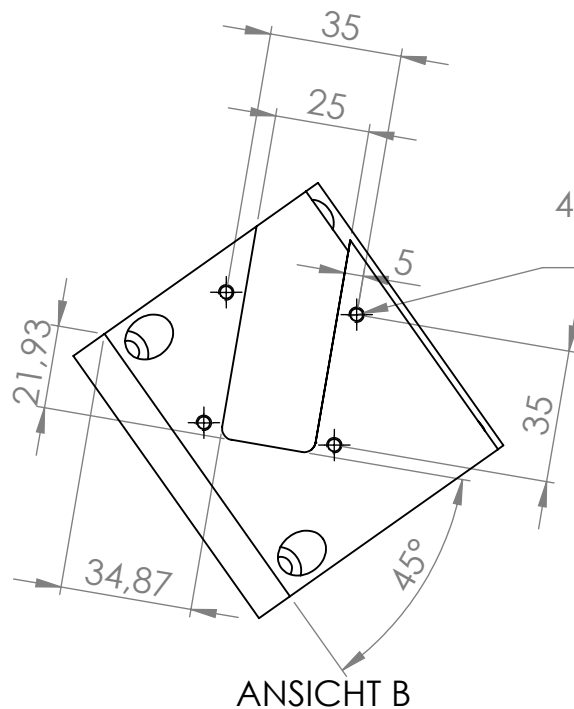
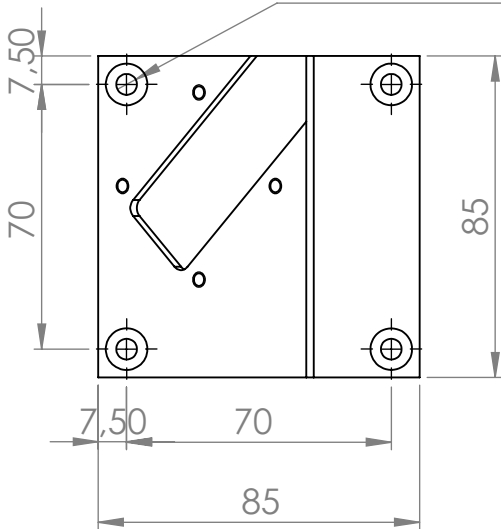
7 x  $\varnothing$  3,30  $\nabla$  18  
M4 - 6H  $\nabla$  12



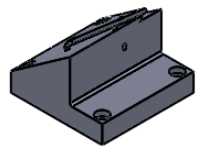
WENN NICHT ANDERS DEFINIERT: BEMASSUNGEN SIND IN MILLIMETER	WERKSTOFF	POM-C	ENTGRATEN UND SCHARFE KANTEN BRECHEN	MASSTAB:1:2
				TEIL
				Transponder_Block_1D
				BLATT 1 VON 1



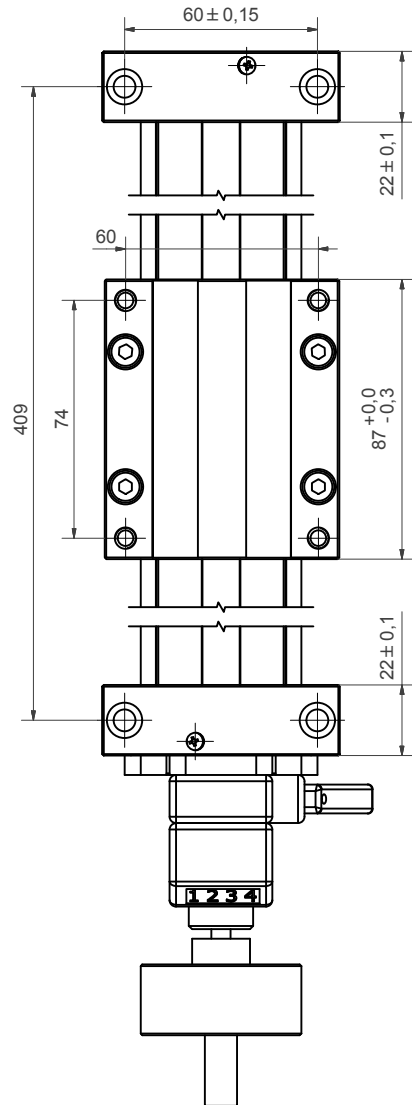
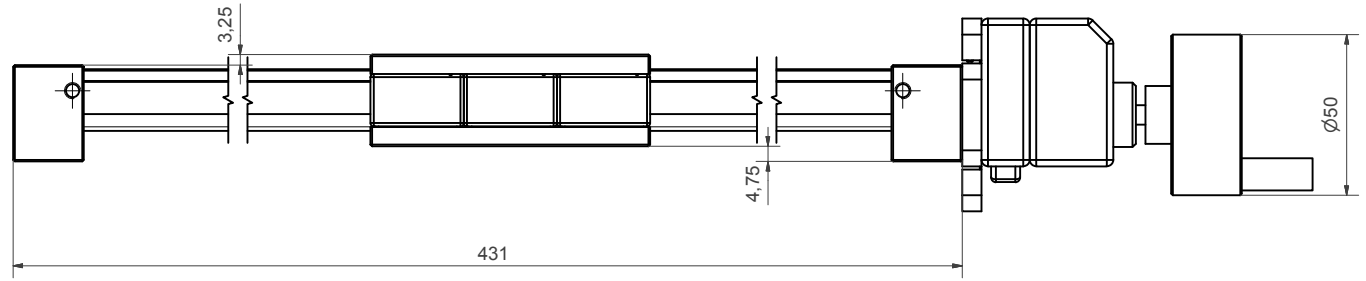
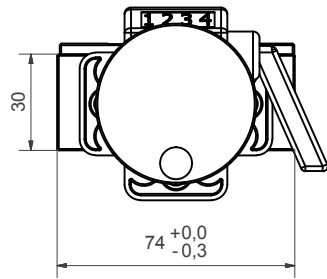
2 x  $\varnothing$  5,50 DURCH ALLES  
 $\square$   $\varnothing$  11  $\nabla$  14,62



4 x  $\varnothing$  3,30  $\nabla$  18  
 M4 - 6H  $\nabla$  12



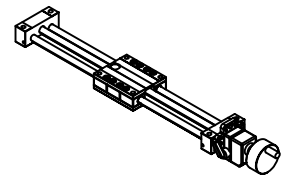
WENN NICHT ANDERS DEFINIERT: BEMASSUNGEN SIND IN MILLIMETER	WERKSTOFF	POM-C	ENTGRATEN UND SCHARFE KANTEN BRECHEN	
				MASSTAB:1:2
				TEIL
				Transponder_Block_3D
				BLATT 1 VON 1



**Besondere Merkmale:**

- a) Spindel TR10x3
- b) Handrad SHT-HR-6-50-52-FG

**Hub: 300mm**  
**Spindellänge: 484mm**  
**Schienenlänge: 407mm**



**weitere Maße und Details:**

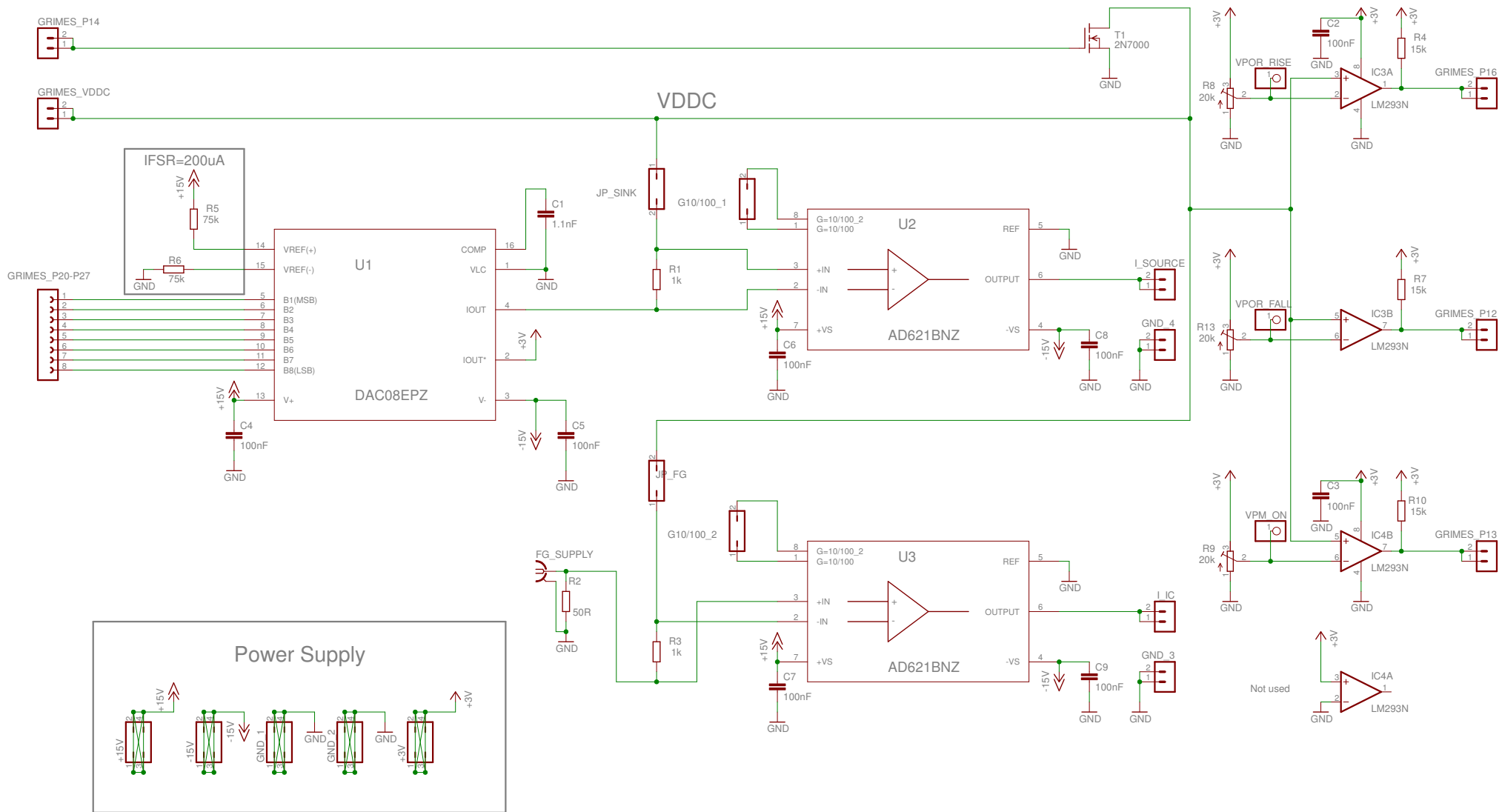
igus® Katalog  
[www.igus.de](http://www.igus.de)

Freigabe:	Datum:	Name:	Unterschrift:	Schutzvermerk nach DIN ISO 16016 beachten
Für Entscheidungen über die Geeignetheit der von igus® zu liefernden Produkte für bestimmte Anwendungsfälle und Konstruktionen, in die die igus®-Produkte einbezogen sind, ist ausschließlich der Kunde verantwortlich. Die ausschließliche Verantwortung des Kunden für die Konstruktion und/oder Verwendung liegt auch dann beim Kunden, wenn igus in die Entwicklung eines vom Kunden geschaffenen Produktes einbezogen wird und dabei, etwa durch Ratschläge oder Empfehlungen, mitwirkt.				
Zeichnungsänderungen:	Maßstab:	-		
	Zeichnungsstand:	-		
	Datum:	Name:	Zeichnungsnummer: 3881100-140514	
	erstellt:	14.05.14	Rheindorf	<b>Spindel-Lineartisch</b> basiert auf: SLW-PT-1040
	geprüft:			
	 Spicher Str. 1a 51147 Köln www.igus.de <small>Plastics for longer life</small>			Artikelnummer:
				SLW-S-3881100-140514
index	Änderung	Datum	Name	Datenname: 3881100-140514.dwg
3				
				Blatt 1 A2

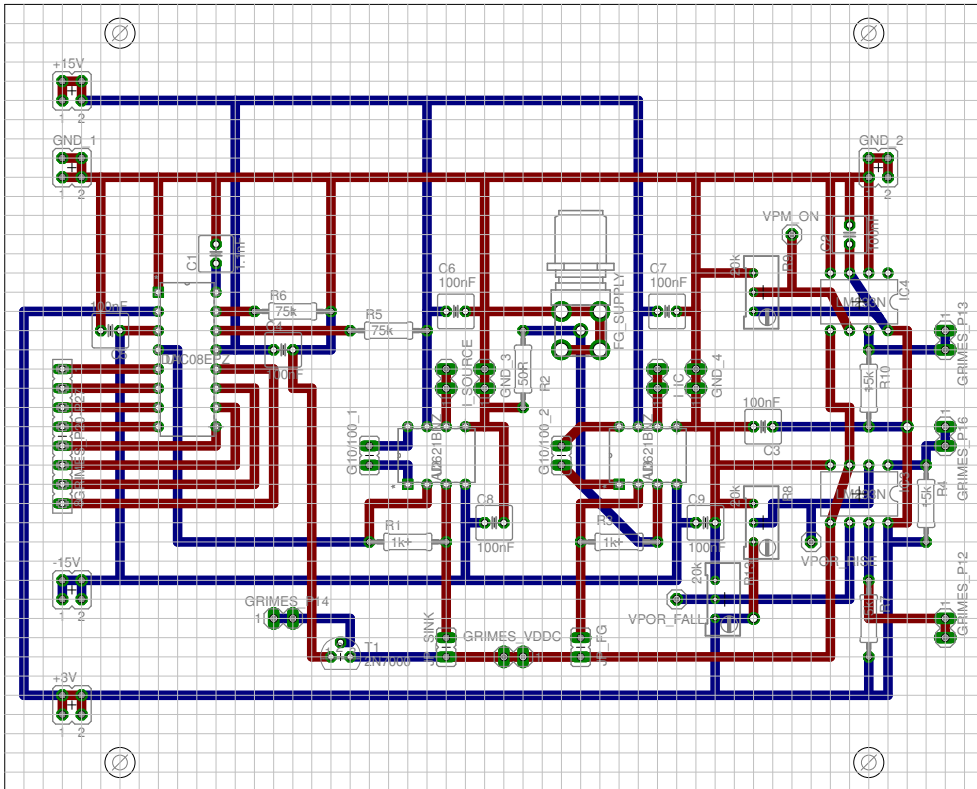


## Appendix C

# Schematic and Layout of the Transponder Adapter Board



TITLE: Transponder_Adapter_Board	
Document Number:	REV:
Date: 09.12.2014 09:02:13	Sheet: 1/1

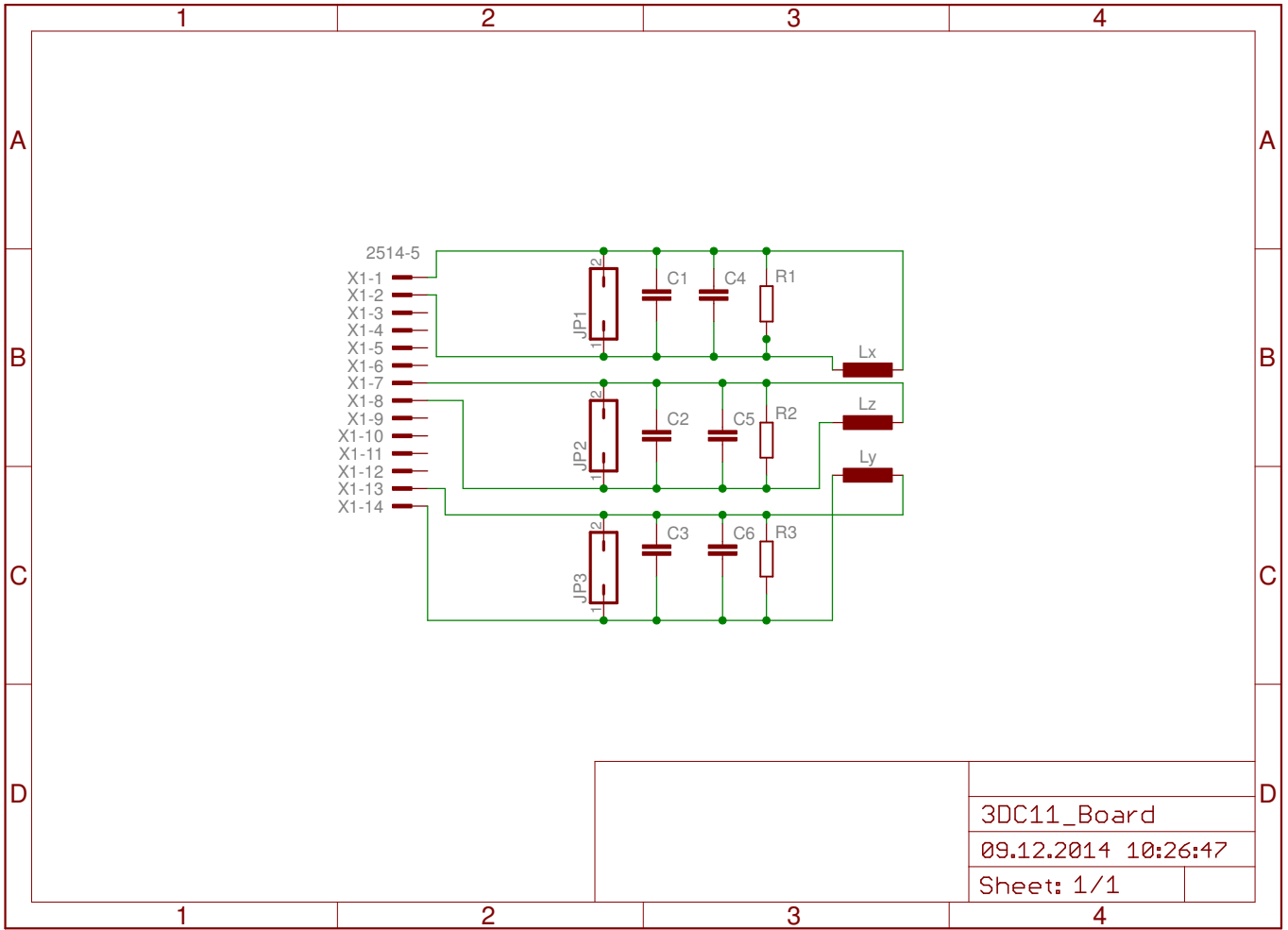


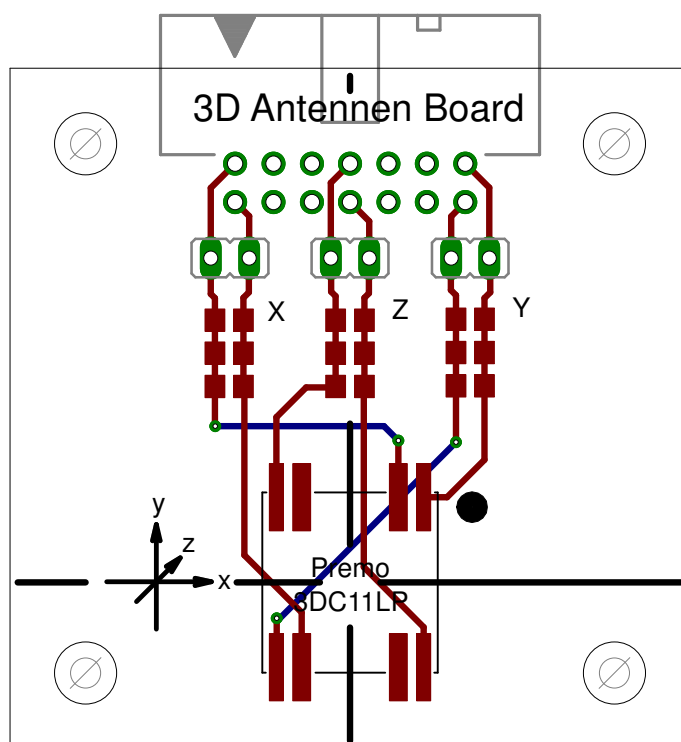
Scale: 1:1



## Appendix D

# Schematic and Layout of the Transponder Coil PCB



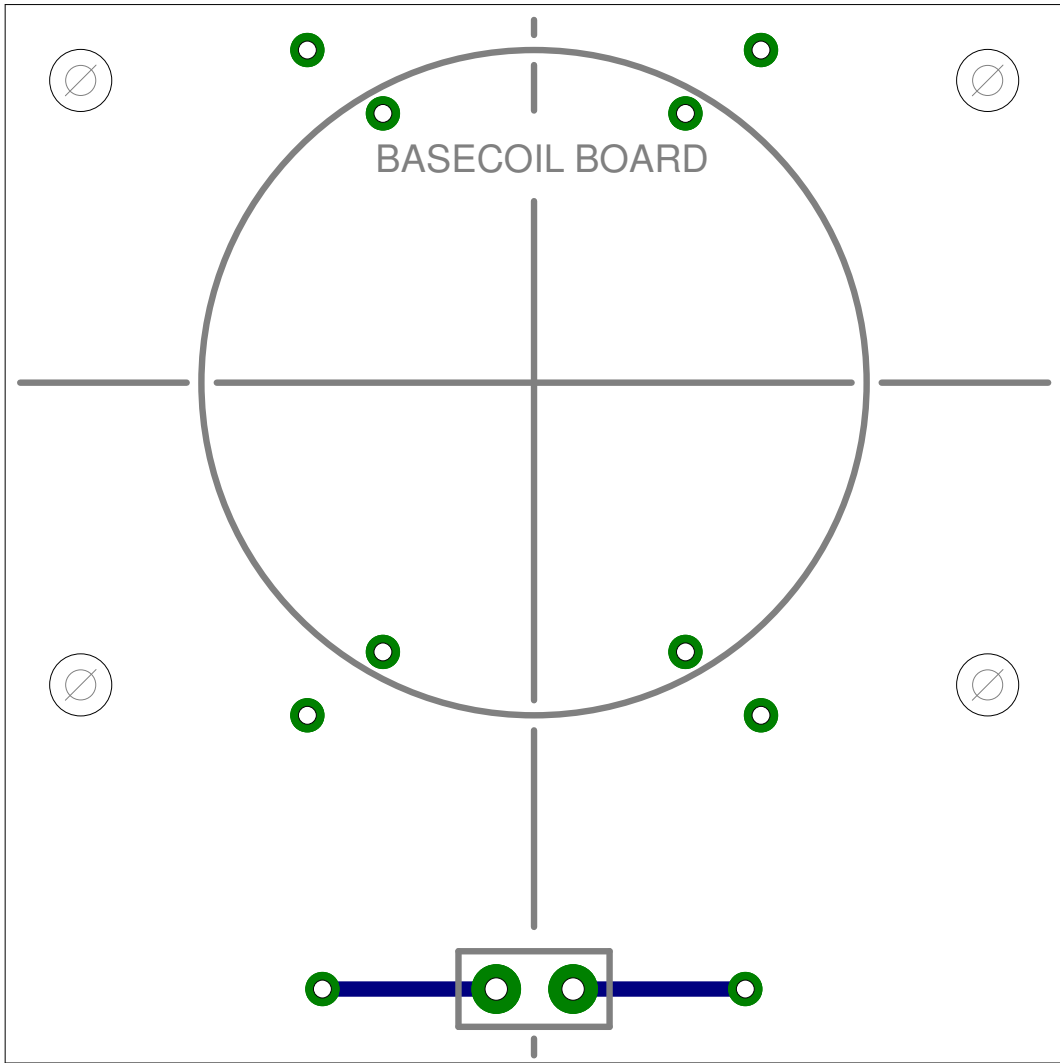


Scale: 2:1



## Appendix E

# Layout of the Basestation Coil PCB



Scale: 2:1